UNMANNED AERIAL VEHICLES FOR ESTIMATING FOREST CANOPY FUELS IN PONDEROSA PINE FOREST

BY PATRICK C. SHIN

A Thesis

Submitted in Partial Fulfillment

of the Requirements for the Degree of

Master of Science

in Environmental Science and Policy

Northern Arizona University

May 2018

Approved:

Temuulen T. Sankey, Ph.D., Chair

Margaret M. Moore, Ph.D.

Andrea E. Thode, Ph. D.

ABSTRACT

UNMANNED AERIAL VEHICLES FOR ESTIMATING FOREST CANOPY FUELS IN PONDEROSA PINE FOREST

BY PATRICK C. SHIN

Forests in the southwestern United States are becoming increasingly susceptible to large wildfires with significant environmental and economical impacts. As a result, forest land managers are planning and conducting forest fuel reduction treatments, in which spatial forest fuels and structure information are necessary, but currently have coarse spatial resolution and limited accuracies. This study tested the feasibility of using an unmanned aerial vehicle (UAV) with a multispectral sensor for estimating forest canopy fuels and structure in a southwestern ponderosa pine forest. The UAV-derived 2D multispectral orthomosaic images and 3D Structure-from-Motion point clouds were used to estimate canopy cover, canopy height, tree density, canopy base height, and canopy bulk density. The estimates were validated with field measurements within 57 plots, 10 x 10 m in dimension, and commonly used aerial photography from the National Aerial Imaging Program with 1 m spatial resolution. The results indicate that the 15 cm resolution UAV images can be used to accurately estimate forest canopy cover in 10 m cells (R^2 = 0.82, RMSE = 8.9% canopy cover). Tree density estimated from individual tree segmentation outputs resulted in true positive detection of 74% of the field-mapped trees with a 16% commission error rate. The individual tree height estimates were strongly correlated to field measurements (R^2 = 0.71, RMSE = 1.83 m), while canopy base height estimates had a weaker correlations with an R^2 of 0.34 and RMSE of 2.52 m. Estimates of canopy bulk density showed

no correlation to estimates derived from field measurements. The UAV-derived canopy cover, canopy height, and canopy base height resulted in drastically different estimates of potential crown fire behavior compared to the coarse resolution LANDFIRE dataset. In particular, estimates from LANDFIRE data showed the study area as 86% active crown fire, 14% passive crown fire, and 0% surface fire. Whereas, UAV-derived estimates showed 100% surface fire and no active or passive crown fire. These results suggest that the spatial resolution of the data can have a large impact on the estimated crown fire behavior and, therefore, on the final forest fuels reduction treatment prescription and monitoring.

Acknowledgements

I would like to thank my thesis committee for their support and guidance through my research and graduate studies. Thanks to members of the Remote Sensing and Geoinformatics Lab at Northern Arizona University, specifically Jonathon Donager and Adam Belmonte, for sharing their experience and knowledge in operating UAV equipment, processing spectral and point cloud data, and their assistance in conducting fieldwork for my research. Also, thanks to members of the Flagstaff forest management community for their support. I am also grateful to the Wyss Foundation for their financial support through my graduate studies. Lastly, I would also like to thank Alexandra Wunsch for all her help throughout my studies and this project.

Table of Contents

Table of Tables

Table of Figures

Chapter 1 Introduction

The southwestern US is home to the largest contiguous ponderosa pine (*Pinus ponderosa*) forest in the world (Cooper, 1960; Allred, 2015). The southwestern ponderosa pine forests serve an ecologically important role by providing biodiversity, carbon storage and sequestration functions (Van Mantgem et al., 2009), and wildlife habitat. These forests are home to many plant species and over 250 species of vertebrates (Patton & Severson, 1989; Laughlin et al., 2006). Ponderosa pine forests in the Southwest also provide economic and social values from wood products, recreation opportunities, and watershed values (Baker, 1986; Allen et al., 2002; Noss et al., 2006; Mueller et al., 2013). Fire suppression, heavy grazing, logging, and climate change in these forests have created characteristics that are more susceptible to high-intensity crown fires putting these values, and neighboring communities, at risk (Cooper, 1960; Covington & Moore, 1994a; Savage et al., 1996; Moore et al., 2004).

Historically, southwestern forests experienced frequent low-intensity fires that effectively thinned younger trees and consumed forest fuels keeping a low tree density. Euro-American settlement brought changes in land use and introduced fire suppression which removed this natural balancing mechanism (Covington et al., 1997). The forests that were naturally maintained by frequent low-intensity fires are now characterized by an overabundance of forest fuels (Fitzgerald, 2005; Westerling et al., 2006; Miller et al., 2009; Stephens et al., 2013). Southwestern forests are now densely stocked with an excess of small trees making them increasingly susceptible to high-intensity crown fires (Covington & Moore, 1994b).

The Schultz Fire of 2010 was an example of the disastrous effects of a high-intensity crown fire just outside of Flagstaff, AZ. The wildfire burned over 6,000 hectares and caused an estimated $133-147 million in damage from the wildfire and subsequent flood events (Combrink

et al., 2013). Shortly after the Schultz Fire, residents of the City of Flagstaff voted for the Flagstaff Watershed Protection Project (FWPP) that allocated a $10 million bond for fuel reduction treatment in key areas around Flagstaff and its watershed (Figure 1). The FWPP is a multiple agency partnership with the City of Flagstaff, Arizona State, and Coconino National Forest with the goal to protect the city from wildfire, and subsequent flooding, which could damage key city infrastructure including its water supply. The FWPP is also the first fuel reduction treatment in the United States to be funded by a municipal bond (Mottek Lucas, 2015).

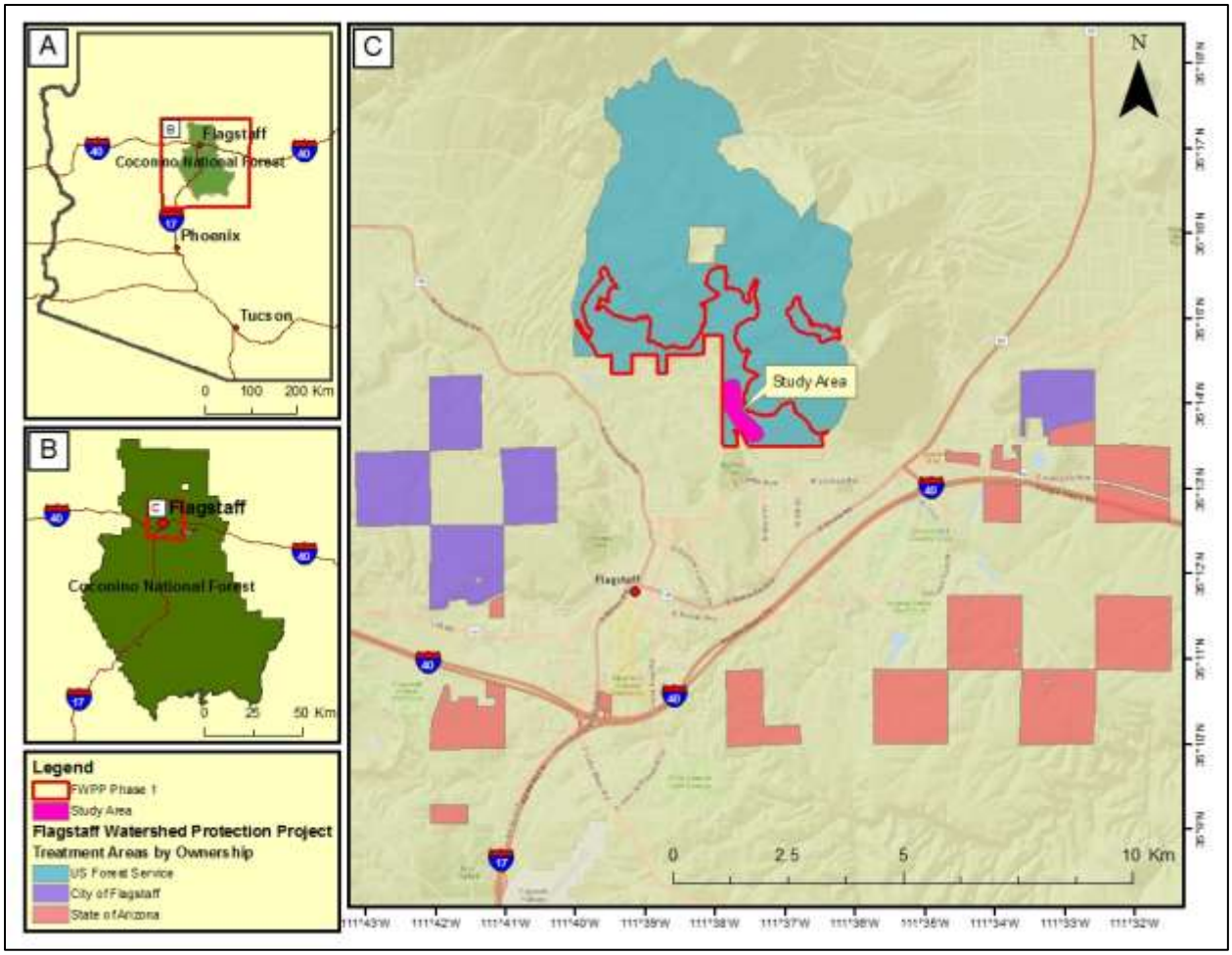

Figure 1: Study area map. The study area is located near Flagstaff, AZ and the Coconino National Forest within the state of Arizona (Panels A and B). This study focused on a Phase 1 area of the Flagstaff Watershed Protection Project (FWPP) treatment area (Panel C), which was scheduled for fuel reduction thinning in Summer and Fall 2017. Other areas of the FWPP and associated land ownership by the US Forest Service, City of Flagstaff, and the State of Arizona are also shown (Panel C).

Forest fuel reduction treatments, such as those treatments within the FWPP, often include a combination of mechanical, or hand thinning followed by the reintroduction of periodic low-intensity fire. Forest thinning is designed to manipulate forest structure such as canopy cover, canopy height, crown base height, and crown bulk density, to produce forest conditions within the natural range of variability and less susceptible to catastrophic crown fires (Graham et al., 2004; Agee & Skinner, 2005; Larson & Churchill, 2012; Reynolds et al., 2013). Reintroduction

of low-intensity fire is used to restore the natural fire regime and maintain a balance of forest fuels (Landres et al., 1999; Mast et al., 1999). These techniques can decrease the risk of wildfire, lessen the impacts of wildfire, reduce outbreaks of insects and disease, and help mitigate the effects of a changing climate (Savage et al., 1996; Kolb et al., 1998; Covington et al., 2001; Moore et al., 2004; Van Mantgem et al., 2009; Stoddard et al., 2015).

Land managers often use detailed spatial forest structure information when planning, implementing, and monitoring forest fuels treatments. This information, in addition to data from field measurements, is used to prioritize areas that require treatment and to develop treatment prescriptions for specific areas. In addition to treatment planning, this information is also used to monitor forest characteristics and determine the effectiveness of the treatments at accomplishing desired management objectives (Lackey, 1998; Mueller et al., 2013).

Currently, most fuels treatment projects use spatial fuels information from the Landscape Fire and Resource Management Planning Tools Project (LANDFIRE) database. LANDFIRE is an interagency partnership between the United States Department of Agriculture (USDA) Forest Service and the United State Department of Interior (DOI). Major partners to the program include the US Geological Survey (USGS), US Bureau of Land Management (BLM), Natural Resources Conservation Service (NRCS), National Agricultural Statistics Service (NASS), National Association of State Foresters, Texas Forest Service, and the Nature Conservancy. The LANDFIRE data production process is designed to be fully repeatable and is based on the latest science. LANDFIRE utilizes a combination of several geospatial technologies including biophysical gradient analysis, remote sensing, vegetation modeling, ecological simulation, landscape disturbance, and succession modeling (Rollins, 2009). First, a field-referenced database is created using field data primarily from the US Forest Service Forest Inventory and

Analysis program, but also including data from the US Geological Survey Gap Analysis Program, Bureau of Land Management, State agencies, and other partners. Next, spatial layers such as topography, satellite imagery, biophysical gradients, and training data from field-referenced data are used to predict existing vegetation type, vegetation height, and canopy cover. These data are then used to model fire regime departure from historical conditions, as well as current vegetation characteristics.

The field-reference data, spatial layers, and modeled vegetation characteristics are then used to estimate surface and canopy fuel components including fire behavior fuel models, canopy base height, and canopy bulk density (Reeves et al., 2006; Rollins, 2009). An overview of the LANDFIRE data production process from Rollins (2009) is shown in Figure 2. Specifically, canopy fuels products of LANDFIRE are a function of 40 separate predictor variables that are derived from LANDSAT satellite imagery (Homer et al., 2004), DAYMET meteorological database (Thornton et al., 1997), LANDSUM fire succession model (Keane et al., 2006), USGS elevation data (USGS, 2008), and previously modeled vegetation characteristics from LANDFIRE (Zhu et al., 2006) (Appendix A).

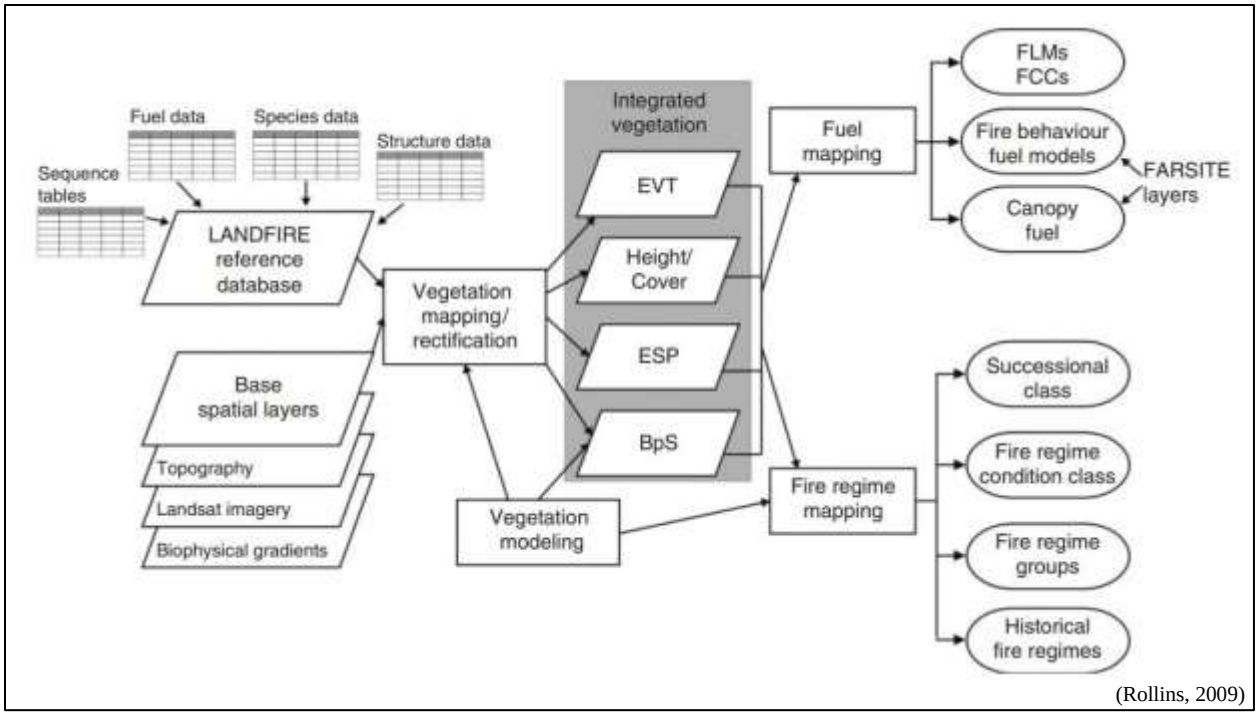

Figure 2: Overview of the LANDFIRE data production procedure. LANDFIRE mapping processes begin with the creation of the LANDFIRE reference database, which comprises a set of all available georeferenced plot information from within each mapping zone. The reference and spatial databases are used in a classification and regression tree-based framework for creating maps of environmental site potential (ESP) and biophysical settings (BpS), existing vegetation type (EVT) and structure (canopy height, EVH and cover, EVC). These core vegetation maps formed the foundation for the simulation of historical fire regimes and the subsequent calculation of current departure from historical vegetation conditions. In addition, the vegetation maps served as the basis for mapping surface and canopy fuel for simulation of fire behavior and effects. LANDFIRE fire effects data products include Fuel Loading Models (FLMs) and Fuel Characterization Classes (FCCs).

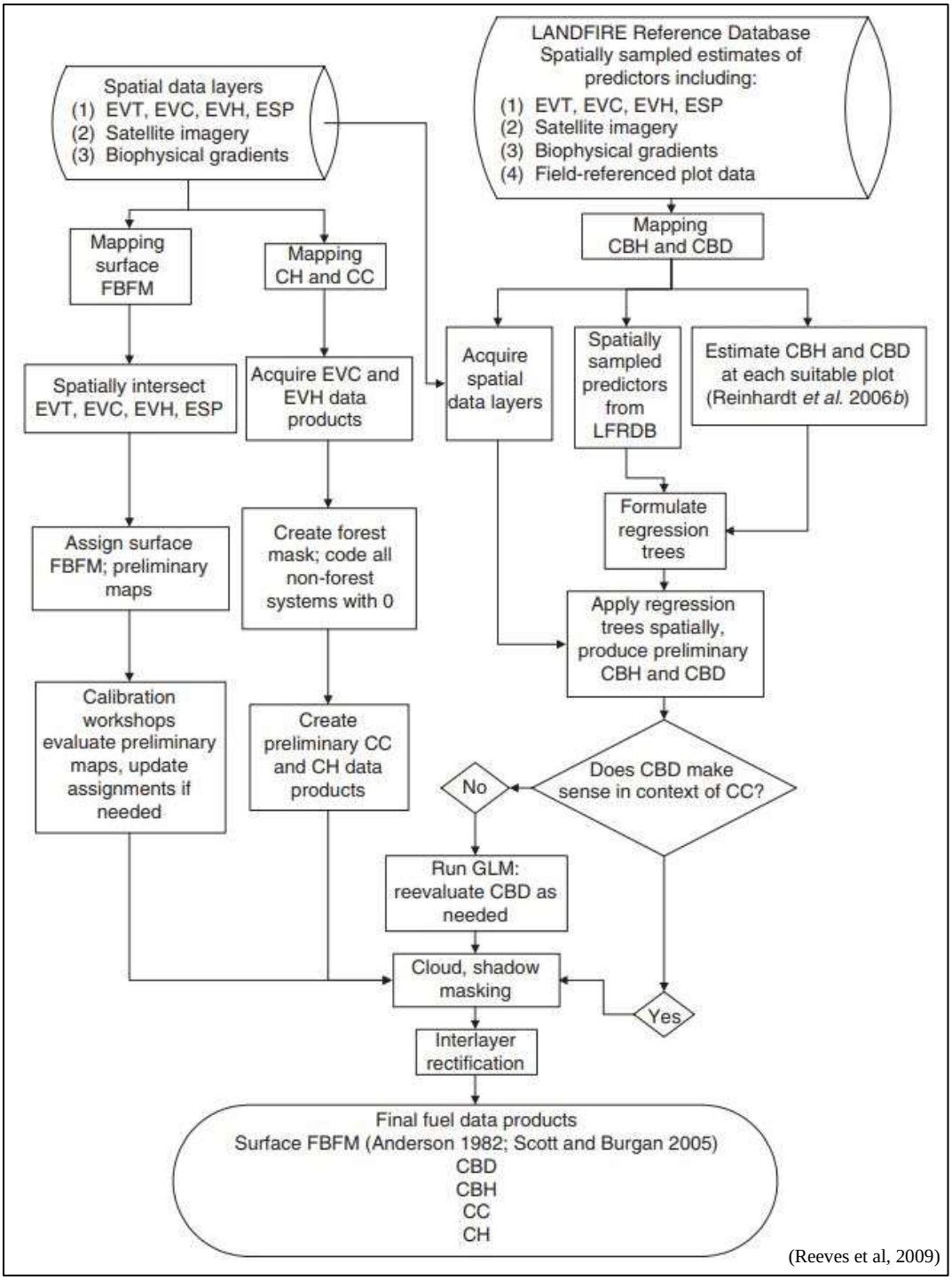

Figure 3: The LANDFIRE fuels product data processing diagram. Spatial data layers and field-referenced data are used to model fire behavior fuel models (FBFM), canopy height (CH), canopy cover (CC), canopy base height (CBH), and canopy bulk density (CBD). A subsequent process using a combination of model output evaluation, and expert opinion, are then used to develop the final LANDFIRE fuel data products.

Data from LANDFIRE is relatively easy to acquire from the federal website (www.landfire.gov) and comes at no cost to the user. The database offers nationwide coverage of spatial forest fuels data in 30 m spatial resolution, and is updated every 2-5 years (Table 1). The spatial fuels products produced by the LANDFIRE project include: canopy cover, canopy height, crown base height, crown bulk density, and fire behavior fuel models. Canopy cover is the percent of horizontal space that is covered by tree canopy within a 30 m grid cell. Canopy height describes the average height of the forest canopy within a 30 m grid cell (Reeves et al., 2009). Crown bulk density is the mass of canopy fuel per canopy volume that would burn in a crown fire (Wagner, 1977; Scott & Reinhardt, 2001; Keane et al., 2005). Crown base height is the lowest point at which there is sufficient canopy fuel for ignition ($\geq$0.012 kg/m^3) (Reeves et al., 2006). The fire behavior fuel models refer to the 13 Anderson Fire Behavior Fuel Models (Anderson, 1982) and the 40 Scott and Burgan Fire Behavior Fuel Models (Scott & Burgan, 2005), which describe surface fuel composition and associated fire behavior (Rothermel, 1972). These forest fuels raster products can be useful for prioritizing and planning at a landscape scale. However, their accuracy can vary by location compared to field-based measurements and often need to be adjusted to better represent actual site-specific conditions (Rollins, 2009). For example, in a study conducted by Reeves et al. (2009) across 12 different sites, LANDFIRE canopy base heights had R^2 values that ranged from 0 to 0.93 when compared to field data.

Table 1: Spatial fuel products of LANDFIRE. The spatial fuels products produced by the LANDFIRE program with associated units that are binned into different categories. For example, canopy cover is presented in 10% bins, and canopy height is in 5 m height bins.

LANDFIRE Spatial Fuels Products

*All products are in 30 m spatial resolution and updated every 2-5 years

Data Type	Units	Bin Size
Canopy Cover	Percent Cover (%)	10%
Canopy Height	Meters (m)	5 m
Canopy Base Height	Meters (m)	0.1 m
Canopy Bulk Density	Kilograms per cubic meter (kg/m^3)	0.01 kg/m^3
Fire Behavior Fuel Model	Fuel Type and Fire Behavior	N/A

The spatial fuels data from the LANDFIRE database are formatted for use with fire behavior modeling software, such as FlamMap (Stratton, 2006) (Figure 4). FlamMap is used to combine forest fuel characteristics, topography, fuel moisture, and weather factors to model fire behavior outputs. Some of these outputs include: flame length in meters, rate of spread in meters per minute, and crown fire activity. These are all generated with geospatial attributes and can be analyzed in a spatial environment (Finney, 2006). This study used FlamMap to model potential crown fire activity which uses spatial fuels data to model a particular area as potential surface, passive crown, or active crown fire. Surface fire is defined as a fire burning through the fuels on the ground surface. Passive crown fire occurs in an area that exhibits surface fire and contains a canopy base height low enough to initiate crown fire, however the canopy bulk density is insufficient to carry the crown fire. Active crown fire occurs where crown fire initiation is achieved and canopy bulk density can adequately carry a crown fire (Cruz et al., 2002; Scott, 2006).

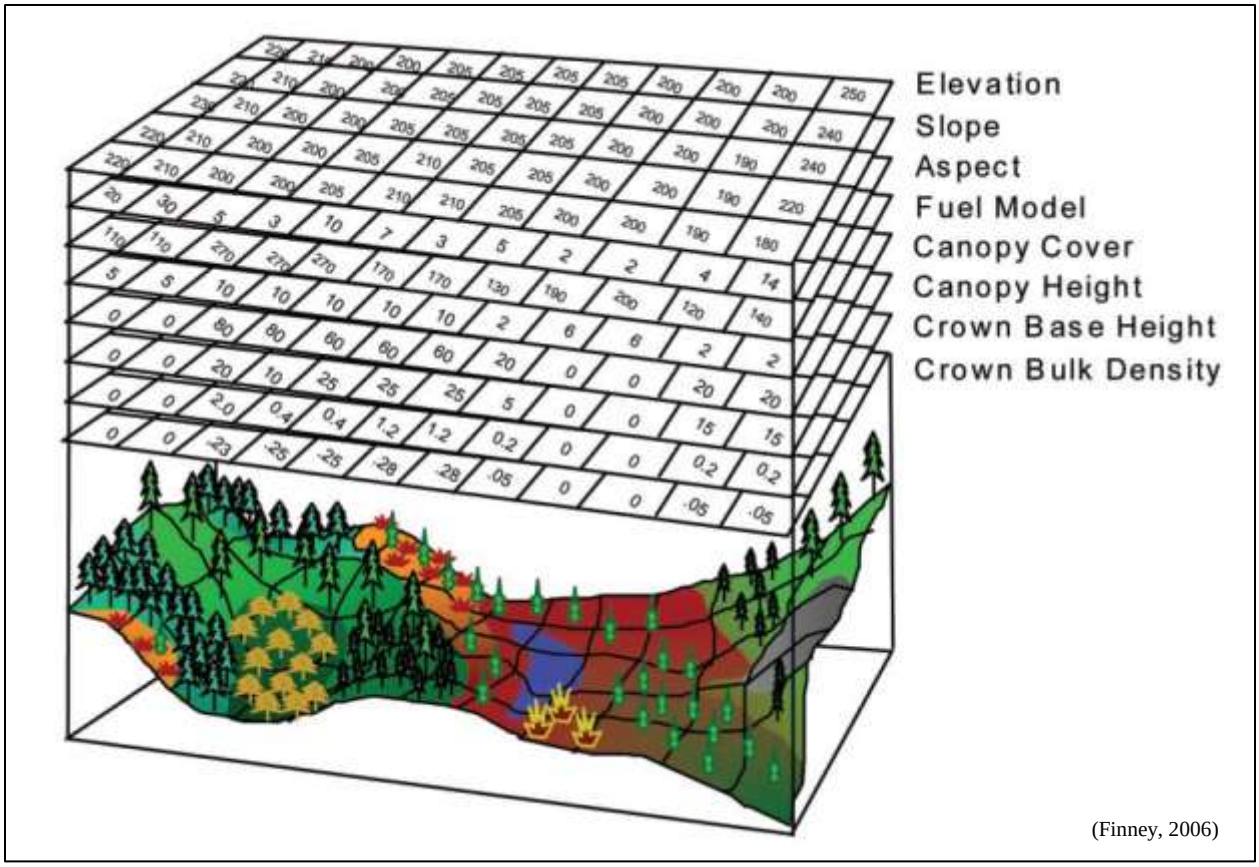

Figure 4: Topographic and spatial fuels variables that comprise the FlamMap landscape file. These variables are required to model fire behavior with FlamMap. These layers are readily available as 30 m rasters from the LANDFIRE database.

By using the spatial fuels products from LANDFIRE with FlamMap fire behavior software, users can model fire behavior on a landscape scale in an area of their interest. In planning the FWPP treatment, the Coconino National Forest utilized LANDFIRE data, with supplementary field surveys, as inputs to FlamMap software to spatially model fire hazard and behavior near Flagstaff, AZ. They were able to use this information to examine the different alternatives that were analyzed in the Environmental Impact Statement (EIS). During this analysis, the Coconino National Forest found that the fuel reduction treatment could reduce the

potential active and passive crown fire area by about 83% in the Dry Lake Hills area of the project (Table 2).

According to the Environmental Impact Statement prepared by the Coconino National Forest (Coconino National Forest, 2015) for the FWPP, fire behavior analyses was performed by utilizing spatial fuels data from LANDFIRE, that were supplemented with field surveys. These field surveys were conducted across approximately 50% of the Dry Lake Hills area and were collected using the US Forest Service Field Sampled Vegetation (FSVeg) protocols (https://www.fs.fed.us/nrm/fsveg/). Local weather conditions from those that were exhibited during the 2010 Schultz Fire were used in modelling potential fire behavior in FlamMap. By using FlamMap in conjunction with Forest Vegetation Simulator (FVS), which is used to model the growth of forests, simulate management actions, and predict future forest structure, the Coconino National Forest staff modeled future potential fire behavior for simulated treatments representing each of the alternatives that were analyzed during the EIS process (Coconino National Forest, 2015).

Table 2: Outputs from the crown fire potential model conducted by the Coconino National Forest during the FWPP Environmental Impact Statement analysis, which estimated the amount of total area in each fire behavior category (active crown fire, passive crown fire, and surface fire) for the Dry Lake Hills area. The weather conditions used in modelling were those exhibited during the 2010 Schultz Fire near Flagstaff. By implementing alternatives 2 and 3, the total active and passive crown fire was reduced by about 83%. See Figure 5 for associated crown fire potential maps.

Crown Fire Potential in the Dry Lake Hills Area as Modelled in the FWPP EIS by the Coconino National Forest		
Fire Behavior	Existing Crown Fire Potential	Post-treatment Crown Fire Potential
Active Crown	1,550 hectares	266 hectares
Passive Crown	303 hectares	38 hectares
Surface	1,166 hectares	2,706 hectares

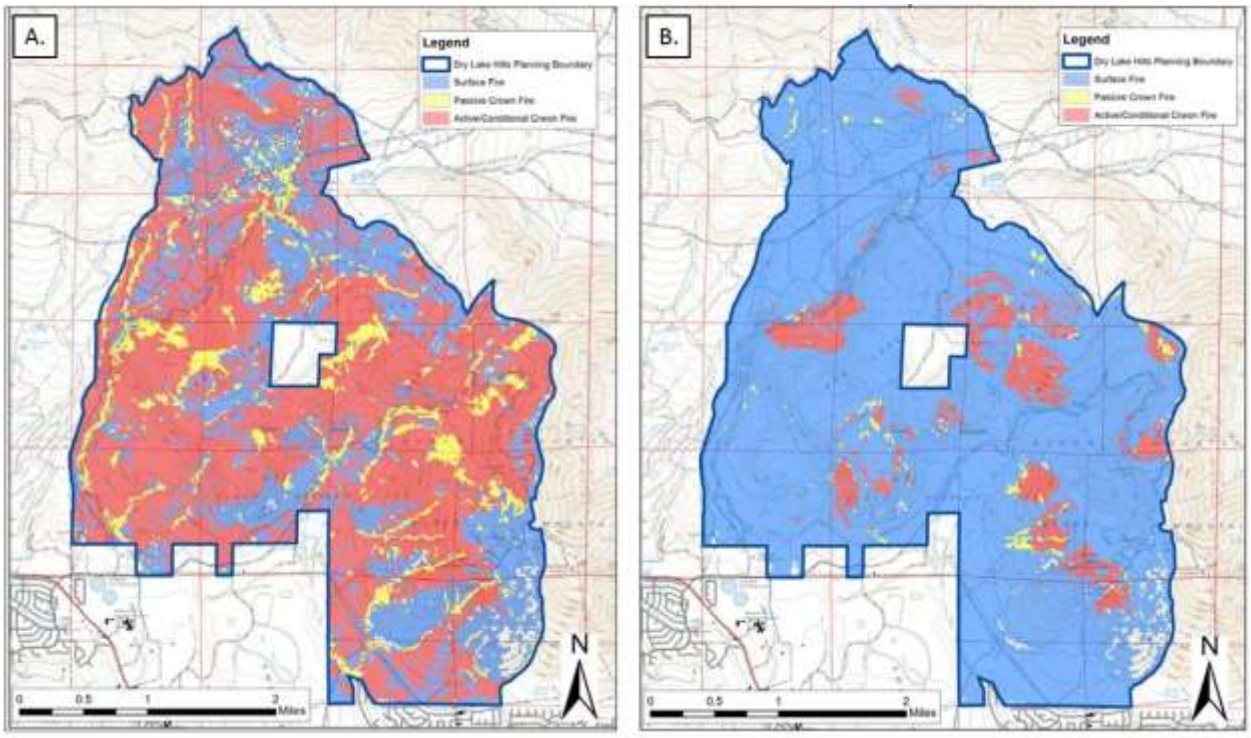

Figure 5: Crown fire potential maps for the Dry Lake Hills area of Flagstaff Watershed Protection Project as illustrated in the Environmental Impact Statement conducted by the Coconino National Forest. Crown fire potential with the existing forest conditions (Panel A) contains more area modeled for potential active crown fire than post-treatment conditions (Panel B). Both models used weather conditions found during the 2010 Schultz Fire. See Table 2 for acreages by each modeled fire behavior type.

Although LANDFIRE provides comprehensive U.S. nationwide coverage, the spatial information from the database is too coarse to represent the variations of forest fuels in an area smaller than landscape scale (Stratton, 2004). In southwestern ponderosa pine forests, landscape scale is defined as being >405 hectares, mid-scale is 4-405 hectares, and fine-scale is <4 hectares (Reynolds et al., 2013). Planning and evaluating fuels treatments with LANDFIRE data are limited to landscape scale applications and often requires supplementary data to make it applicable on a local level (Reeves et al., 2006; Stratton, 2009). Additionally, the LANDFIRE database is updated every 2-5 years making it further difficult to use as a timely monitoring tool. Therefore, land managers often conduct monitoring through traditional field surveys that can be

time-consuming and costly, often leading to a lack of comprehensive monitoring and evaluation of the treatment.

Remote Sensing of Forest Characteristics

Remote sensing offers a valuable method for understanding forest characteristics and lessens the need for costly field inventory campaigns. Spectral remote sensing in a form of passive remote sensing measures electromagnetic radiation that is reflected by objects of interest, and is commonly conducted using satellite- and aerial-based platforms. In forestry applications, these data can be used to estimate canopy cover, as well as species composition and arrangement (X. Li & Strahler, 1985; Franklin et al., 2000; Key et al., 2001; Ozdemir & Karnieli, 2011). However, passive remote sensing is less effective at estimating three-dimensional forest attributes such as tree height, canopy base height, tree density, and diameter at breast height (DBH) (Roberts et al., 2004; Hyde et al., 2006; Wulder et al., 2009).

Light detection and ranging (lidar) is a form of active remote sensing that emits laser pulses towards the ground and measures the energy that is reflected back to the sensor. The resulting data is in the form of a 3D point cloud, where each point represents a surface, or feature, that reflected a pulse. The resolution of lidar data is measured by point density, or the number of points per area (points/m^2).

Manned aerial lidar uses a manned aircraft as a platform for a lidar sensor. Generally, when applied to measuring forest structure, a relatively high point density is desired ($\geq$ 6-8 points/m^2) (Hummel et al., 2011; Edson & Wing, 2011). Manned aerial lidar has become a proven method for measuring forest structure across various regions and forest types. Aerial lidar was used to estimate forest canopy fuels in a coniferous forest west of the Cascade Range in Washington State within the Capitol State Forest managed by the Washington State Department

of Natural Resources (WA DNR). The study site was primarily composed of Douglas-fir (*Pseudotsuga menziesii*) and western hemlock (*Tsuga heterophylla*), with a small hardwood component of red alder (*Alnus rubra*) and bigleaf maple (*Acer macrophyllum*). The study area was located within a commercial forest that had varying age and tree density due to harvesting, however specific forest metrics for the study area were not given. The study compared field-based canopy fuel estimates to those derived from lidar data and had strong relationships for crown bulk density ($R^2 = 0.86$), canopy base height ($R^2 = 0.77$), and tree height ($R^2 = 0.98$) (Andersen et al., 2005). Additionally, a study was also conducted in Washington State in the drier ponderosa pine forests east of the Cascade Range within the Ahtanum State Forest managed by WA DNR. The study site contained mostly ponderosa pine and additional components of Douglas-fir, grand fir (*Abies contorta*), lodgepole pine (*Pinus contorta*), Engelmann spruce (*Picea engalmanii*), and western larch (*Larix occidentalis*). Similar to the Capitol Forest site in Andersen et al (2005), the Ahtanum State forest is an active commercial forest which led to varying tree ages and tree density across the study site. Field data from this study showed that the study area contained an average canopy cover of 49.24% (SD = 18.74%) and average tree density of 423.98 tree per acre (SD = 344.34). When comparing field-based estimates to lidar-derived estimates, strong positive relationships were shown for tree heights ($R^2 = 0.94$), canopy base height ($R^2 = 0.78$), and canopy bulk density ($R^2 = 0.83$) (Erdody & Moskal, 2010). Another study used aerial lidar to measure canopy base height, tree height, and crown diameter in eastern Texas within the Sam Houston National Forest. The study site was described as pine plantations of various ages and also contained upland and bottomland hardwood species. However, specific species and forest metrics for the site are not described. The study compared lidar-derived crown base heights, tree heights, and crown widths to field measurements. Crown base height was

positively correlated with an R^2 of 0.80 (0.79 for pines, 0.74 for hardwoods). Tree heights were positively correlated with an R^2 of 0.95 (0.96 for pines, 0.90 for hardwoods). Lastly, crown widths were also positively correlated, although less strongly, with an R^2 of 0.53 (0.57 for pines, 0.59 for hardwoods) (Popescu & Zhao, 2008). A study in southwestern Norway used aerial lidar to estimate tree height and height to live crown. The study contained two areas, the Ostmarka Nature Reserve and a forest near the municipality of Valer, both of which were in southeast Norway and dominated by Norway spruce (*Picea abies*). When compared to field measurements, lidar-derived estimates for tree heights were positively correlated ($R^2 = 0.75$). Lidar-derived estimates for height to live crown were less strongly correlated ($R^2 = 0.53$) (Naesset & Bjerknes, 2001). Additionally, manned aerial lidar has the advantage of being able to cover a large area from 5,000 ha (Edson & Wing, 2011) to over 12,000 ha (Hummel et al., 2011) for a single acquisition. However, it can be very costly ($78,900 for ~12,000 ha acquisition (Hummel et al., 2011)) making it inaccessible for some land managers.

Recent miniaturization of sensors have allowed them to be deployed on small unmanned aerial vehicles (UAVs). Remote sensing with UAVs offers an efficient method for gathering information about forest characteristics. Similar to aerial- and satellite-based spectral remote sensing, UAVs equipped with spectral sensors are able to produce data that can be used to classify vegetation types and estimate canopy cover (Dunford et al., 2009; Makynen et al., 2011; Saari et al., 2011; Getzin et al., 2012; Sankey et al., 2017). Compared to the resolution of aerial images (1 m resolution) or satellite data (2 - 30 m resolution), imagery acquired from UAVs tends to have very high spatial resolution (15 cm) due to a lower altitude of acquisition and less atmospheric interference. The higher spatial resolution allows users to detect finer scale variability within images (Woodcock & Strahler, 1987), and may be more representative of the

actual target. Additionally, UAVs offer the ability to control the image acquisition process, timing, and obtain overlapping images to the users' specifications. If acquired with high-overlap, these images can be used with Structure-from-Motion (SfM) algorithms to produce 3D point cloud data similar to aerial lidar.

SfM is a photogrammetric method that allows users to create 3D models of a feature of interest (buildings, vegetation etc.) by using overlapping 2D images taken from a wide range of angles and perspectives. The concept behind SfM is similar to stereoscopic photogrammetry where users rely on the parallax between images to measure 3D structure. However, SfM can recreate feature geometry, camera position, and orientation through the use of computer algorithms and is not reliant on ground targets. SfM algorithms detect matching features in multiple, overlapping images and estimates the camera positions and feature geometry (Westoby et al., 2012). With this information, SfM can then generate a point cloud of the feature, similar to those generated with lidar. For some applications, SfM can provide an economical alternative to lidar (Morgenroth & Gomez, 2014). SfM produces the most accurate models when using images with high overlap and taken from many positions around the feature of interest. These images are best acquired from a moving platform that is able to take many images as it travels around the feature (Westoby et al., 2012). When conducted over forests, images taken from a UAV can be processed using SfM software to produce point clouds that represent both the ground surface and vegetation in 3D (Westoby et al., 2012; Dandois & Ellis, 2013). Using this method, remote sensing with UAVs offers an efficient method for gathering forest structure information.

A study was conducted in temperate deciduous forests across three sites in Maryland that produced high-density (14+ points/m^2), 3D point cloud data to derive forest canopy height estimations and compare them to field measurements. The first site was located on the University

of Maryland Baltimore County campus and contained a mixed-age of deciduous tree species including American beech (*Fagus grandifolia*), oak (*Quercus* spp.), hickory (*Carya* spp.), white ash (*Fraxinus americana*), and tulip-poplar (*Liriodenron tulipifera*). The second site contained similar forest composition as the first, however it included a riparian area that consisted of black locust (*Robinia pseudoacacia*), honey locust (*Gleditsia triacanthos*), and green ash (*Fraxinus pennsylvanica*). The third site was located at the Smithsonian Environmental Research Center (Maryland) and contained mostly tulip-poplar, American beech, and oak species. Aside from species composition, other forest metrics information was not given for this study. UAV-derived canopy height was strongly correlated to field measurements (R^2 = 0.86, RMSE = 3.6 m) (Dandois & Ellis, 2013; Dandois et al., 2015). A study in Tasmania, Australia compared UAV-derived canopy height and canopy cover to those estimated from aerial lidar and field measurements. This study was conducted in a dry sclerophyll eucalypt forest that was dominated by white peppermint (*Eucalyptus pulchella*). The entire study area was a 30 x 50 m rectangular plot and contained a range of tree density and canopy cover. Field measured canopy cover was 59%, UAV canopy cover was estimated to be 50%, and lidar canopy cover was estimated to be 63%. Field measured tree density was 907 trees per hectare (tph), and was estimated to be 747 tph with UAV data, and 813 tph from lidar data indicating 82% and 90% detection. UAV-derived tree height was positively correlated with field measurements (R^2 = 0.68, RMSE = 1.3 m), although lidar tree height estimates were more highly correlated to field measurements (R^2 = 0.84, RMSE = 0.92 m) (Wallace et al., 2016). In southeast Norway, another study used UAV imagery to estimate forest inventory metrics including tree heights, basal area, and stem volumes. The study area was across a 195 ha boreal forest that was mainly composed of Norway spruce and Scots pine (*Pinus syvestris*), and also included a small component of downy birch

(*Betula pubescens*). Although specific forest metrics for canopy cover and density are not given, a qualitative assessment of the sample UAV imagery of the study site shows conditions that appear relatively denser and more continuous canopy cover than the study area in the present study. The study estimated forest inventory metrics using UAV imagery, however ground points from aerial lidar were used to establish a digital elevation model (DEM) across the study area. When compared to field estimates, the UAV-derived estimates for Lorey's mean height, dominant height, stem numbers, basal area, and stem volume were measured with respective R^2 values of 0.71, 0.97, 0.60, 0.60, and 0.85 with RMSE values of 1.4 m, 0.7 m, 538.2 ha, 4.5 m^2/ha, and 38.3 m^3/ha (Puliti et al., 2015). In a study conducted in the Northern Territory, Australia, the authors used UAV imagery to delineate individual trees and estimate aboveground biomass. The study area was mainly composed of Darwin woollybutt (*Eucalyptus miniata*) and Darwin stringybark (*Eucalyptus tetrodonta*) and exhibited >30% canopy cover. When compared against aerial lidar-derived data, UAV-derived estimates were able to detect 70% of dominant or co-dominant trees, and 35% of suppressed trees. However, when compared to field-derived estimates, aboveground biomass estimates were relatively poor using UAV data (R^2 = 0.15) (Goldbergs et al., 2018). A study was conducted near Flagstaff, AZ that used UAV imagery to estimate individual tree heights, crown diameters, canopy cover, and tree density. The primary overstory tree species in this study was ponderosa pine which varied in tree density and canopy cover across the study area. The study area contained both an ecotone area and forest area. The ecotone area was described as the transition zone of shrubland-grassland meadow and ponderosa pine forest. The forest area contained primarily a ponderosa pine overstory and contained an untreated control site, and three treatment sites including a burn-only, thin-only, and a thin-and-burn. According to field measurements in the forest area, the control site had the highest mean

canopy cover (50%) and tree density (3.5 trees/100 m^2). In descending order this was followed by the burn-only site with 43% canopy cover and 2.7 trees/100m^2, the thin-only site with 33.8% canopy cover and 1.3 trees/100m^2, and the thin-and-burn site with 21.8% canopy cover and 1 tree/100m^2. Across the study area, UAV-derived canopy cover estimates were highly correlated to field measurements (R^2 = 0.74, RMSE = 8.5%). Tree height estimates had an R^2 of 0.93 (RMSE = 1.5 m) in the less dense ecotone area, and R^2 of 0.64 (RMSE = 2.9 m) in more dense forest areas. Crown diameter estimates had an R^2 of 0.66 (RMSE = 0.72) in the ecotone area, and R^2 of 0.70 (RMSE = 1.9 m) in the forest area. However, the individual tree delineation showed a weaker correlation in both the ecotone and forest areas (R^2 = 0.36, RMSE = 0.83 trees/100 m^2 and R^2 = 0.53, RMSE = 2.2 trees/100 m^2 respectively) (Sankey et al., 2017). The forested area found in the study conducted by Sankey et al (2017) represented the most comparable site characteristics to those found in our study area. Therefore, we expect similar results for our estimations of canopy cover, tree heights, and individual tree delineation. At the time of this study, no previous literature has used UAV-SfM methods to estimate canopy base height or canopy bulk density.

With modern advances in UAV platforms, sensor capabilities, and SfM computer vision algorithms, UAV SfM is becoming a potential economical alternative to aerial lidar for some applications (Dandois & Ellis, 2013; Morgenroth & Gomez, 2014; Dandois et al., 2015; Puliti et al., 2015; Jensen & Mathews, 2016; Wallace et al., 2016). Currently, UAV SfM has a smaller footprint than aerial lidar, but it is often higher in resolution (10+ points/m^2 (Dandois et al., 2015)) due to the interpolated nature of the points. Additionally, the lower cost allows a higher frequency of surveys and gives the user the option to survey a small area (40-120 hectares) without paying for an aerial lidar acquisition that is often not economically justifiable to obtain at

this scale. Relative to the cost of aerial lidar acquisitions, the cost of UAV SfM equipment (roughly around $30,000 for UAV and sensor) makes it possible for landowners to purchase their own and conduct surveys as needed. When compared to field surveys, UAVs can offer more comprehensive coverage and a less human-biased assessment of forest structure characteristics. The average cost to conduct fixed-radius forest inventory is $104-180/plot (Hummel et al., 2011) and field-based survey is often implemented at a sampling frequency of one plot for every 2-3 ha. UAV surveys can potentially be cheaper, thus being an easier method for land managers to conduct more frequently (Puliti et al., 2015) leading to adaptive management opportunities and more informed decision-making.

Objectives

The overall objective of this project is to use UAV imagery and SfM method to estimate forest canopy fuels and estimate crown fire behavior. Specific objectives include the following:

1. Test and quantify UAV SfM capabilities in measuring forest structure in the FWPP area:
    a. Estimate canopy cover in 10 m cells using orthomosaic images from the UAV
    b. Delineate individual trees by segmenting the UAV SfM-derived point cloud to estimate tree density in 10 m cells and estimate for each individual tree: total tree height, canopy base height, and canopy bulk density.
2. When the above variables are reasonably accurately derived, estimate the following variables in 10 m cells using the UAV data: elevation (m), slope (degrees), aspect (azimuth), total canopy cover (%), mean canopy height (m), mean canopy base height (m), and mean canopy bulk density (kg/m^3) for use in FlamMap software for fire behavior modeling.

3. Conduct sensitivity analysis in FlamMap using each UAV-derived raster variable individually to determine the effects of these variables on modeled potential crown fire behavior.

Hypotheses

1. UAV images can be used to accurately estimate canopy cover in 10 m cells.
2. Detection of individual trees from UAV SfM will decrease with increasing tree density.
3. UAV-derived estimates of total tree heights for individual trees will be accurate when compared to field measurements.
4. UAV-derived individual tree canopy base height will have relatively lower accuracies, since below-canopy variables are challenging to detect with SfM-derived 3D data.
5. If canopy base height cannot be reliably estimated, canopy bulk density estimates will not be accurate, since it is directly related to canopy base height estimates.
6. Due to the finer spatial resolution, UAV-derived crown fire behavior models will show more spatial variation than LANDFIRE-derived models leading to varying estimates of forest fire behavior.

Implications of Research

UAV-derived imagery can produce high spatial resolution data that can be used to more accurately and cost-efficiently represent forest fuels. These data could offer a fuels measurement method that is more efficient than field surveys and potentially more accurate with less bias introduced by the observer. By supplementing, or replacing, LANDFIRE data (30 m spatial resolution, 2-5 year temporal resolution) forest fuels can be assessed at a fine- to mid-scale giving land managers the ability to conduct more precise and targeted treatments and monitoring. UAVs also have the added benefit of being relatively less costly and more repeatable than other

methods. Thus, UAVs can also provide land managers with a means to perform rapid assessments of fuels treatments. This would make it possible for managers to prioritize treatments, calibrate ongoing treatments, and conduct responsive adaptive management. The results of our project can be used to assist forest land managers with integrating UAV technology in their future land management activities, potentially increasing efficiency of fuels reduction treatments.

Chapter 2 Methods

Study Area Description

This study focused on a 12.14 ha area located about 3 km northeast of downtown Flagstaff, AZ and about 0.5 km north of Buffalo Park, a park owned and managed by the City of Flagstaff (Figure 1). The study area is under Coconino National Forest land ownership and is within the wildland-urban interface of Flagstaff, AZ. It is within 200 m from the nearest residential structure. Due to the close proximity to residential structures, the City of Flagstaff has identified this area as a high priority for treatment and has planned it to be mechanically thinned as part of Phase 1 FWPP in 2017. Phase 2 is located north of Phase 1 on Coconino National Forest ownership and includes operationally complex thinning areas mostly due to steep slopes. Phase 2 is planned to include helicopter and skyline cable harvesting techniques and planned to be treated in future years. The final treatment area, Phase 3, is located about 25 km southeast of Flagstaff in the Mormon Mountain area.

The elevation of the study area ranges from 2,158 to 2,188 meters above sea level with a southwest aspect of 0-10 degrees slope. The Flagstaff Pulliam Airport weather station is about 20 km south of the study area and provides the most representative climate data. Annual records from this station between 1981 and 2010 include a mean annual precipitation of 55.5 cm, which

predominantly occurs during summer monsoon events and winter snowfall, and a mean annual temperature of 7.9° C, with a mean low temperature of 0.1° C, and a mean high temperature of 16.0° C. On average the coolest month is December with an average temperature of -1.3° C, whereas July is the warmest month with an average temperature of 18.9° C (National Oceanic and Atmospheric Administration, n.d.).

The dominant overstory vegetation type is ponderosa pine (*Pinus ponderosa*) forest with a small Gambel oak (*Quercus gambelii*) component. Native understory vegetation is primarily comprised of Arizona fescue (*Festuca arizonica*), bottlebrush squirreltail (*Elymus elymoides*), mountain muhly (*Muhlenbergia montana*), and Fendler's ceanothus (*Ceanothus fendleri*). Common invasive species in this area include Dalmatian toadflax (*Linaria dalmatica*), common mullein (*Verbascum thapsus*), and cheatgrass (*Bromus tectorum*).

The climate, vegetation, and soils of the study area are similar to those found in most of the forested areas that surround the City of Flagstaff. Forests with similar characteristics are also commonly found across northern Arizona among ponderosa pine forests of comparable elevation ranges. According to the Natural Resources Conservation Service (NRCS) Web Soil Survey tool, the study area contains Baldy stony loam soils, which have a rhyolite parent material, are well-drained, and have a medium runoff potential (Natural Resources Conservation Service, 2017).

The area surrounding the study area is a popular location for recreationists, specifically hikers and mountain bikers. Although the area only contains one sanctioned trail, the Pipeline Trail No 42 (Coconino National Forest, n.d.a.), there are numerous unsanctioned social trails that have been developed over time, most likely due to the close proximity to residential areas. Most recent management activity in the study area occurred in 2016 when a noxious weed treatment was implemented on approximately 0.73 ha. The study area has not seen any timber harvesting

between 1970 and present. However, there is evidence of historical logging activity in the form of historical cut stumps. In 1998, there was one wildfire within the study area that was documented to be human caused and less than 4 ha in size in the southernmost end of the study area. The southwest perimeter of the Radio Fire of 1977 (1800 ha in size) is about 1.5 km due east, and the southern boundary of the Schultz Fire of 2010 (6000 ha in size) is about 4.2 km due north of the study area (Coconino National Forest, n.d.b).

Data Collection

Site Selection

The FWPP Phase 1 area was examined using ArcMap 10.4 software (ESRI, 2015) to locate areas for potential UAV surveys. Adequate take-off and landing space to safely implement UAV flights proved to be the most limiting factor in site selection. The study area was chosen due to its operational feasibility for UAV use. After identifying an appropriate study area, two UAV surveys were planned: Flight 1 and Flight 2. Although the flights are in close proximity to one another, the areas do not overlap and are about 60 m apart.

UAV Platform and Sensor

This study utilized a SenseFly eBee fixed-wing UAV platform (Figure 6). The eBee aircraft weighs approximately 537 g with no payload, has a maximum takeoff weight of 750 g, and a wingspan of 96 cm (Puliti et al., 2015; Sankey et al., 2017). The eBee has a cruising speed of 40-90 km/h, maximum flight duration of 50 minutes, and maximum flight coverage of 12 km^2 under optimal conditions (SenseFly, n.d.a.). The eBee is launched by hand and lands by reducing speed and altitude until it "belly lands" (Sankey et al., 2017). The eBee operates with eMotion 2, a custom flight planning software package (SenseFly, n.d.b). In this study, this software was used to develop the flight mission plan and carry out the mission. A Microsoft Surface™ tablet was

used to run the eMotion 2 software and the ground station. The eBee performed an autonomous flight on the planned flightpath, collected images at preset intervals, and returned to the landing area.

The eBee UAV was equipped with an Airinov Multispec 4C multispectral sensor. The sensor collected images in four different spectral bands via four separate lenses (Figure 6). These wavelengths are centered at green (550 nm), red (660 nm), red edge (735 nm), and near-infrared (790 nm).

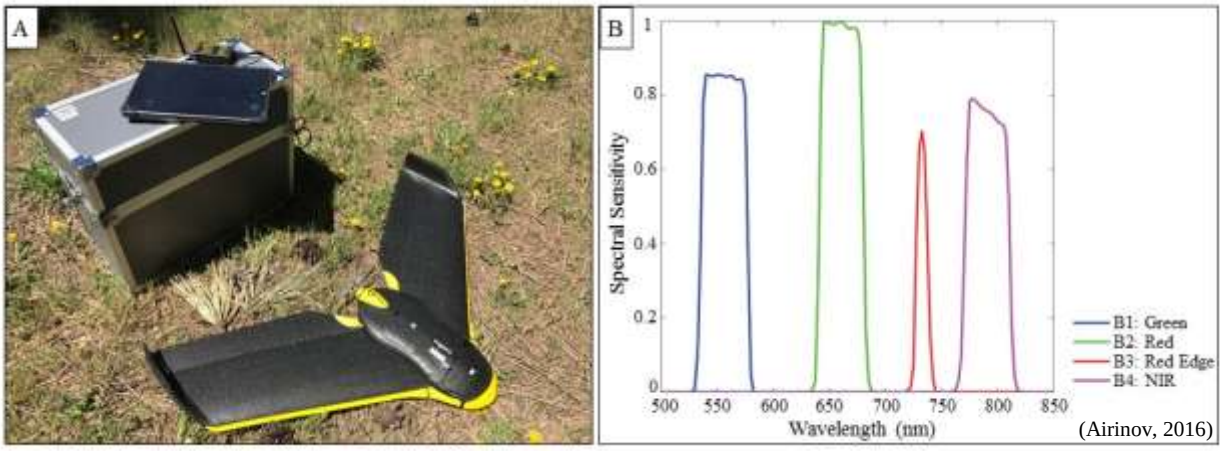

Figure 6: The eBee fixed-wing UAV with the Microsoft Surface tablet used for flight planning and operation (Panel A) and the spectral bands of the Airinov Multispec 4C sensor used aboard the UAV (Panel B). Bands 1 through 4 respectively are the green, red, red edge, and near infrared wavelengths. They have corresponding mean wavelengths of 550 nm, 660 nm, 735 nm, and 790 nm.

UAV Image Acquisition

Flight 1 was completed on August 21, 2016 and Flight 2 on November 22, 2016. Both surveys were conducted with 85-90% latitudinal and longitudinal overlap, respectively, at a maximum flight altitude of 120 m. This flight altitude resulted in pixel resolution of 15 cm. Both flights were performed close to solar noon to minimize shadowing. Flight 1 lasted for 15 minutes

resulting in 960 individual images taken (240 images x 4 bands). Perpendicular flight lines were planned for both flights to maximize the number of images collected and to achieve higher image overlap. However, Flight 1 only obtained perpendicular flight lines for approximately half of its survey area before landing due to impending weather. Flight 2 was successful at acquiring perpendicular flight lines for its entire survey area. Flight 2 took 22 minutes to complete and acquired a total of 1,828 individual images (457 images x 4 bands).

Field Validation Data Collection

Field measurements were designed to provide a validation dataset for the forest characteristics and individual tree measurements derived from the UAV data. Two specific forest stand-level variables that required validation data were: tree canopy cover and tree density. In this study, both of these variables were estimated in 10 x 10 m cells (100 m^2). Additionally, within each plot individual trees were measured to provide a validation dataset for UAV-derived individual tree measurements.

Using ArcMap 10.4 software (ESRI, 2015) along with polygons of the study areas imaged with the UAV, field plot locations were chosen by first overlaying a 10 m grid across both flight polygons to produce the 10x10 m grid cells. Within this grid, 100 non-adjacent cells with a minimum distance of 10 m (one cell) between cells were randomly chosen. An initial tree density (trees/cell) for each random cell was visually estimated by examining the high-resolution (~15 cm) orthomosaic image from the UAV surveys. Field sampling was then stratified by tree density with a goal of sampling 10 cells with a density of 1, 2, 3, and 4 trees/cell. The study area contained only a few areas of higher tree density, but the desired goal of this study was to measure and evaluate tree canopy cover and tree density estimates across the entire possible range of tree densities. I, therefore, actively sought and located at least 5 cells with 5, 6, and 7

trees/cell, respectively (Table 3). The sampling goal was achieved at all density levels with a total 57 plots distributed across the study area.

Table 3: Distribution of the field samples. Field sampling was stratified by tree density to collect individual tree measurements in areas of varying density. The sampling goal was to measure 10 cells with a density of 1, 2, 3, and 4 trees/cell, and 5 cells with a density of 5, 6, and 7 trees/cell. The sampling goal was met at all densities.

Tree Density (trees/cell)	Sampling Goal (cells)	Actual Measured (cells)
1	10	12
2	10	10
3	10	10
4	10	10
5	5	5
6	5	5
7	5	5
Total	55	57

Once the final plot locations were identified, an iPad tablet was connected to a Bad Elf GPS PRO and used to navigate to each plot location. Although the tablet was equipped with a GPS, the tree location was based on the UAV-derived georeferenced orthomosaic image (see "UAV Image Pre-Processing"), which was used as a basemap in Avenza Maps software. I navigated to the four corners of each plot to match the locations of the field plots with the 10 m cells derived in ArcMap 10.4. Plot boundaries were then delineated and trees were determined to be either in or out of the plot based on their canopy position on the orthomosaic map. At each plot, the GPS location of each tree was digitized on the orthomosaic map. For the purpose of this study, the recorded tree locations were relative to the orthomosaic map and not true locations on the ground. However, this procedure ensured that the exact matching area and individual trees

were examined in both the field plots and UAV images, and also eliminated the need for high-precision GPS and correcting for GPS errors.

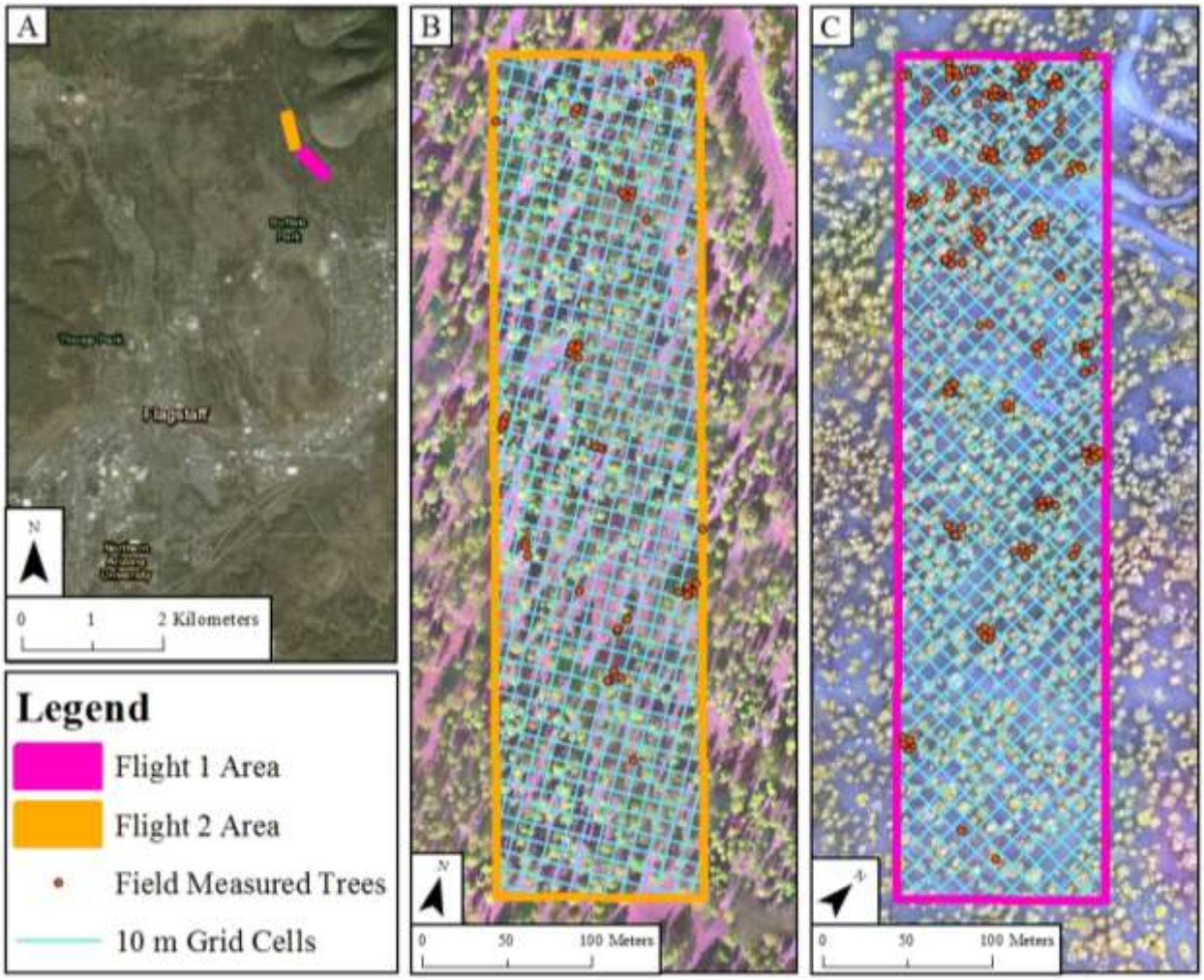

Figure 7: Map of study area with field sampling points. General vicinity of the study area with the two flight areas and their proximity to the City of Flagstaff (Panel A). Flight 2 Area with a 10 m grid and locations of field measured trees (Panel B). Flight 1 Area with a 10 m grid and locations of field measured trees (Panel C).

The following measurements were then recorded for each tree: species, DBH, canopy diameter in the North-South axis, canopy diameter in the East-West axis, tree height, and canopy base height. The DBH was measured using a diameter tape at a height of 1.37 m on the upslope side of the tree. Canopy diameter was measured using a Leica DISTO E7500i laser rangefinder

in both the North-South and East-West axes, which were determined using a Suunto MC2 compass with 10° E magnetic declination adjustment. Canopy height and canopy base height were measured by using the laser rangefinder to determine horizontal distance to the tree, and a Suunto PM-5 clinometer to measure the angles to tree base, canopy top, and canopy base. Canopy base was the lowest point of continuous canopy. The distance and angle measurements were then used to calculate tree height and canopy base height. Canopy bulk density was calculated by first estimating canopy mass using DBH and allometric equations (eq. 1, 2, 3) by Kaye et al. (2005). The canopy volume was then calculated using the average canopy radius, overall tree height, and canopy base height, and assuming a cylindrical canopy model (eq. 4). Crown mass was divided by crown volume to estimate a crown bulk density for each tree (eq. 5).

$$Mass\ of\ Live\ Branch\ Wood\ and\ Bark\ (kg) = 1.0425e^{-6.0278+\ln(dbh)\times 2.8655} \quad \text{eq. 1}$$

$$Mass\ of\ Dead\ branch\ wood\ and\ bark\ (kg) = 1.1322e^{-5.3589+\ln(dbh)\times 2.250} \quad \text{eq. 2}$$

$$Mass\ of\ Foliage\ (kg) = 1.0672e^{-4.1317+\ln(dbh)\times 2.0159} \quad \text{eq. 3}$$

$$Canopy\ Volume = [\pi\ (avg.canopy\ radius)^2] \times (tree\ height - canopy\ base\ height) \quad \text{eq. 4}$$

$$Canopy\ Bulk\ Density = \frac{Sum\ of\ Canopy\ Mass}{Canopy\ Volume} \quad \text{eq. 5}$$

The individual tree measurements were appended as attributes to the GPS coordinates corresponding to each tree location. The resulting spatial data represents the location of each tree

with the associated attributes and was used as a validation dataset for the UAV-derived individual tree measurements.

UAV Image Pre-Processing

Following the UAV survey flights, the acquired images and flight logs were retrieved from the UAV. These files were then processed using Pix4D (Pix4D, Switzerland) to create a single orthomosaic image and 3D point cloud of each of the surveyed areas. The MultiSpec 4C sensor captures images in four bands through four separate cameras. The Pix4D software effectively coregisters and merges these images together to create an orthomosaic for each band. These four orthomosaics were then spectrally stacked with ENVI 5.3 (Harris Geospatial Solutions) to produce one four-band orthomosaic for each flight area. The edges of the resulting orthomosaic images were heavily distorted due to lack of image overlap. Therefore, the original flight polygons were used to spatially subset the orthomosaic images and remove the distorted areas. The resulting orthomosaic images for both flight areas were 15 cm in spatial resolution and contained four separate bands (green, red, red edge, and NIR).

Similar to the orthomosaic images, the Pix4D software creates lidar-like, 3D point cloud data for each spectral band via the photogrammetric method known as Structure-from-Motion (SfM). These point clouds were merged using CloudCompare to create a single point cloud file with a high point density for each flight area. The point cloud data were then spatially subset to the same area as the orthomosaic images. The point cloud for Flight 2 contained a few areas with spurious points that were well below the ground. The Statistical Outlier Removal tool in CloudCompare was used to remove outliers that were outside one standard deviation from any group of six points. This process effectively removed extraneous points below the ground

without removing desirable points. The average point densities for the point clouds were 32 points/m^2 and 56 points/m^2 for Flights 1 and 2, respectively.

Deriving Forest Measurements

Canopy Cover from UAV imagery

UAV canopy cover was primarily derived using the orthomosaic images and a normalized difference vegetation index (NDVI)-based segmentation method. The orthomosaic image for each flight were used in ENVI 5.3 software where the Band Math tool was used to create an NDVI raster with the following equation (eq. 6):

$$NDVI = \frac{(NIR - Red\ Edge)}{(NIR + Red\ Edge)} \quad \text{(eq. 6)}$$

Preliminary testing showed that using the NIR & Red Edge band combination generated a better NDVI raster than the NIR & Red band combination. Additionally, all values were converted to a floating point data type for the band math operation. After the NDVI raster was generated, the Segmentation Image tool was used to classify canopy pixels by setting a minimum and maximum NDVI value threshold, and a population minimum. These parameters define the criteria for the canopy classification (Table 4). A pixel that meets the minimum and maximum thresholds, and has enough qualifying pixels surrounding it to meet the population minimum were classified as areas of crown.

Table 4: Parameters used in the ENVI Image Segmentation tool for UAV and NAIP canopy cover estimates. The minimum population used for NAIP data was significantly less than UAV due to the large (1 m) resolution relative to the UAV data (15 cm).

Parameter name	UAV Flight 1	UAV Flight 2	NAIP
Minimum Threshold:	0.1	0.1	0.15
Maximum Threshold:	1	1	1
Population Minimum:	100	100	4
Neighbor Rule:	8	8	8

The resulting raster classified areas of tree canopy and assigned them with unique object ID numbers. A band math equation was then applied to create a binary canopy raster in which all trees were assigned a value of 1, whereas all other pixels had a value of 0. This raster was then exported from ENVI as a .tif file and imported in R software. The binary canopy raster was overlaid on a canopy height model raster to remove all canopy pixels with a tree canopy height of less than 1.37 m. Within R (R Development Core Team 2008), and using the *raster* package, the point cloud for each flight was imported and canopy height models were produced. This canopy height model (CHM) was then used to create a raster to identify all values less than 1.37 m. This process effectively removed areas of high NDVI and low canopy height (eg. herbaceous vegetation) to produce a canopy raster more representative of only tree canopy. This raster was then resampled to 20 cm resolution, for an even fit into a 10 m cell, and imported to ArcMap 10.4 where it was converted from a binary canopy raster into a 10 m percent canopy cover feature (Figure 8).

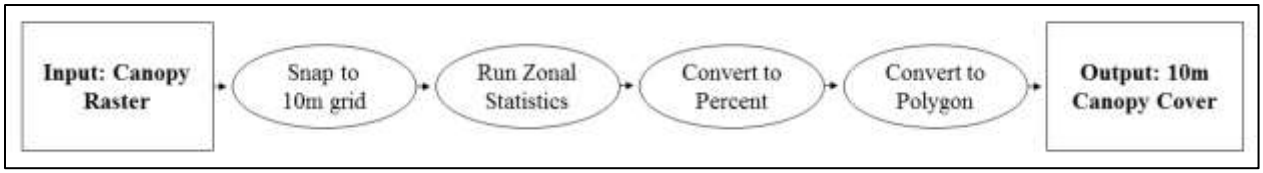

Figure 8: Canopy cover processing workflow. Process used to convert the binary canopy raster to summarize canopy percent cover in a 10 m cell.

To summarize the binary canopy cover raster to tree canopy percent cover estimates in 10 m cells, the input raster was first snapped to match the desired 10 m grid. The zonal statistics tool was then run to summarize the number of canopy pixels within every 10 m grid cell. This sum was then converted to a percent by dividing by the total number of input raster cells (N=2,500) in the 10 m grid. The resulting raster was converted to a polygon for comparison with the other data types. The same process for both the UAV and National Agriculture Imagery Program (NAIP) data was used to convert the canopy raster into a 10 m canopy cover feature. However, the total number of raster cells in a 10 m grid cell was 100 to reflect the resolution of the NAIP imagery (1 m).

Canopy Cover Estimate Validation

The UAV image-derived canopy cover estimates were validated using two different independent image sources and field-based canopy cover estimation. First, the National Agriculture Imagery Program (NAIP) image was used for validating the UAV-derived canopy cover estimates in 10 m cells. NAIP is a program through the United States Department of Agriculture (USDA) Farm Service Agency that acquires aerial imagery every 3-5 years. NAIP imagery has a spatial resolution of 1 m and four spectral bands (R, G, B, NIR). For this study, NAIP imagery was acquired by accessing the NAIP server through ArcMap 10.4. Tiles overlapping the study area were selected and then spatially subset to the general study area vicinity.

A similar workflow to the UAV processing was used to estimate canopy cover from NAIP imagery. An NDVI-based segmentation image was created in ENVI 5.3 with the parameters in Table 4 and used create a binary canopy raster. The binary raster was then summarized into tree canopy percent cover estimates in 10 m grids. A pixel-wise regression analysis was used to compare the tree canopy cover estimates from the UAV image classification and NAIP data.

In 2014, the USDA Farm Service Agency acquired imagery similar to NAIP in an area that included our study area. This imagery was acquired using higher specifications than traditional NAIP imagery that resulted in 0.3 m spatial resolution imagery, with four spectral bands (R, G, B, NIR), across a 495,699 ha area of the Coconino and Kaibab National Forests in northern Arizona. Zachmann and Dickson (2017) used this imagery to classify tree canopy at a 0.3 m spatial resolution. During their model evaluation using 621 test samples, the canopy classification had a 98% producer's accuracy (Zachmann & Dickson, 2017). For this study, the Zachmann and Dickson (2017) canopy data provided a relatively high resolution canopy cover raster for comparison and was used as a second validation source. The Zachmann and Dickson (2017) canopy raster was first resampled to 25 cm, using nearest neighbor resampling, to ensure a "perfect fit" into the 10 m grid cells. A pixel-wise regression analysis was conducted between the 10 m canopy cover from the UAV image classification and Zachmann and Dickson (2017) data sources.

Field measurements for canopy diameter were used to calculate an average canopy radius. This canopy radius was then used to create a buffer around each field measured tree location. All field-based tree canopies were combined in ArcMap to estimate canopy cover within each field plot and compared to UAV image-derived estimates.

The primary statistics from the canopy cover regression analyses that were used to assess the correlation between datasets was the adjusted R^2 correlation coefficient and the root mean squared error (RMSE). In order to compare datasets of varying scales, a normalization procedure can be applied to the RMSE by utilizing differences in overall dataset ranges, interquartile ranges, or the coefficient of variation within datasets. However, since all canopy cover data were resampled to percent canopy cover within a 10 x 10 m cell, the datasets shared a common spatial scale and this procedure was not required to make a valid statistical comparison.

UAV image-derived Tree Density Estimates

Tree density estimate was derived by summarizing the number of trees mapped within each field plot. Due to the stratification scheme in field sampling, tree density ranged from 1 to 7 trees per 100 m^2 plot (Table 3). To estimate tree density in the UAV image, the UAV-derived canopy cover estimates for each plot were first used to examine the relationship between canopy and tree density and determine whether tree canopy cover can be used as a predictor variable for tree density estimates. This relationship was analyzed using an ANOVA test with multiple pairwise comparisons, in which the plots were binned into tree density classes along with their corresponding canopy cover values. Statistically significant differences in canopy cover values among the density classes, if observed, might be used as indicators of tree density classes.

Landscape metrics from UAV Canopy Cover

The binary canopy and non-canopy raster (20 cm resolution) from the UAV data was first edited to change the value of all non-canopy pixels from 0 to NA. This effectively gives the canopy raster a single class of "canopy." This raster was then used as an input to FRAGSTATS 4 software (McGarigal, 2012) to calculate the following landscape metrics: number of patches, largest patch index, mean area of a patch, and standard deviation of patch area. All metrics were

calculated using an 8 neighbor rule. The number of patches is simply the number of individual patches that were identified using the 8 neighbor rule. Largest patch index is percentage of the total landscape that is occupied by the largest identified patch. Mean area of a patch is the average area of all patches (reported in square meters). Standard deviation of patch area is the standard deviation between all patch areas (reported in square meters).

Individual Tree Segmentation

Point cloud processing and individual tree segmentation was performed using the lidR package in R statistical analysis software, which contains functions that implement various point cloud processing methods for forestry applications. A progressive morphological filter (Zhang et al 2003) was first used to classify ground points in the point clouds. A digital terrain model (DTM) was then created using the points classified as ground. The DTM values were then subtracted from the point cloud Z values to create a normalized point cloud that effectively converts Z values from meters above sea level to meters above ground. This point cloud normalization is a common pre-processing procedure for individual tree segmentation with point cloud data (W. Li et al., 2012; Wallace, Musk et al., 2014; Wallace, Lucieer et al., 2014; Puliti et al., 2015; Iizuka et al., 2018). The UAV SfM-derived point clouds contained an abnormal amount of "noise" points that were a few meters above the ground surface, but represented neither ground nor vegetation. To remove these points and avoid falsely classified points as trees, two novel methods were used. First, by applying a second progressive morphological ground filter with a higher maximum threshold height (4 m), a larger number of these points were classified as ground points and therefore excluded during tree segmentation. Second, the point clouds were colorized using the NDVI raster generated from the orthomosaic images. This allowed all points with a NDVI value less than 0 to be filtered and ignored during tree segmentation. Applying

these steps generated a point cloud that best represented only tree points which were then used in the tree segmentation algorithm (Figure 9).

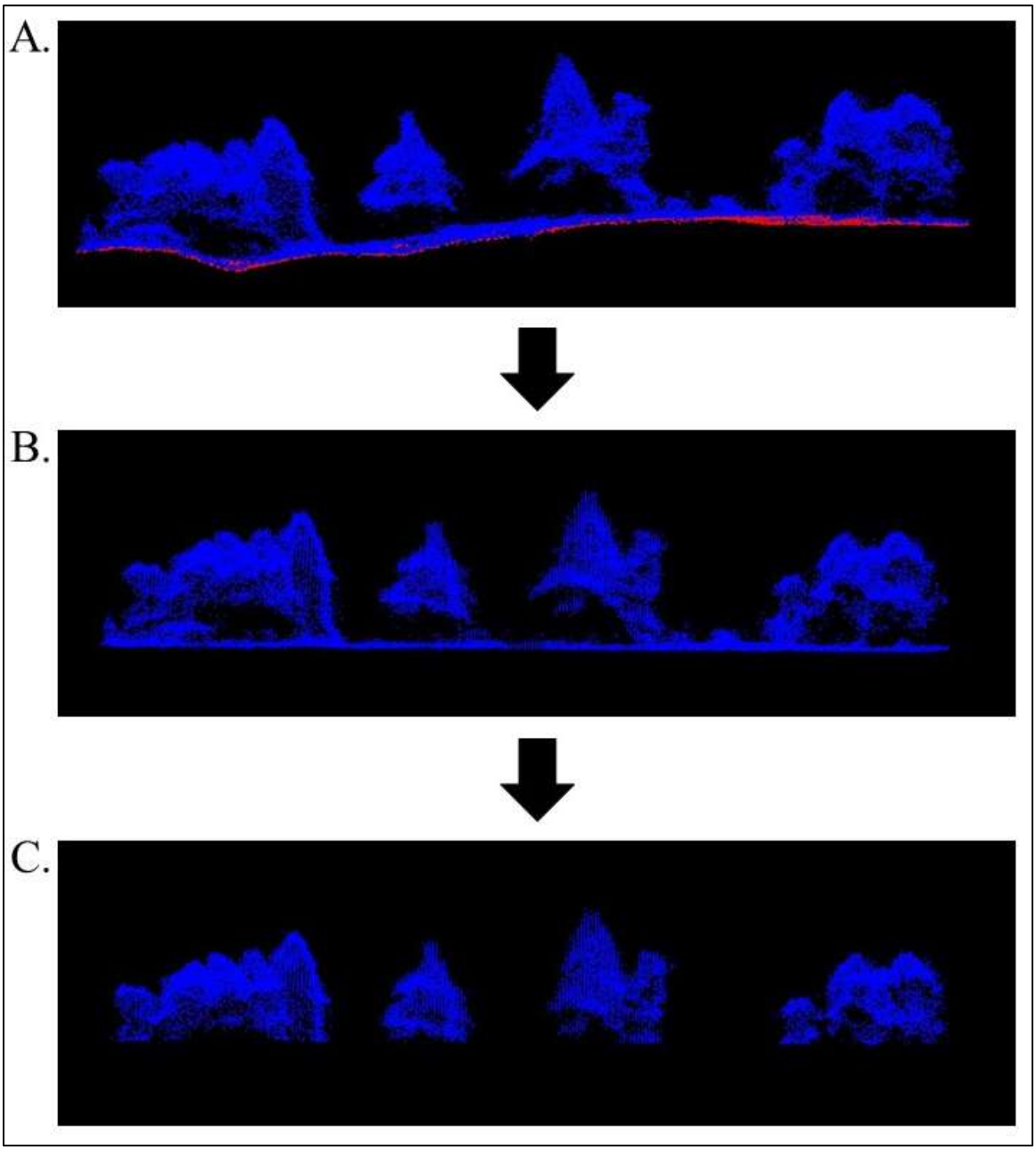

Figure 9: Point cloud preparation for tree segmentation. Side profile views of the same point cloud subset at different stages of processing. Point cloud with initial ground classification (Panel A). The ground points are displayed in red and were used to create a digital terrain model (DTM). Point cloud that has been normalized and ground points removed (Panel B). However, some non-tree points still remain. Point cloud after the second ground filtering and NDVI

threshold have been applied (Panel C). The final point cloud was deemed the most representative of tree-only points and was then used in the tree segmentation algorithm.

The lidR package in R contains several tree segmentation algorithms, most of which are based on canopy height models (CHM). Three of these algorithms were used during preliminary testing: watershed method (Oles et al., 2018), Dalponte method (Dalponte and Coomes, 2016), and Li method (Li et al., 2012). Both the watershed and Dalponte methods are CHM-based, where the user generates a CHM and the tree segmentation is implemented on the CHM raster. The resulting output is used to overlay on the point cloud and assign unique tree identifications to each segmented tree. The watershed method inverts the CHM surface and performs a watershed analysis to determine catchment areas that are then segmented as individual trees (Oles et al., 2018). The Dalponte method uses the CHM and utilizes a decision tree method to grow trees around local maxima in the point cloud (Dalponte and Coomes, 2016). The Li method is the only point-based method implemented by lidR. This method segments trees by analyzing points from tree top to bottom and using the horizontal distance between points to determine if they are part of the tree (Li et al., 2012). During preliminary testing of these three methods, the Li method was chosen as the most effective method for detecting individual trees without over-segmentation.

The Li segmentation used in this study relies on four parameters that are user defined. First, the minimum height of a tree (measured in meters) is set as "hmin," and the maximum crown radius (also measured in meters) is defined as "R." Last, two numeric distance (measured in meters) thresholds are set as "dt1" and "dt2." The function of dt1 and dt2 are to provide a horizontal distance threshold between points for all points above 15 m in height, and below 15 m in height, respectively.

For this study, a minimum tree height of 2 m, and a maximum canopy diameter of 7 m, were deemed appropriate by examining the field-based tree measurements. There were no trees below 2 m in height and no canopies greater than 7 m in diameter in the field data. Although both dt1 and dt2 are used in the Li algorithm, in order to isolate the effects of dt1 and dt2 differences, and limit the possible combinations and iterations in this study, these parameters were run with equal values during each iteration. Both dt1 and dt2 are, hereafter, referred to as "DT". In general, a low DT value results in over-segmentation with many additional trees identified in the point cloud, whereas a high DT value causes under-segmentation, where many tree canopies are merged together into single large canopies. The DT value is site specific and should be defined by the user to best suit their area (Li et al., 2012). In this study, 16 different iterations of the Li segmentation were run with varying DT values.

Tree Detection and Density Estimate Validation

Following the tree segmentation, a shapefile was created that contained the locations of the center of each individual tree. The UAV SfM point cloud-derived trees were first overlaid with the 10x10 m grid to count all trees detected within each cell and then compared to the field-mapped trees to validate and assess the accuracy of the tree segmentation and rates of tree detection. The UAV-derived trees were first spatially joined to the field-mapped tree points. Joining rules were then used to ensure only one-to-one joins. Joining rules were as follows: 1) a join can only occur if the UAV-derived tree is within the crown radius of the field tree; and 2) if there is more than one UAV-derived tree within the crown radius of the field-mapped tree, the closer point maintains the join. This tree detection scheme was used to quantify true positive detection and false negatives (omissions). False positives (commissions) were calculated by

summing the number of UAV point cloud-derived trees within the 10x10m plots that were not matched and joined to a field-mapped tree.

Tree segmentation using the Li method with constant parameters across the entire study area yields different results in areas of higher tree density versus areas of lower tree density. Assuming a linear relationship between tree density and canopy cover, an "optimized" version of the Li segmentation was developed by using tree points from different segmentation iterations based on the above described estimates of canopy cover distribution across my study area. Using the tree canopy cover estimates, I classified my study area into sections of high canopy cover and low canopy cover. In areas of >50% canopy cover, the tree points from a lower DT value iteration were used, and in areas of < 50% canopy cover the tree points from a higher DT value iteration were used.

The combination of true positive, false negatives, and false positives were used to assess each tree segmentation iteration. Validation metrics included recall (r), precision (p), and F-score (F) which were calculated using the following equations (eq. 5, 6, and 7) (Goutte and Gaussier, 2005, Li et al., 2012):

$$r = \frac{True\ Positives}{(True\ Positives + False\ Negatives)} \quad \text{(eq. 5)}$$

$$p = \frac{True\ Positives}{(True\ Positives + False\ Positives)} \quad \text{(eq. 6)}$$

$$F = 2 \times \frac{(r \times p)}{(r + p)} \quad \text{(eq. 7)}$$

The iteration yielding the highest scores represents the best UAV-derived estimate of tree density in this study and was, therefore, used as the final model. This analysis was completed on the

entire study area, and also by grouping plots by their density classes, to determine the effect of tree density on tree detection.

Additionally, ANOVA analysis with multiple comparisons was conducted to compare the UAV point cloud-derived trees with the field-mapped trees to determine if a statistically significant different number of trees were detected between the UAV point cloud data and field-based measurements within each density class.

Individual Tree Metrics

The individual tree measurements derived from the UAV data included the following metrics derived from the point cloud data: total points, tree top coordinates, canopy diameter (north-to-south), canopy diameter (east to west), height max, height min, height mean, height median, height mode, height variance, height standard deviation, height coefficient of variation, height kurtosis, height skewness, and percentile heights (ranging from 5 to 99 in 5 meter increments). Some of these metrics were then used to estimate the final set of individual tree measurements: location, canopy height, canopy base height, and canopy bulk density. These tree metrics were compared to the corresponding field-mapped tree and its associated field measurements for validation: tree height, base height, and canopy bulk density. To estimate canopy base height and canopy bulk density, I explored several possible UAV-derived predictor variables. For canopy base height, these predictor variables included the height percentiles of each segmented tree, as well as the height to crown diameter ratio. Estimates for canopy bulk density involved first establishing a tree height to diameter at breast height (DBH) relationship. This relationship was used to predict tree DBH with the UAV-derived tree height. The predicted DBHs were then used in northern Arizona-specific allometric equations (eq. 1, 2, 3) for ponderosa pine (Kaye et al., 2005) to estimate the canopy mass of each tree. The UAV-derived overall tree height, average

canopy radius, and canopy base height were then used to estimate canopy volume assuming a cylindrical canopy model. Canopy mass was then divided by canopy volume to estimate the canopy bulk density. This process for estimating canopy bulk density directly mirrors the steps used with the field measurements to estimate bulk density. Linear regression models then were used to examine the relationships between the UAV-derived and field-measured variables. A bootstrap resampling analysis (subsample= 100; iterations= 100,000) was conducted with the UAV tree height measurement errors to determine the mean error with a 90% confidence interval.

Fire Behavior Modeling

The Landscape Fire and Resource Management Planning Tools (LANDFIRE) is a multi-agency program with the goal to provide seamless geospatial data products across the entire United States. LANDFIRE provides 27 different data products across 7 categories which include: reference, disturbance, vegetation, fuel, fire regime, topographic, and seasonal. The purpose of these products are to support interagency planning, management, and operations (LANDFIRE n.d.). For this study, only the fuel and topography data were used.

The LANDFIRE spatial fuels data products include total percent canopy cover in 30 m cells, the mean canopy height, the mean canopy base height, total canopy bulk density, mean topographic elevation, mean topographic slope and aspect, and total fuel model. These products are derived using three categories of spatial data: satellite imagery, biophysical gradients, and vegetation structure and composition. Within these categories, 40 different predictor variables are used to derive spatial fuels data in 30 m spatial resolution (Appendix A). These predictor variables include biophysical gradient data such as annual precipitation, temperature, evaporation, evapotranspiration, and others. Vegetation type data are also used in LANDFIRE as

predictor variables for fuels products. Other predictor variables used by LANDFIRE include multispectral imagery from Landsat ETM.

Land managers typically use spatial fuels data from LANDFIRE with FlamMap 5 software (Finney, 2006) to model potential fire behavior in an area of interest. In this study, I used the UAV data to generate inputs to FlamMap and model crown fire behavior to determine if a different image source and resulting input rasters produce substantially different fire behavior models. If the resulting fire behavior model is substantially different than the LANDFIRE-derived model and if many of the input raster layers can be more accurately generated from UAV sensors, land managers might consider UAV platforms as a viable alternative image source.

The UAV data also included the SfM-derived 3D data, whereas the LANDFIRE models currently do not include a 3D predictor variable. The UAV-based canopy height raster was generated by creating a 0.25 m canopy height model across the study area that was then resampled to 10 m resolution by calculating the mean height value and classified into 10 m height classes, similar to LANDFIRE. A canopy base height raster was created by using the percentile height of points within each 10 m cell that was the best indicator of field-measured canopy base heights, and reclassified to units used in LANDFIRE (base height in meters x 10). A 10 m resolution UAV-based canopy cover raster was already created during earlier canopy cover processing (see "Deriving Forest Measurements – Canopy Cover from UAV images") and used as an input to FlamMap. The elevation, slope, and aspect rasters were created by first generating a DEM in ENVI LiDAR 5.3. The DEM was generated at a 1 m resolution, which was used to create the slope and aspect rasters in ArcMap 10.4. It is important to note that the accuracy of topographic data layers were not assessed during this study. However, a previous study assessed the accuracies from the same UAV platform and sensor in a similar area (Sankey et al., 2017)

and reported that UAV SfM derived DEMs were well correlated to those derived from both terrestrial and UAV-based laser scanning (R^2 = 0.71 and 0.73, RMSE = 0.17 m and 0.5 m, respectively). After creating a DEM for the study area, all three topographic raster layers were resampled to 10 m resolution to match all other raster layers. Canopy bulk density was estimated with UAV data, however these estimates showed poor relationships to field estimates from field data thus the bulk density raster was used directly from the LANDFIRE database for crown fire modeling. Additionally, the fuel model raster was not measured using UAV data and was also used directly from the LANDFIRE database.

Crown fire behavior models were then performed using various combinations of LANDFIRE (2012 version) and UAV data (Table 5). Additional parameters in FlamMap for modeling crown fire behavior include a fuel moisture file, wind speed, and wind direction. These additional parameters remained constant across all iterations (Table 6). A sensitivity analysis was conducted by substituting one LANDFIRE raster input at a time with a single UAV-derived raster for each iteration to determine the effects of using UAV-derived layers for each input. All FlamMap iterations were conducted using 10 m resolution input raster layers. Since LANDFIRE data is in 30 m resolution, they were resampled to 10 m to be compatible with the UAV data.

Table 5: Inputs used in FlamMap to model crown fire behavior. The outputs from these iterations were then compared to assess the differences in fire behavior models with the UAV-derived inputs (UAV) versus LANDFIRE-derived inputs (LF). All LANDFIRE data used were from the 2012 version. All raster input files were either resampled from LANDFIRE 30 m, or resampled from original UAV data resolution, to a matching resolution of 10 m. Iteration 0 modeled crown fire behavior using 30 m LANDFIRE data, Iteration 1 used LANDFIRE data resampled to 10 m. Iterations 2 to 5 tested UAV-derived rasters for topography, canopy cover, canopy height, and canopy base height. Iteration 6 used all available UAV-derived rasters.

Input Raster	Data Source for Each Iteration						
	Iteration 1	Iteration 2	Iteration 3	Iteration 4	Iteration 5	Iteration 6	Iteration 7
Elevation	LF	LF	UAV	LF	LF	LF	UAV
Slope	LF	LF	UAV	LF	LF	LF	UAV
Aspect	LF	LF	UAV	LF	LF	LF	UAV
Canopy Cover	LF	LF	LF	UAV	LF	LF	UAV
Canopy Height	LF	LF	LF	LF	UAV	LF	UAV
Canopy Base Height	LF	LF	LF	LF	LF	UAV	UAV
Canopy Bulk Density	LF	LF	LF	LF	LF	LF	LF
Fuel Model	LF	LF	LF	LF	LF	LF	LF

Table 6: FlamMap parameters that remained constant through all crown fire behavior iterations. Constants used were those observed during the Schultz Fire of 2010. Fuel moisture refers to the percent of dry weight of the fuel type. 1 hour fuels are dead fuels 0.66 to 2.5 cm in diameter, 10 hour fuels are 2.5 to 7.6 cm in diameter, and 100 hour fuels are 7.6 to 20.3 cm in diameter. The crown fire calculation method refers to the particular method used to calculate the potential for surface, passive, or active crown fire.

Fuel Moisture					Winds		Canopy Characteristics	Crown Fire Calculation Method
1 hour fuel	10 hour fuel	100 hour fuel	Live Herbaceous	Live Woody	Azimuth	Speed	Foliar Moisture Content	
2%	2%	6%	65%	65%	215 degrees	25 MPH @ 20'	100%	Scott/ Reinhardt (2001)

Chapter 3 Results

UAV images and Field Data

The fixed-wing UAV image orthomosaic from Flight 1 covered 6.7 ha area, when all 960 images were mosaicked together and subset to the area of interest. Flight 2 also covered 6.7 ha area in the final orthomosaic image subset. Both Flight 1 and Flight 2 also had corresponding 3D point cloud data with an average of 32 and 56 points/m^2, respectively. The final field dataset collected for validation purposes included 192 individual trees that were mapped and measured in a total of 57 plots distributed across the study area with the two flights.

Canopy Cover Estimates

An equal number of UAV- and NAIP-derived percent canopy cover pixels (N=1,371) were analyzed using a pixel-wise regression covering the entire areas imaged by the two UAV flights. The regression model resulted in adjusted R^2 of 0.72. As indicated by the regression coefficients, the NAIP-derived canopy cover estimates are higher than UAV-derived estimates, especially in areas of high canopy cover (Figure 10).

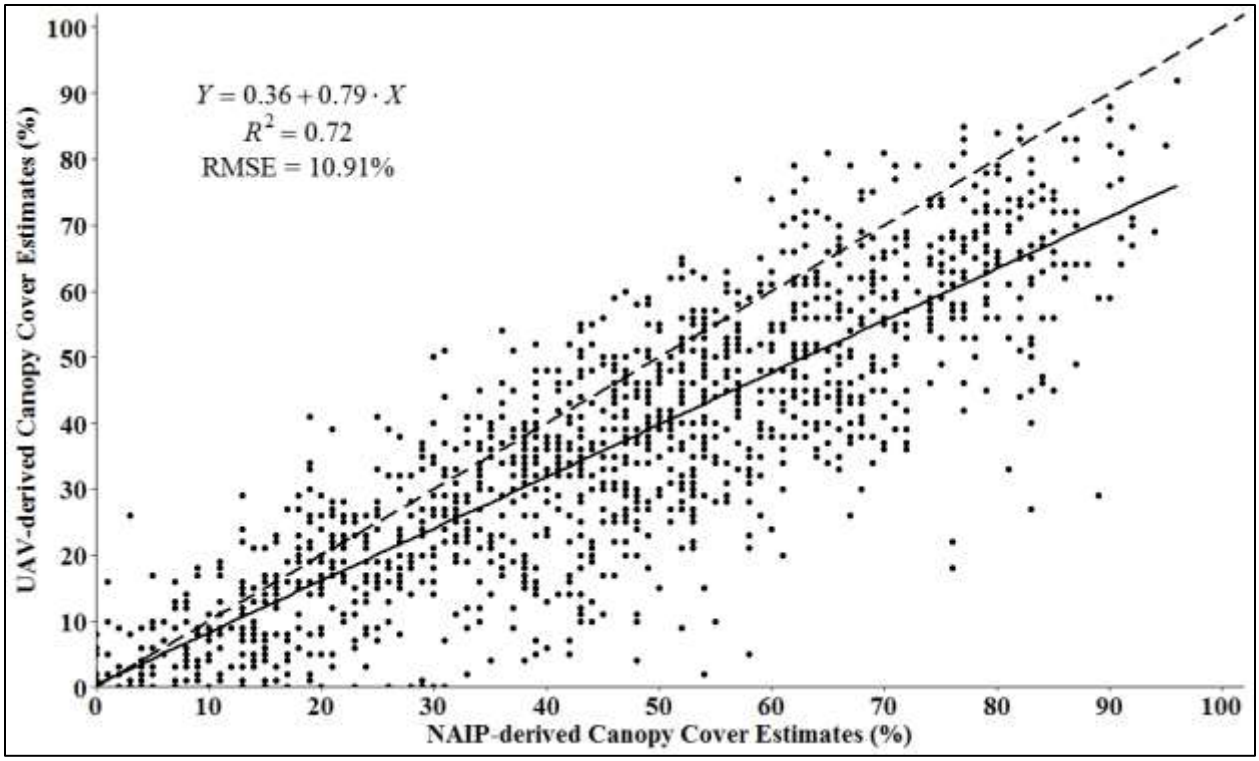

Figure 10: Pixel-wise regression between UAV- and NAIP-derived canopy cover estimates in 10 m resolution. The dashed line represents the 1:1 line, and the solid line is the fitted linear regression line.

The UAV image-derived canopy cover estimates were also compared with the Zachmann and Dickson (2017) canopy cover data summarized in 10 m cells via pixel-wise regression analysis using all pixels (N = 1,371). The regression model indicated a strong agreement between the two estimates with an adjusted R^2 of 0.82 and RMSE of 8.9% canopy cover. The regression model also indicated that the UAV data slightly underestimated canopy cover in greater canopy cover areas compared to the Zachmann and Dickson estimates (Figure 11).

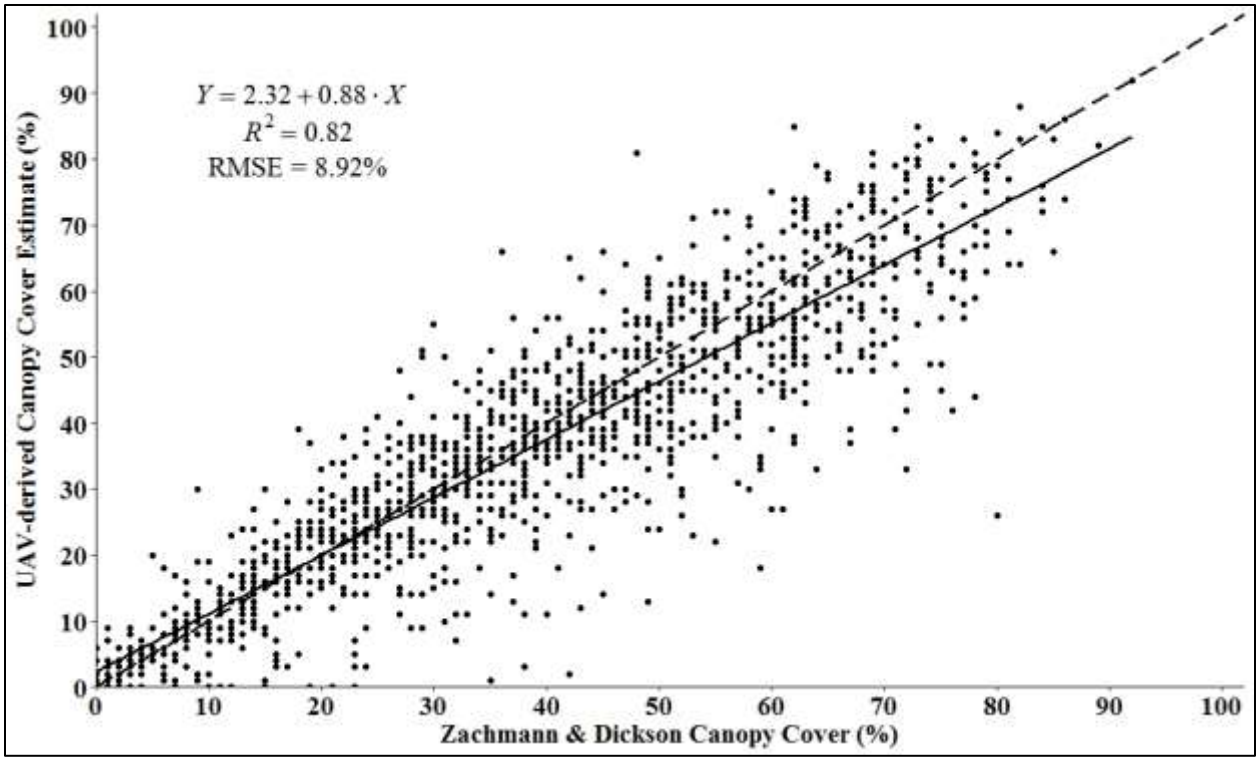

Figure 11: Pixel-wise regression between the UAV image-derived canopy cover estimates and Zachmann and Dickson (2017) canopy cover estimates summarized in 10 m cells. The dashed line represents the 1:1 line and the solid line is the fitted linear regression line from the data.

UAV image-derived canopy cover estimates were also compared to field-based estimates using a pixel-wise regression analysis. This analysis was conducted using field plots (N = 57) and showed a positive correlation (R^2 = 0.67, RMSE = 11.87% Canopy Cover). When compared to field-based estimates, the UAV image-derived estimates tend to underestimate canopy cover, especially in areas of high canopy cover (Figure 12).

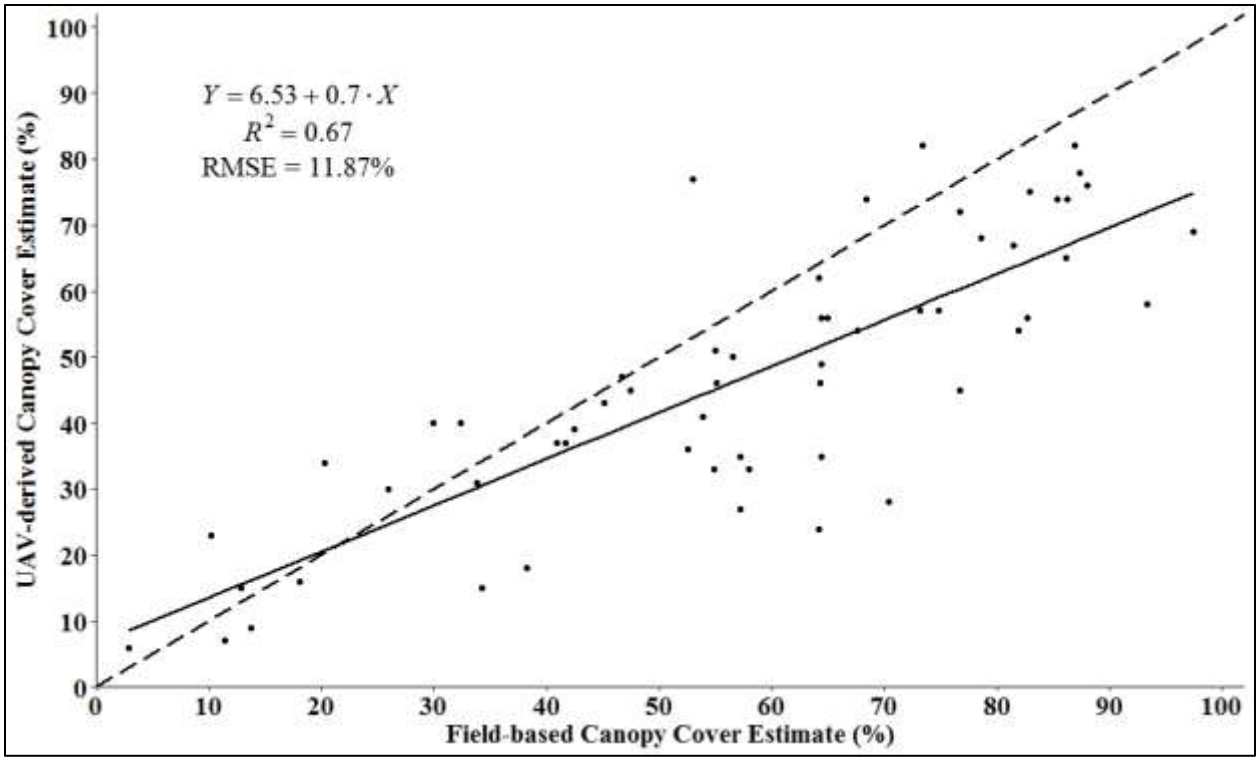

Figure 12: Pixel-wise regression between UAV-image derived canopy cover estimates and Field-based canopy cover estimates. Canopy cover estimates are summarized in 10 m cells for all field plot locations (N=57). The solid line represents the fitted regression line and the dashed line is a 1:1 line for reference.

Relationship between UAV-derived Canopy Cover and Tree Density

Since tree density data were only available for the field plot areas, the analysis between UAV-derived canopy cover and tree density only included those areas in 10 m cells (N = 57). Tree density classes ranged from 1 to 7 trees per 10 m plot. Mean canopy cover between the density classes increases steadily from class 1 to class 4. The increase in canopy cover becomes less apparent between classes 4 to 7 (Figure 13). An ANOVA test with Tukey's multiple pairwise comparisons indicated that the mean canopy cover for a density class of 1 (1 tree per 10 m plot) was not significantly different than the mean canopy cover for a density class of 2 (2 trees per 10 m plot). However, the mean canopy cover for a 1 tree plot was significantly different from the

mean canopy cover of all other density classes above 2. The mean canopy cover for a density class of 2 was significantly different than density classes 4, 6, and 7. Canopy cover for density classes 3 through 7 were not significantly different. Across all density classes, no two adjacent classes contained significantly different mean canopy cover (Figure 13). Canopy cover for density classes 1 through 3 could potentially be used as indicators for density. However, density classes 4 through 7 are likely to have similar canopy cover estimates and thus difficult to detect tree density differences between 4 to 7 trees per 10x10 m cell.

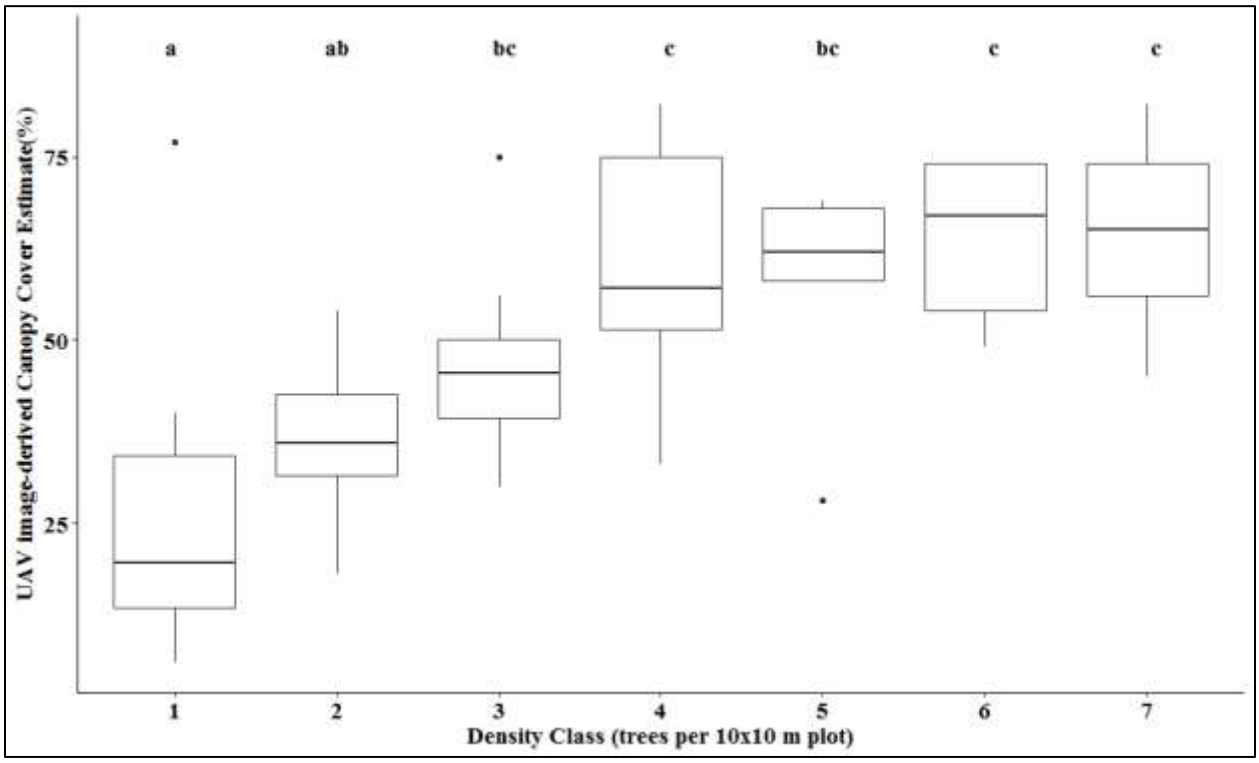

Figure 13: Mean canopy cover (%) for each density class (trees per 10 m plot). The compact letter display for significant differences using the multiple comparisons ANOVA test is shown above each boxplot. Density class 1 is significantly different than class 3 through 7. Density class 2 is significantly different from class 4, 6, and 7. Density classes 4 through 7 are not significantly different. No two adjacent density classes are significantly different. Canopy can potentially be used as an indicator for density in 1, 2, and 3 tree classes. Density classes 4 through 7 will likely show similar values for canopy cover.

Landscape Metrics from UAV Canopy Cover

A total of 1,865 individual patches were identified throughout the study area. Of these, approximately 155 and 167 patches appear to be a single tree canopies in Flight 1 and Flight 2 respectively. The largest patch index was 3.85%, indicating that the largest patch in the study area occupies 3.85% of the total area, which is approximately 1,698 m^2. The mean area of a patch was 24 m^2, with a standard deviation of 75 m^2 indicating a large variability in the size of patches in the study area. Patch identification can be visualized in Figure 14.

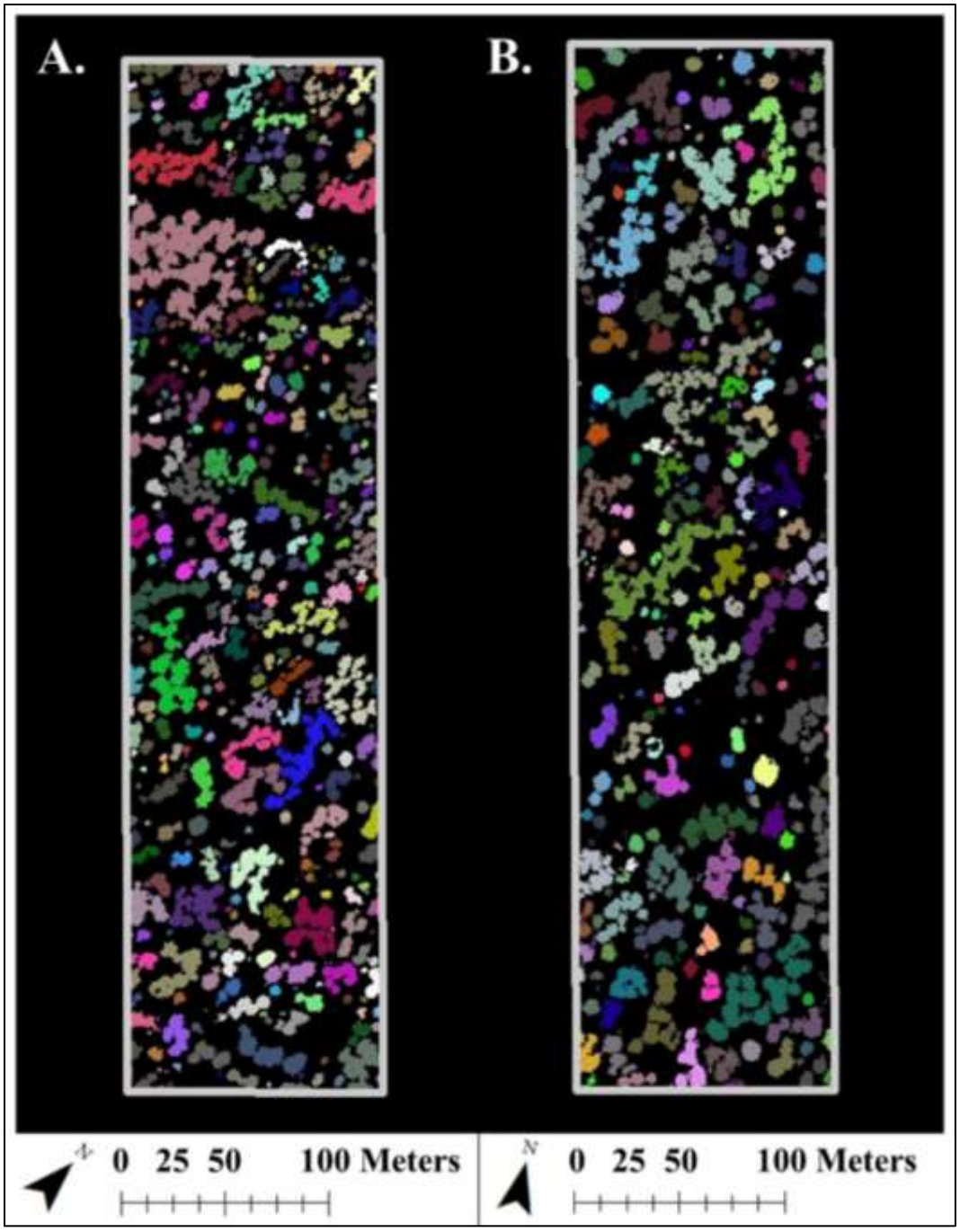

Figure 14: Patch metrics computed by FRAGSTATS with UAV-derived canopy cover classification. Patches were identified using an 8-neighbor rule and colored by their unique patch ID. A total of 1,865 individual patches were identified across both Flight 1 area (Panel A) and Flight 2 (Panel B).

Individual Tree Segmentation

Results from 17 different iterations of the tree segmentation by the Li (2012) algorithm implemented by the lidR package within R were analyzed. In these iterations, the DT parameter ranged from 1.0 to 2.5 meters. In addition, an "optimized" version was tested using results from two different DT iterations based on percent canopy cover across a 10 m grid. Detection was assessed for each iteration using positively detected trees, omission trees, and commission trees (Table 7). The iteration using the smallest DT value had the highest detection of 88%. A total of 159 of the 192 field-mapped trees were accurately detected and segmented. This also produced the highest commission error with 132 additional trees. The iteration using the largest DT value had the lowest detection (109 of 192 trees), but also the lowest commission error (8 trees).

Results from the recall (r), precision (p), and F-score (F) indicated that the lowest DT value iteration had the lowest recall and the highest precision, whereas the highest DT value iteration resulted in highest recall and lowest precision (Table 7). The F-score is a composite measure of both recall and precision. The highest F-scores occurred in the iterations that used a mid-to-high range of DT values. Iterations with a DT value of 1.4 m and 1.7 m had the highest F-score (0.78). Additionally, the optimized iteration also contained a high F-score of 0.78.

Detection, omission, and commission error rates were also analyzed for each density class, and for each tree segmentation iteration. Tree detection was maximized across all densities by using a low DT value in the Li (2012) segmentation algorithm. However, a low DT value also maximized mean commission error, especially in plots with lower tree densities. The iteration using the lowest DT value (1.0 m) resulted in a mean detection of over 80% in all plots except density classes 6 and 7. The low DT value (1.0 m) iteration had a commission error of over 100% (twice as many trees) in both the 1 and 2 density classes. Although the commission error

decreased with an increase in tree density, this error remained over 25% for all density classes except class 7. On the contrary, a high DT value resulted in less detected trees, particularly in the higher density plots. A high DT value also minimized the amount of commission error across all plots. The iteration using the highest DT value (2.5 m) resulted in an average detection of 75% for 1 and 2 tree plots. In general, the detection rate decreased as the plot density increased with lowest detection rates of less than 50% in density classes 5, 6, and 7. When using the optimized DT values of 1.4-1.7 that were based on canopy cover, a balance of omission error and commission error was achieved for lower density classes and higher density classes. The optimized DT iteration achieved this balance across all density classes better than any other iteration using a single DT value (Table 7).

Table 7: Individual tree detection results for each iteration. A total of 192 trees were detected. The DT value was changed by 0.1 m for each iteration to determine the effects of the parameter. The optimized iteration contains two DT values: 1.4 m for areas with >50% canopy cover, and 1.7 m for areas of ≤50% canopy cover. Recall (r), precision (p), and F-score (F) are standardized measures of detection, omission, and commission, respectively (eq. 2, 3, 4).

DT value	Detected Trees (%)	Omitted Trees (%)	Commission Error (%)	r	p	F
1	83	17	69	0.83	0.55	0.66
1.1	79	21	38	0.79	0.68	0.73
1.2	77	23	32	0.77	0.71	0.74
1.3	76	24	21	0.76	0.78	0.77
1.4	73	27	15	0.73	0.83	0.78
1.5	71	29	14	0.71	0.84	0.77
1.6	69	31	11	0.69	0.86	0.77
1.7	68	32	7	0.68	0.9	0.78
1.8	66	34	7	0.66	0.91	0.77
1.9	66	34	7	0.66	0.91	0.76
2	61	39	6	0.61	0.91	0.73
2.1	59	41	5	0.59	0.93	0.72
2.2	61	39	3	0.61	0.96	0.75
2.3	56	44	5	0.56	0.92	0.7
2.4	57	43	5	0.57	0.92	0.71
2.5	57	43	4	0.57	0.93	0.71
Optimized (1.4/1.7)	74	26	16	0.74	0.83	0.78

In addition to analyzing the study area as a whole, separate analyses were also conducted by grouping the plots into density classes. First, the mean number of segmented trees were compared between each density class with each iteration (Figure 15). The mean number of segmented trees for plots with 1, 2, and 3 trees closely matched the number of trees mapped in the field plots. However, plots with 5, 6, and 7 trees also show a greater variance around their

means, making the density classification challenging based on the tree segmentation output. An ANOVA test with multiple pairwise comparisons was also conducted to test for significant differences among the mean segmented trees between all density classes. Using an alpha of 0.05, confidence level of 95%, and all p-values adjusted using Tukey's adjustment for family of 7, there was no significant difference in the mean number of segmented trees between any adjacent density classes. However, density class 1 contained a significantly different mean number of segmented trees than density class 3, 4, 5, 6, and 7. Density class 2 had significantly different mean number of segmented trees compared to density class 6 and 7. Mean segmented trees are not significantly different between density classes 2, 3, 4, and 5. Additionally, density classes 3 to 7 are not significantly different (Figure 16).

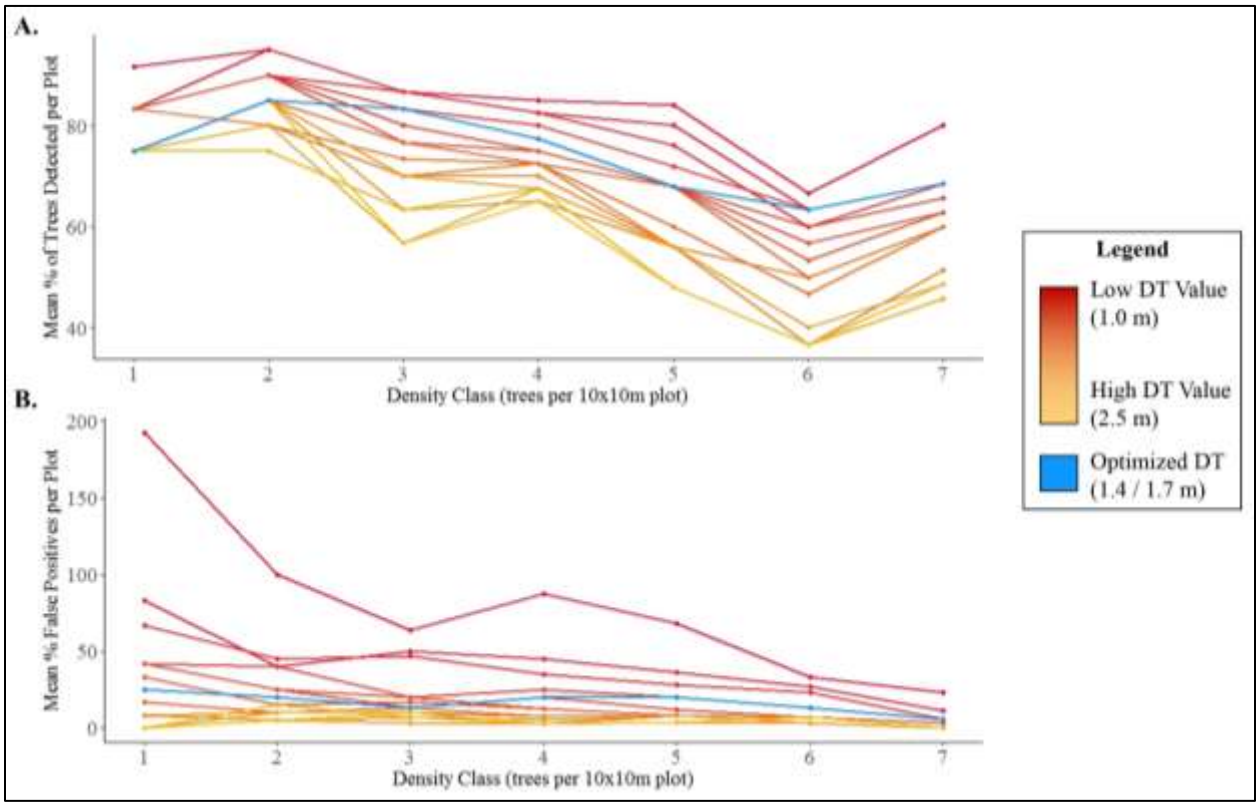

Figure 15: Tree detection and commission error by density class. Each line represents a separate tree segmentation iteration and is colored according to the DT value used (see legend). Mean

percentage of trees detected decreases with increasing density and higher DT value (Panel A). Mean percent of false positives (commission error) also decreases with increasing density and higher DT value (Panel B).

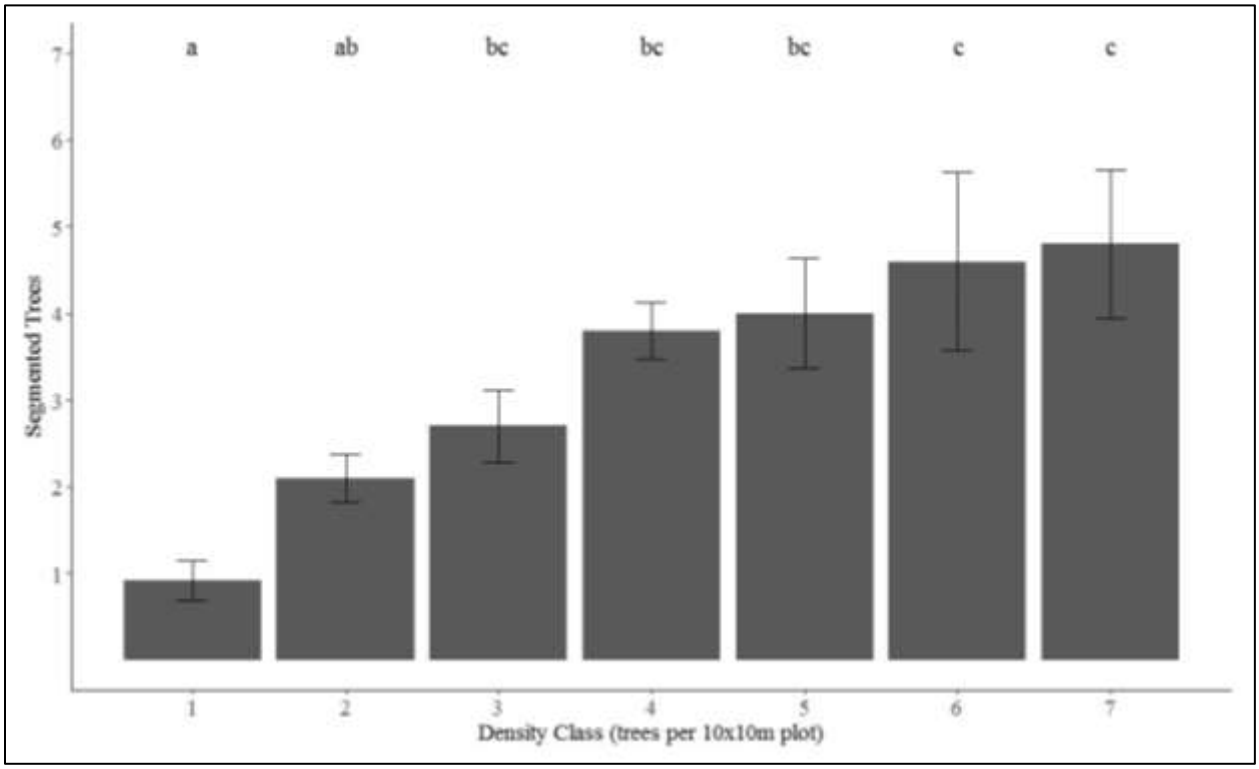

Figure 16: Mean number of segmented trees per each density class. Density class represents the number of trees within each 10 x 10 m plot. Error bars represent the standard error of the means for each class. The compact letter display for significant differences using the multiple comparisons ANOVA test is shown above each bar. The mean number of segmented trees in density class 1 is not significantly different than density class 2, however it is significantly different than density class 3, 4, 5, 6, and 7. Density class 2 contains a significantly different mean number of segmented trees than density class 6 and 7. Density classes 3, 4, 5, 6, and 7 do not contain a significantly different mean number of segmented trees.

Individual Tree Metrics

A comparison of UAV-derived and field-based individual tree metrics was conducted to evaluate the accuracy of the UAV measurements. This analysis was only completed using the trees that were positively detected with the optimized DT iteration (N = 142) since this validation required

field measurements for every UAV-derived tree, and only the detected trees had both measurements to compare.

A regression model of UAV-derived tree height and field-measured tree heights indicated a positive correlation with an adjusted R^2 of 0.71 (RMSE = 1.83 m) (Figure 17).

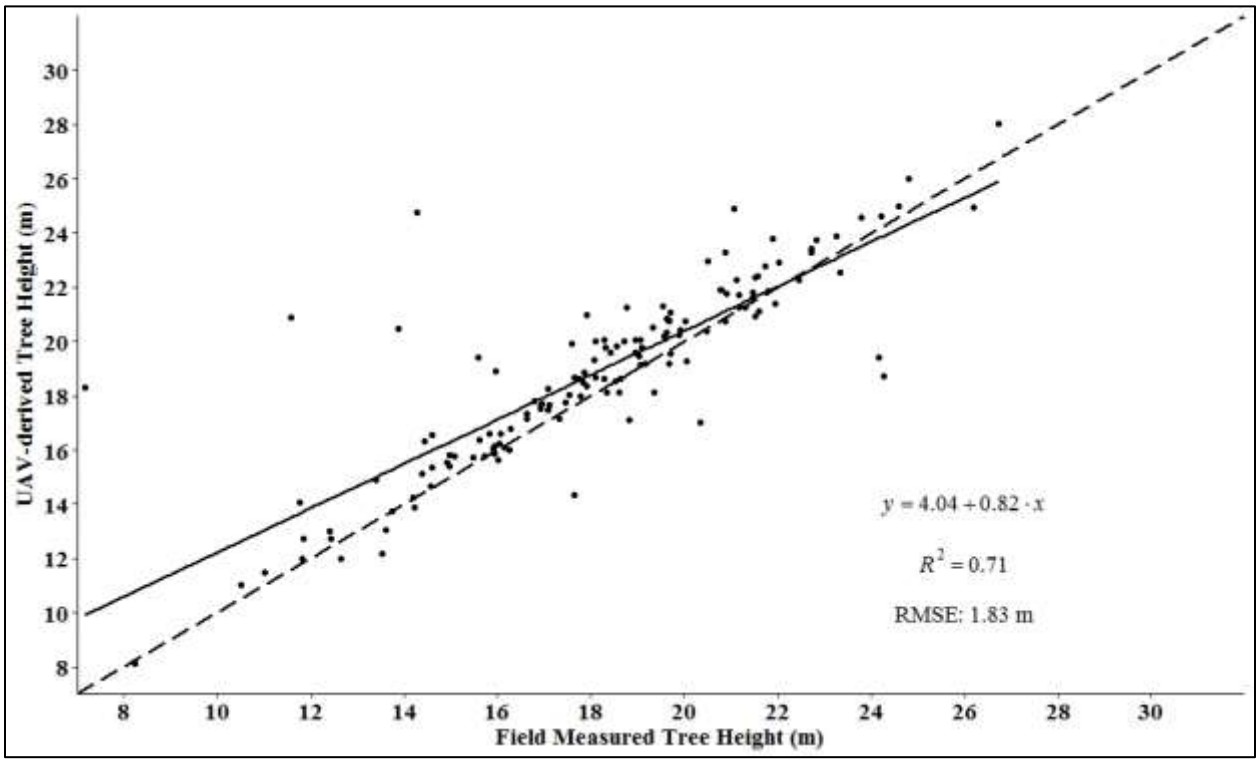

Figure 17: Linear regression model between UAV-derived tree heights and field measurements. The solid line represents the fitted regression line and the dashed line is a 1:1 line for reference.

A bootstrap resampling analysis was then conducted to determine the mean error between UAV-derived tree height and field measurements. A subsample of 100 error rates was taken to calculate a mean height error. This occurred over 10,000 iterations to determine a 90% confidence interval of mean error rates. The mean error rate of the UAV-derived tree height was 5.29% of the field measured heights. The lower end of the 90% confidence interval was 2.79%, whereas the upper end was 8.32%.

To determine a predictor for canopy base height, a regression analysis was conducted using the field measured base heights compared to UAV-derived predictor variables. These included all height percentile estimates and the height to canopy diameter ratio from the UAV-derived crown metrics for each tree. All height percentiles had a positive correlation to canopy base height with adjusted R^2 values ranging from 0.25 to 0.40, and RMSE ranging from 1.67 to 2.88 m. In comparison, LANDFIRE base height estimates have an average R^2 value of 0.09 (Reeves et al., 2009). However, no single height percentile was a clear best predictor of base height. Height to canopy diameter ratio did not have any statistically significant correlation with field-measured canopy base heights (Table 8).

Table 8: Results from regression analyses using each UAV-derived height percentile and height to canopy diameter compared to field-measured base heights.

UAV-derived predictor variable	Correlation to Base Height (adj R^2)	RMSE (m)	Intercept (m)	Slope	p-value
5th	0.34	2.52	4.70	0.62	2.63E-14
10th	0.35	2.55	5.36	0.65	4.03E-15
15th	0.38	2.50	5.81	0.69	1.16E-16
20th	0.38	2.49	6.51	0.68	1.39E-16
25th	0.39	2.52	6.99	0.69	9.73E-17
30th	0.39	2.53	7.44	0.70	8.61E-17
35th	0.39	2.52	7.84	0.70	8.52E-17
40th	0.39	2.52	8.27	0.69	1.04E-16
45th	0.39	2.48	8.66	0.69	3.61E-17
50th	0.40	2.47	9.00	0.69	3.07E-17
55th	0.39	2.48	9.38	0.69	5.56E-17
60th	0.37	2.50	9.85	0.67	3.49E-16
65th	0.36	2.53	10.35	0.65	3.00E-15
70th	0.34	2.57	10.81	0.64	2.27E-14
75th	0.32	2.61	11.22	0.62	1.17E-13
80th	0.28	2.73	12.20	0.59	7.51E-12
90th	0.26	2.79	12.67	0.58	3.65E-11
95th	0.25	2.84	13.13	0.58	8.95E-11
99th	0.25	2.88	13.78	0.57	2.03E-10
Height to Canopy Diameter ratio	0.00	1.67	3.22	0.04	3.57E-01

Since many of the UAV-derived height percentiles were correlated to canopy base height, and no single variable was the clear “best” predictor, another analysis was completed to determine which predictor variable had the closest to a 1:1 relationship with canopy base height.

The analysis completed was a qualitative assessment of the predictor variable and a 1:1 relationship with field measured canopy base height (Figure 18). Using this assessment, it was determined that the 5th height percentile had the closest to a 1:1 relationship with field measured canopy base height compared to all other predictor variables. Also, as the height percentile increased, the relationship between predictor variable and field measured canopy base height migrated further from the 1:1 line. The height to canopy diameter ratio did not show a 1:1 relationship with field measured canopy base height.

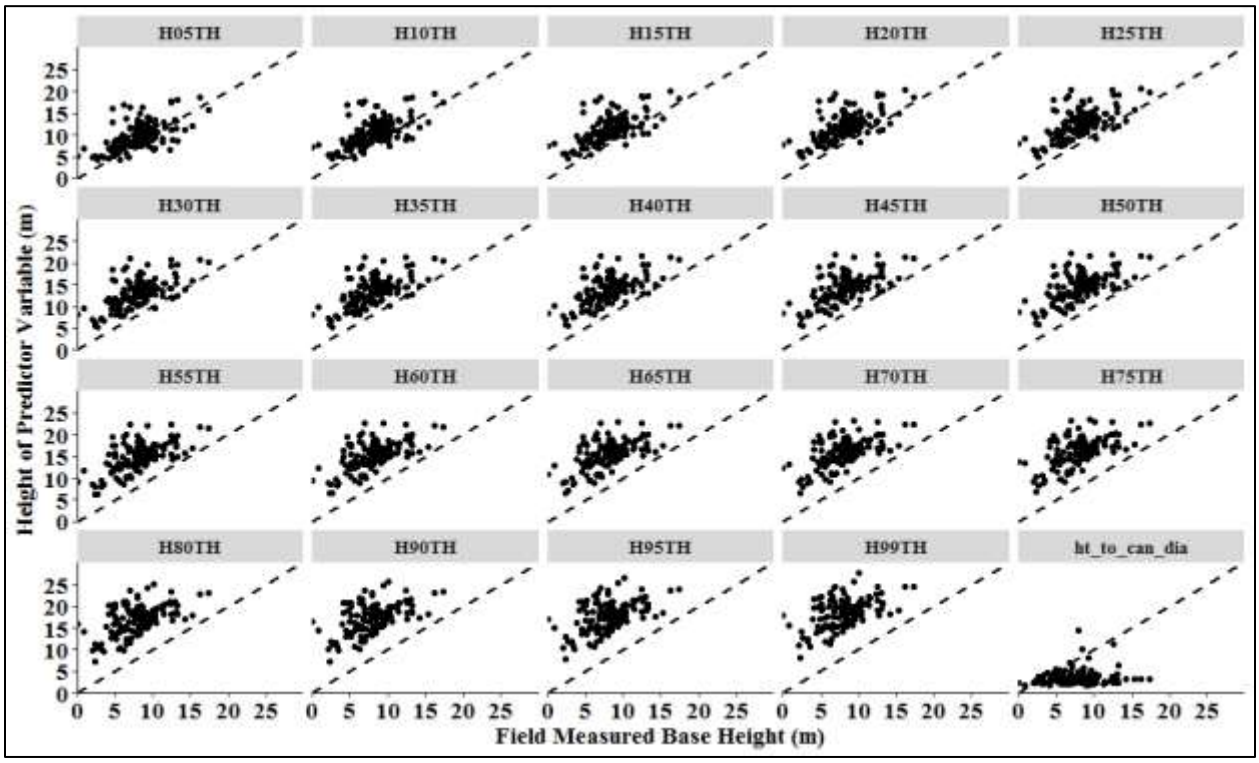

Figure 18: UAV-derived predictor variables and the field measured canopy base heights of all detected trees. The dashed line represents a 1:1 line relationship.

Using the UAV image-derived 5th percentile height as a predictor for canopy base height, a bootstrap resampling analysis was conducted to determine the mean error of the UAV estimate compared to the field measurement. A subsample of 100 error rates was taken to calculate a mean base height error. This occurred over 10,000 iterations to determine a 90% confidence

interval of mean error rates. On average, the error between the UAV-derived estimates were 32.29% of the field measured base height. At the 90% confidence level, the mean canopy base height error rate was 22.03% to 45.54%.

Canopy bulk density was estimated by first estimating the canopy mass and volume of each detected tree. Canopy mass was estimated using a tree height to DBH relationship that was established using the field data and used to predict the DBH of individual trees given their UAV-derived tree height. The UAV-derived DBH predictions ranged from 12.34 to 51.15 cm, with a mean of 38.22 cm. UAV-derived DBH had an adjusted R^2 of 0.38 with an RMSE of 4.82 cm when compared to field measurements. The UAV-derived DBH predictions were then used to estimate the canopy mass of each tree using allometric equations from Kaye et al (2005). These UAV-derived estimates of canopy mass ranged from 7.6 to 283.1 kg, with a mean of 138.8 kg, and were then compared to estimates using field measurements which produced an adjusted R^2 of 0.39 with an RMSE of 39.25 kg. To estimate the canopy volume of each tree, three UAV-derived canopy measurements were used: tree height, canopy base height, and average canopy radius. Comparisons between UAV-derived and field measured tree heights and canopy base heights were conducted in previous analyses. UAV-derived average canopy radius ranged from 0.49 to 5.42 m, with a mean radius of 2.97 m. When compared to field measured canopy radius, the UAV-derived radius had an adjusted R^2 of 0.26 and an RMSE of 0.88 m. The resulting UAV-derived canopy volume estimates ranged from 4.08 to 1651.15 m^3 with a mean volume of 323.15 m^3. UAV-derived canopy volume had an adjusted R^2 of 0.33 and an RMSE of 246.13 m^3. The UAV-derived mass and volume estimates were then combined to estimate canopy bulk density. The relationship between UAV and field estimates for canopy bulk density was not correlated (adj. R^2 = 0.0005, RMSE = 0.30 kg/m^3).

Fire Behavior Modeling

A baseline model was first established by using only LANDFIRE data layers in 30 m resolution to model crown fire behavior for the study area. After establishing the baseline, the LANDFIRE raster layers were resampled to 10 m resolution for comparison with the UAV-derived raster layers. To analyze the effects of resolution on crown fire behavior, the 10 m LANDFIRE data were used to model crown fire and compare to the 30 m LANDFIRE output. Crown fire behavior outputs for both the 30 m and 10 m LANDFIRE datasets were equal with 0% surface fire, 14% passive crown fire, and 86% active crown fire predicted for the study area (Table 9: Iteration 1, Iteration 2).

A reliable estimate of canopy bulk density could not be produced from the UAV images, given the relatively low correlation coefficients. However, UAV-derived estimates for the critical variables had similar accuracies to the LANDFIRE-derived variables. Therefore, UAV-derived estimates for elevation, slope, aspect, canopy cover, and canopy base height were produced in 10 m resolution for use in FlamMap. These data represented the mean of each variable for the 10 m grid cell. These variables were then used to supplement LANDFIRE data and model crown fire behavior for the study area.

A sensitivity analysis was completed by substituting each UAV-derived layer individually, except topographic variables which were used as a group, and comparing the resulting outputs from each iteration for crown fire behavior across the study area. First, the UAV-derived topographic variables (elevation, slope, and aspect) were substituted to model crown fire (Table 9: Iteration 3). This resulted in a reduction of active crown fire with an increase of passive crown fire. Crown fire behavior across the study area with the UAV-derived

topographic variables resulted in 0% surface fire, a larger passive crown fire of 23%, and a lower active crown fire of 77% compared to the LANDFIRE outputs.

The next iteration substituted LANDFIRE-derived canopy cover with the UAV-derived canopy cover estimates (Table 9: Iteration 4). This resulted in a slight reduction in active crown fire and passive crown fire. These reductions resulted in a slight increase in the surface fire category. Crown fire behavior with the UAV-derived canopy cover layer resulted in 3% surface fire, 13% passive crown fire, and 84% active crown fire across the study area. UAV-derived canopy height was then substituted into the crown fire behavior model (Table 9: Iteration 5). The UAV-derived canopy height layer had a larger effect than either topography or canopy cover. Active crown fire was reduced from 86% in the LANDFIRE-only models to 44% with the UAV image-derived canopy height. Additionally, surface fire increased from 0 to 49% and passive crown fire decreased from 14 to 7%.

Canopy base height was the next variable that was substituted for the sensitivity analysis (Table 9: Iteration 6). The inclusion of the UAV-derived canopy base height layer caused an extreme reduction of active crown fire and a drastic increase of surface fire. Active crown fire was reduced to 2%, passive crown fire to 0%, and surface fire increased to 98%. Lastly, crown fire was modeled using all the available UAV-derived variables including topography, canopy cover, canopy height, and canopy base height (Table 9: Iteration 7). Crown fire behavior was modeled as 100% surface fire, 0% passive crown fire, and 0% active crown fire.

Overall, when modeling crown fire behavior with only LANDFIRE data, the 30 m resolution and resampled 10 m resolution produced the same results. Substituting UAV-derived canopy cover showed a slight reduction in active crown fire and an increase in surface fire. In increasing order, UAV-derived topography, canopy height, and base height had substantial

impacts on the crown fire behavior model by reducing the percentage of active crown fire and increasing surface fire. The UAV-derived crown base height layer almost eliminated crown fire initiation completely with only 2% active crown fire and 98% surface fire. When all UAV-derived variables were used, crown fire initiation was completely reduced to 0% active crown fire and 0% passive crown fire with 100% of the study area being modeled as surface fire.

Table 9: Crown fire behavior model outputs for each iteration. Inputs for Iteration 1 included the original data layers from the LANDFIRE database in 30 m resolution. Iteration 2 utilized the resampled LANDFIRE data in 10 m resolution. Iteration 3 used UAV-derived elevation, slope, and aspect rasters with LANDFIRE data as other inputs. Iteration 4 substituted UAV-derived canopy cover with LANDFIRE data for all other inputs. Iteration 5 included the UAV-derived canopy height estimate with LANDFIRE data for other inputs. Iteration 6 used the UAV-derived canopy base height estimate along with all other LANDFIRE data inputs. Iteration 7 included UAV-derived topography, canopy cover, canopy height, and canopy base height.

	Percent of Fire Type (%)					
	Iteration 1 & 2	Iteration 3	Iteration 4	Iteration 5	Iteration 6	Iteration 7
Fire Type	LANDFIRE	UAV Topo	UAV CC	UAV CH	UAV CBH	UAV all
Surface	0	0	3	49	98	100
Passive Crown	14	23	13	7	0	0
Active Crown	86	77	84	44	2	0

Chapter 4 Discussion

Canopy Cover and Data Sources

The UAV-derived canopy cover estimates were very high in spatial resolution originating from 15 cm resolution data. The accuracy of the UAV-derived canopy cover estimates was relatively high, when compared with two different data sources used to estimate canopy cover: NAIP imagery and a canopy cover classification dataset from Zachmann and Dickson (2017), which was derived from aerial imagery. The original resolution from each of these data sources was 1 m for NAIP imagery and 30 cm for the Zachmann and Dickson (2017) canopy classification. Each data source was then resampled to a 10 m canopy cover percent raster to directly compare among the three image sources (N=1,371).

The UAV-derived canopy cover estimate was positively correlated with the NAIP-derived canopy cover estimate (R^2=0.72, RMSE= 10.9% canopy cover). In this comparison, there were several occurrences of the NAIP-derived estimate both over- and under-estimating canopy cover compared to the UAV-derived estimate. However, in general the NAIP-derived estimate tends to overestimate canopy cover across the study area, especially in areas of high canopy cover. This was evident when examining the intercept and slope of the fitted regression line (intercept= 0.18% canopy cover, slope= 0.79). Canopy cover estimates from NAIP data become increasingly greater than UAV estimates as canopy cover increases. This difference can be largely explained by the difference in spatial resolution between the original datasets. Canopy cover for the UAV imagery was being derived from an original image resolution of 15 cm, whereas the NAIP imagery was in 1 m resolution. Finer resolution imagery is able to detect variation in the data that would otherwise be undetected using coarser resolution imagery (Woodcock & Strahler, 1987). Therefore, the UAV imagery may be able to detect areas of no-

canopy, or sparse canopy, within a 1 m area that the NAIP imagery cannot leading to an overestimation of canopy cover with the NAIP estimate. Another possible source of this discrepancy could be from the date of UAV image acquisition in the Flight 2 area. This flight was conducted during the month of November during leaf-off season. Since canopy cover was derived using an NDVI-based procedure, canopies without leaves, such as oaks, would not have been detected. Although there are few deciduous tree species in the Flight 2 Area, this could have also lead to an underestimation of canopy cover with the UAV imagery.

A comparison between UAV-derived canopy cover and the Zachmann and Dickson (2017) canopy classification was completed to compare these estimates with more similar spatial resolution. Original resolution of UAV imagery was 15 cm, and the Zachmann and Dickson classification was 30 cm, which were both resampled to 10 m percent canopy cover estimates for comparison. The pixel-wise regression between the UAV-derived and Zachmann and Dickson estimates showed a positive correlation stronger than the UAV vs NAIP comparison. The R^2 value between UAV and Zachmann and Dickson percent canopy cover was 0.82, with an RMSE of 8.77% canopy cover. Additionally, the fitted linear regression equation between the UAV and Zachmann and Dickson canopy cover estimates had an intercept of 2.1% canopy cover, and a slope of 0.88, indicating a relationship closer to 1:1, when compared to the UAV vs NAIP relationship. Overall, the UAV and Zachmann and Dickson comparison showed a stronger relationship than UAV versus NAIP. One possible reason is that the spatial resolution of the Zachmann and Dickson classification (30 cm) was much closer to the UAV imagery (15 cm) than the NAIP imagery (1 m).

In addition to comparing UAV-derived canopy cover with remotely sensed data sources, we also compared these estimates to field-based estimates. In this comparison, UAV-derived

canopy cover estimates were positively correlated to field-based estimates (R^2 = 0.67, RMSE = 11.87% canopy cover). Sankey et al. (2017) found a similar, though slightly stronger, relationship between UAV-derived canopy cover and field-based estimates (R^2 = 0.74, RMSE = 8.5% canopy cover) in a comparable study site. When comparing our UAV-derived canopy cover estimates to field-based estimates, we found that UAV methods tend to underestimate, especially in areas of high canopy cover. An underestimation of canopy cover using UAV imagery was also found in a study conducted by Wallace et al (2016). UAV-derived canopy cover estimates are capable of fully representing the unevenness of tree crowns, whereas the field-based estimates used in our study rely on average crown radii that are used to assume an even, circular, crown around each tree. Additionally, UAV-derived canopy cover estimates are able to represent small gaps within a single crown, whereas field-based estimates assume continuous, gapless, crowns. These assumptions could account for the general underestimation of canopy cover when comparing UAV-derived estimates to those calculated from field measurements.

The positive correlation between UAV-derived canopy cover to both NAIP and Zachmann and Dickson estimates shows that the UAV canopy cover estimates have similar uses and implications to both NAIP and Zachmann and Dickson. Additionally, UAV data has the added benefit of temporal resolution that can, to a certain extent, be defined by the user. This characteristic make UAV surveys particularly useful for applications requiring fine temporal resolution that can be difficult and costly to acquire with aerial imagery.

Canopy Cover and Tree Density Relationship

The relationship between canopy cover and tree density was explored using the UAV-derived 10 m percent canopy cover estimate and the field measurements from varying tree densities. Tree

density was defined in 7 classes that represent the number of trees within a 10 x 10 m plot. These density classes ranged from 1 to 7 trees per plot. Mean canopy cover varied statistically significantly and had a steady increase between 1 to 4 tree density classes. However, when examining the mean canopy cover between 4 to 7 trees per plot, this difference becomes less pronounced. An ANOVA test with multiple pairwise comparisons indicated that the 1 tree density class was significantly different than all classes from 3 to 7 trees. Additionally, the 2 tree density class was significantly different than the 4, 6, and 7 tree density classes. Overall, no two adjacent density classes showed significantly different mean canopy cover. Therefore, canopy cover cannot be used to predict tree density of 1 versus 2. However, it may be used to separate areas of very low density from areas of high density.

The findings from the canopy cover and tree density analysis could be explained by the varying widths of tree canopies across the study area. An open-grown single tree may occupy the same amount of horizontal space as a few trees growing close together. The difference between single, large and several small canopies could not be detected with the UAV-derived canopy cover alone. Additionally, this analysis also only included 10 m plots, which can inherently reach a point of canopy closure regardless of how many individual trees are present (eg. 4, 5, 6, or 7 trees can fill a 10 x 10 m space with canopy). Interestingly, mean canopy cover across all field plots seems to reach a maximum around 65-70% suggesting it becomes less common for tree canopies to reach closure beyond that amount in the study area. However, it's also important to consider the sampling method was random and stratified by density, and therefore not an even representation of the entire study area.

Landscape Metrics with Canopy Cover

FRAGSTATS software computes landscape metrics using an input raster that has been classified by the user. This study used the 15 cm canopy cover classification raster derived from the UAV data. The software can handle images that contain several classifications. However, the data used in this study only contained a binary classification of tree canopy and no-tree canopy. An 8 neighbor rule was used in this study to aggregate adjacent canopy pixels into patches. The 8 neighbor rule aggregates pixels into a "patch" if they share adjacent sides or adjacent corners. In general, an 8 neighbor rule allows more aggregation of pixels into a single patch thus creating larger, but fewer, total patches, when using coarse spatial resolution data. Since the UAV images had 15 cm resolution, the FRAGSTATS application did not encounter this limitation and identified many small patches.

A total of 1,865 patches were identified across the study area. The largest patch index was 3.85%, meaning the largest patch occupied 3.85% of the total landscape (1,698 m^2). Additionally, the mean area of a patch was 24 m^2, with a standard deviation of 75 m^2. The large standard deviation relative to the mean suggests that patch sizes are highly variable across the study area. However, further interpretations from these metrics alone are limited. The utility of such metrics becomes greater with more datasets. A UAV survey of the study area after restoration treatment could be used to answer questions about the change of these metrics such as: Has the landscape become more fragmented? How has the average patch size changed? How has the variability in patch sizes changed? Additionally, similar procedures could be used to answer these questions when comparing multiple landscapes in different areas.

Future Considerations for Canopy Cover

The UAV imagery used in this study to derive canopy cover data was relatively high in spatial resolution (15 cm). A comparable high resolution dataset, that has been independently validated, was not available for comparison. Instead, a comparison of NAIP imagery and a third-party canopy cover classification (Zachmann and Dickson, 2017) was conducted to assess the accuracy of UAV-derived canopy cover. Results from these comparisons supported the hypothesis that UAV-derived estimates of canopy cover can be accurate. Future research might consider more high-resolution validation datasets to estimate UAV canopy cover accuracy. Seasonality of the data acquisitions being used should also be considered. Factors such as sun-angle and leaf-on vs leaf-off conditions can potentially effect canopy cover estimates that are derived from NDVI.

A problem that was encountered when processing UAV imagery to produce a canopy cover estimate was that the UAV imagery often contained areas of high NDVI between tree canopies. Aside from true areas of high NDVI (low vegetation: grass, forbs, shrubs), there were also areas of image distortion likely from misalignment during the orthomosaic building process. However, the UAV data estimates have the benefit of including a 3D SfM point cloud which can be used to provide height attributes to the UAV imagery. A novel method was used to leverage this height information to create a height mask and apply it to the canopy cover classification and eliminate areas classified as canopy that were below a certain height (1.37 m). This produced a canopy cover estimate that was more representative of only tree canopy. This method could be explored more in-depth with not only UAV data, but also using aerial imagery and lidar.

Potential applications of UAV-derived canopy cover estimation include conducting change detections to estimate mortality and regeneration. A process similar to the one used in this study could be conducted at several timesteps to conduct a canopy cover change detection.

Tree mortality could be estimated by examining areas of canopy that decrease over time. Additionally, the same process could be used to estimate post-disturbance regeneration by examining the areas of increasing canopy cover. Albeit each of these, applications would require customization of the parameters used to address site-specific changes. Additionally, this study did not attempt to conduct a spectral classification of different cover types or species, since the study are was dominated by ponderosa pine. By including such classification, information regarding the composition and configuration of various cover types, or species, could be conducted.

Additionally, information such as canopy cover that can be derived from UAV imagery can have far reaching implications in forest ecology. Forest canopy cover has been shown to be directly related to wildfire behavior and fuel loading (Fule et al., 2004; Lydersen et al., 2013). Increased canopy cover causes higher susceptibility to insect outbreak and forest pathogens (Covington & Moore, 1994a; Covington et al., 1997; Feeney et al., 1998). Diversity in forest canopy cover can provide habitat and forage areas for Mexican spotted owl (*Strix occidentalis*) (Ganey et al., 1999; Prather et al., 2008). Changes in canopy cover due to restoration treatments have been shown to have implications towards water yield and nutrient outflow (Kaye et al., 2002; Simonin et al., 2007). Understory species that provide species biodiversity and forage for wildlife have an inverse relationship with forest canopy cover (Jameson, 1967; Covington et al., 1997; Laughlin et al., 2006; Moore et al., 2006). UAV surveys offer scientists and land managers a way to further examine these ecosystem responses by providing spatial canopy cover information across user-defined areas and frequency.

Individual Tree Segmentation and Subsequent Density Estimates

This study implemented tree segmentation algorithms, originally intended for use with lidar point cloud data, to identify individual trees from a SfM-derived point cloud. Depending on the parameters used in the algorithm, varying levels of detection, and omission and commission rates were achieved. When maximizing the F-score of tree detection, the tree segmentation algorithms detected 74% of trees with an F-score of 0.78. This detection rate was consistent with a study that used SfM point clouds to segment individual trees in Australian savannas (Goldbergs et al., 2018), which had a detection rate of 70% and an F-score of 0.71. However, this study achieved a lower rate than the 85% detection rate documented in open canopy mixed conifer forest (Mohan et al., 2017). Similar to findings by Goldbergs et al. (2018), the detection rates in this study declined with increasing tree density. This finding supported the hypothesis that detection of individual trees using the UAV SfM method would decrease with increasing tree density.

The parameters used in a given tree segmentation algorithm must be "tuned" to match the specific site and user's needs. The parameters used in this study should not be used in another location without verification and fine-tuning. This study utilized a point-based algorithm (W. Li et al., 2012) to segment individual trees from the point cloud. The main parameter that affected the segmentation was the DT parameter- a distance threshold between points that determined whether a point was, or was not, part of a particular tree. Within the Li (2012) segmentation algorithm, there are two different DT values. DT 1 is the distance threshold above 15 m, and DT 2 is the distance threshold below 15 m. For this study, both of these thresholds were set equal. In future studies, these values can be set differently to potentially achieve better segmentation results.

This study explored an optimization of SfM tree segmentation by taking advantage of the multispectral orthomosaic image from the UAV in addition to the point cloud. The availability of both orthomosaic image and SfM point cloud offered the opportunity to leverage the 2D canopy cover information with 3D point cloud data. After running the segmentation using various DT parameters, grid cells of higher canopy cover (> 50%) used trees that were segmented with parameters designed to detect more trees, whereas grid cells of low canopy cover (≤ 50%) used trees that were segmented with parameters that minimized commission error and found less trees. This optimization proved to be successful at detecting marginally more trees with less commission error.

The results from the optimized tree segmentation were then used to explore a relationship between the mean number of trees detected per plot across each density class (trees per 10 x 10 m plot). In this analysis, a perfect segmentation would result in the number of trees segmented being equal to the density class of the particular plot. Mean numbers of segmented trees follow this trend within the 1, 2, 3, and 4 tree density classes. However, the 5, 6, and 7 tree density classes no longer show this trend. The tree segmentation used in this study rarely detects more than 5 trees in any of the study plots. An ANOVA test indicated that the variance in the number of trees segmented for each density class was relatively high creating no significant difference in mean values between any adjacent density class. However, the 1 tree class was significantly different than classes 3 through 7, and the 2 tree class was significantly different than class 6 and 7.

Other studies using UAV-SfM for individual tree segmentation have had varying results. In a spruce forest in southeast Norway, Puliti et al (2015) estimated stem numbers of trees with an R^2 of 0.60. Although specific values for tree density and canopy cover are not given, the

example imagery appears to show a much denser forest relative to our ponderosa pine study area. This study utilized similar UAV-SfM methods as our study, however they supplemented their data with aerial lidar data for ground points, which may have increased their accuracies compared to using only UAV-derived data. In the Northern Territory of Australia, similar UAV-SfM methods were used by Goldbergs et al (2018) to segment trees in a eucalyptus forest that had >30% canopy cover. In this study, UAV-derived estimates detected 70% of dominant and co-dominant trees, and 35% of suppressed trees. In a ponderosa pine forest in northern Arizona that had an average canopy cover of 37%, Sankey et al (2017) segmented individual trees with UAV-SfM methods and had a positive, albeit weaker, correlation to field tree counts (R^2 = 0.53). In comparison to these studies, our study area had an average canopy cover of 36% (SD = 20.8%) as measured with the UAV imagery. Therefore, the most comparable study sites would be the eucalyptus forest in Australia (Goldbergs et al., 2018), and the ponderosa pine forest in northern Arizona (Sankey et al., 2017). In our study, we had marginally higher detection rates with a positive detection of 74% of our field-measured trees with a 16% commission error.

In this study, changing the DT value resulted in changes in tree detection rates, as well as commission error. When the parameter was set to detect more trees, the commission error increased. Although the F-score is a composite score between true detections and commission error, this score does not necessarily indicate the "best" segmentation. The evaluation of tree segmentation and detection rates should be conducted by the user for a given objective. For example, some situations might prefer over-segmentation of trees, which would allow overestimates of tree density that can then be filtered with another variable. The objective of the survey, or study, should be the primary driver behind choosing tree segmentation parameters.

Individual Tree Metrics

After individual trees were segmented from the point cloud, crown metrics were calculated for each tree. These metrics included tree center coordinates, canopy diameter, canopy height, and percentile heights that represent the meters above ground for different percentiles of points. These metrics were then used to estimate the height, canopy base height, and canopy bulk density for each tree. These measurements were compared to field data for validation (N = 142).

Using the segmented point cloud, the highest point for a given tree was considered the overall tree height. A positive correlation was found when comparing these values to field measurements for tree height (R^2 = 0.71, RMSE = 1.83 m), which supported the hypothesis that UAV estimates for tree height would be accurate when compared to field measurements.

Several other studies have estimated tree heights with UAV-derived data. The results from these studies generally show a strong relationship between UAV-derived tree height estimates and field-based measurements. Dandois et al (2015) found a strong correlation between UAV-derived and field-based tree height estimates (R^2 = 0.86, RMSE = 3.6 m) in a mixed age deciduous forest in Maryland. Wallace et al (2016) showed a weaker correlation (R^2 = 0.68, RMSE 1.3 m) in a dry sclerophyll eucalypt forest in Australia. Puliti et al (2015) had a strong correlation when comparing the Lorey's mean tree height metric derived from UAV data and field measurements (R^2 = 0.71, RMSE = 1.4 m) in a spruce forest in southeast Norway, however they supplemented the UAV data with aerial lidar data which likely increased the accuracy of their estimates. Sankey et al (2017) showed a positive correlation (R^2 = 0.64, RMSE = 2.9 m) when comparing UAV and field-based tree height estimates in a ponderosa pine forest. Although these studies were conducted across a wide range of vegetation types, the tree height estimate

accuracies found in our study (R^2 = 0.71, RMSE = 1.83 m) are generally consistent with previous studies.

When examining UAV-derived tree heights compared to field measurements, some outliers were apparent. During field data collection, canopies that were "significantly overlapping" were noted in the comments field for trees that appeared to have overlapping canopies. This attribute was used to designate trees as "clumped" which was then used to remove 38 trees from the dataset. The tree height regression was then re-performed without the clumped trees to determine if the relationship changed. This analysis showed that removing clumped trees strengthens the relationship between UAV-derived tree heights and field measured heights (R^2 = 0.82, RMSE = 1.6 m) suggesting that the overlapping canopies may contribute more error in UAV tree height measurements (Figure 19). Similar results were found by Goldbergs et al (2017) where tree detections were much higher for dominant and co-dominant trees (70%), than they were for suppressed trees (35%) that may have been crowded by other trees leading to suppressed growth. In addition to overlapping canopies, during preliminary data analysis, Gambel oak (*Quercus gambelii*) often posed problems for UAV height estimates due to relatively low height and clumpy nature. However, only five Gambel oak trees were within field plots across the entire study area and only 1 was positively detected during tree segmentation. In the height regression omitting clumped trees, the detected Gambel oak tree was removed due to its clumped designation.

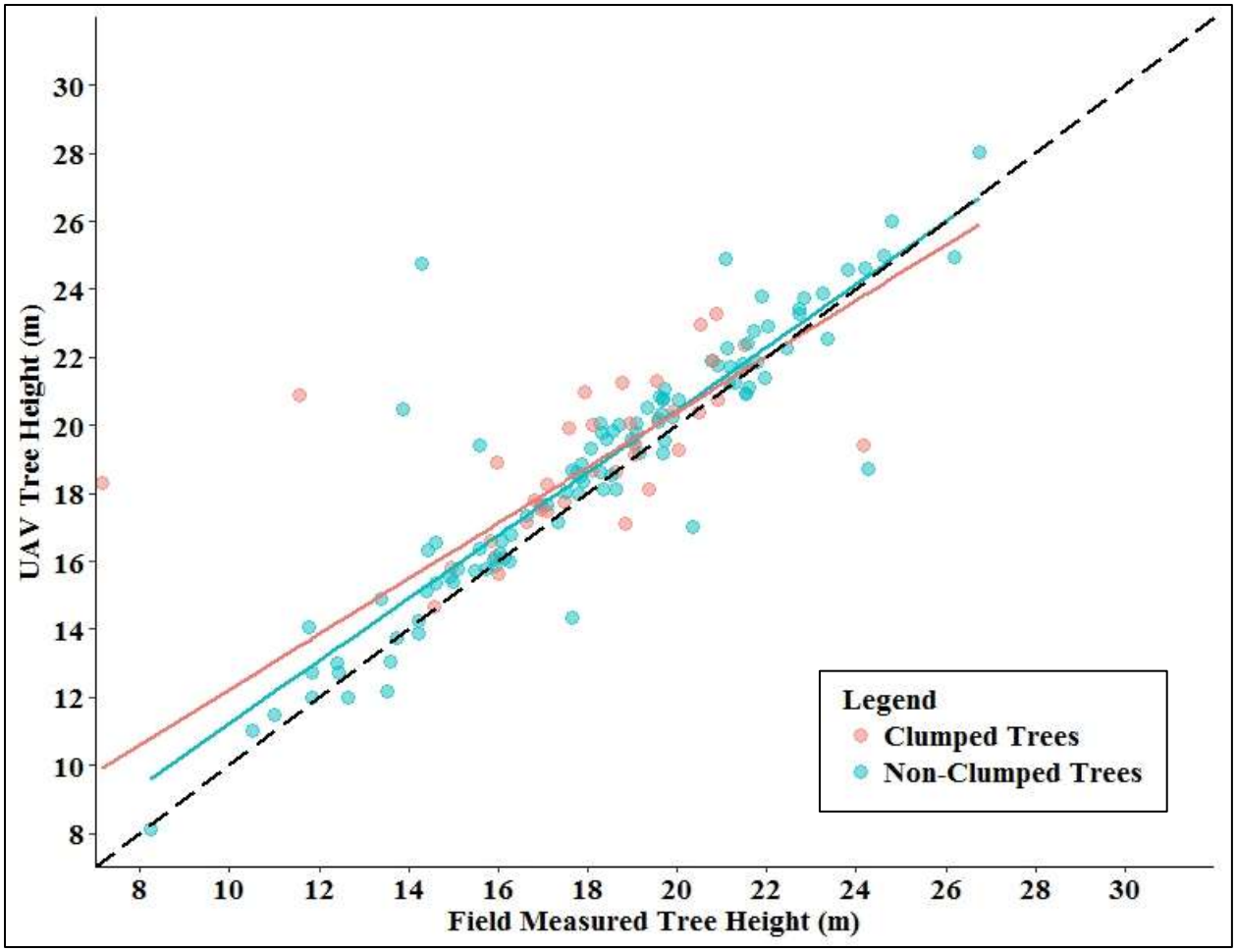

Figure 19: Regression relationships between UAV-derived tree heights and field measurements, with clumped and non-clumped trees. The fitted regression line for all trees is shown in red, the fitted regression line for only non-clumped trees is shown in blue, and the 1:1 line is shown as a black dotted line. By removing the clumped trees, the tree heights regression improved from an R^2 of 0.71 (RMSE = 1.83 m) to an R^2 of 0.82 (RMSE = 1.6 m) and showed a relationship that was generally closer to 1:1 than the relationship between all trees.

Canopy base height was estimated with UAV data by examining the relationship between field measured canopy base heights and the height percentiles of points within the point cloud for each tree. It was believed that the height percentiles could potentially provide a good predictor for canopy base height. When tested, several height percentiles showed a positive correlation with field measured canopy base height. However, there was no clear "best" predictor found. Several height percentiles had a correlation coefficient (R^2) ranging from 0.38 to 0.40. When

deciding on a height percentile to use as a predictor of canopy base height, rather than choosing the variable with the strongest correlation coefficient, an additional analysis was conducted to decide which variable resulted in a regression line closest to the 1:1 line with field measured base height. The 5th height percentile had a regression line closest to the 1:1 line with an R^2 of 0.34 and RMSE of 2.52 m. In addition, the tree height to canopy diameter relationship was also tested assuming that a tall tree with small canopy diameter would have a high base height. However, this relationship did not hold true when compared against field measurements. This discrepancy was mostly caused by the inaccurate measurement of canopy diameter with UAV-based methods.

Although the relationship between field-measured canopy base height and UAV-derived 5^{th} percentile height was somewhat low, the current standard of remotely sensed canopy base height data for use in modeling crown fire potential is based on the LANDFIRE database. Canopy base height data from LANDFIRE has been shown to have poor, and highly variable relationships with actual field observations. Correlation coefficients between LANDFIRE base height and field measurements were highly variable between an R^2 of 0 to 0.93, with a mean of 0.09 across 12 sites (Reeves et al., 2009). For this reason, the 5^{th} percentile estimate derived from the UAV data was believed to be sufficient as a predictor for base height in this study and, therefore, used as an input layer in FlamMap to model potential crown fire behavior.

At the time of this study, no other studies were found that attempted to estimate canopy base height using similar UAV-derived methods. However, canopy base height has been accurately measured using aerial lidar. In a western Washington douglas-fir forest, Andersen et al (2005) found aerial lidar estimates for canopy base height that were positively correlated to field measurements ($R^2 = 0.77$). Additionally, a separate study in a ponderosa pine dominated

forest in eastern Washington also showed a positive correlation between aerial lidar-derived and field-based measurements for canopy base heights (R^2 = 0.78) (Erdody & Moskal, 2010).

Canopy bulk density relies on estimates of both canopy mass and canopy volume. Using field measurements, canopy mass was estimated using the tree DBH and allometric equations for local ponderosa pine (Kaye et al., 2005). Canopy volume was estimated by determining the canopy height and average canopy radius to estimate the cylindrical volume of the canopy. Mass was divided by volume to estimate the overall canopy bulk density in kg/m^3. I attempted to mirror this process with UAV data, however there was no reliable estimate of DBH to use to estimate canopy mass. To overcome this, I established a tree height to DBH relationship which was used to predict the DBH of a tree given the overall height. This provided DBH estimates for each tree that was based on the UAV-derived tree height, and subsequently canopy mass was estimated for each tree. UAV-derived canopy volume was predicted similarly to field data. First, the canopy base height estimate was subtracted from the overall tree height to estimate the overall height of the canopy. Then, canopy diameters were used to calculate the average canopy diameters. The canopy height and diameter were then used to estimate canopy volume assuming a cylindrical canopy model. UAV-derived canopy mass and volume were then used to estimate the canopy bulk density of each tree.

The UAV-derived estimates of canopy bulk density showed a weak relationship with the field-based bulk density estimates. Differences between UAV-derived and field-derived estimates of canopy bulk density may have been caused by several factors. Rather than directly measuring DBH directly with UAV data, the UAV-derived estimates of canopy mass were based on DBH predicted from the tree height to DBH relationship created with field data. A logarithmic relationship was established between tree heights and DBH with an R^2 of 0.48 and p-

value of 3.11e-6. The UAV-derived tree height was used as an input to this model to predict a UAV-derived DBH. The UAV-derived DBH in this study was positively correlated with field-measured DBH, but the relationship was fairly weak (R^2= 0.38, RMSE= 4.82 cm). The DBH predictions were then used to estimate the canopy mass of each tree. When comparing canopy mass derived from the UAV data, and the canopy mass derived from field data, the relationship was also poor (R^2= 0.39, RMSE= 39.25 kg) (Figure 20).

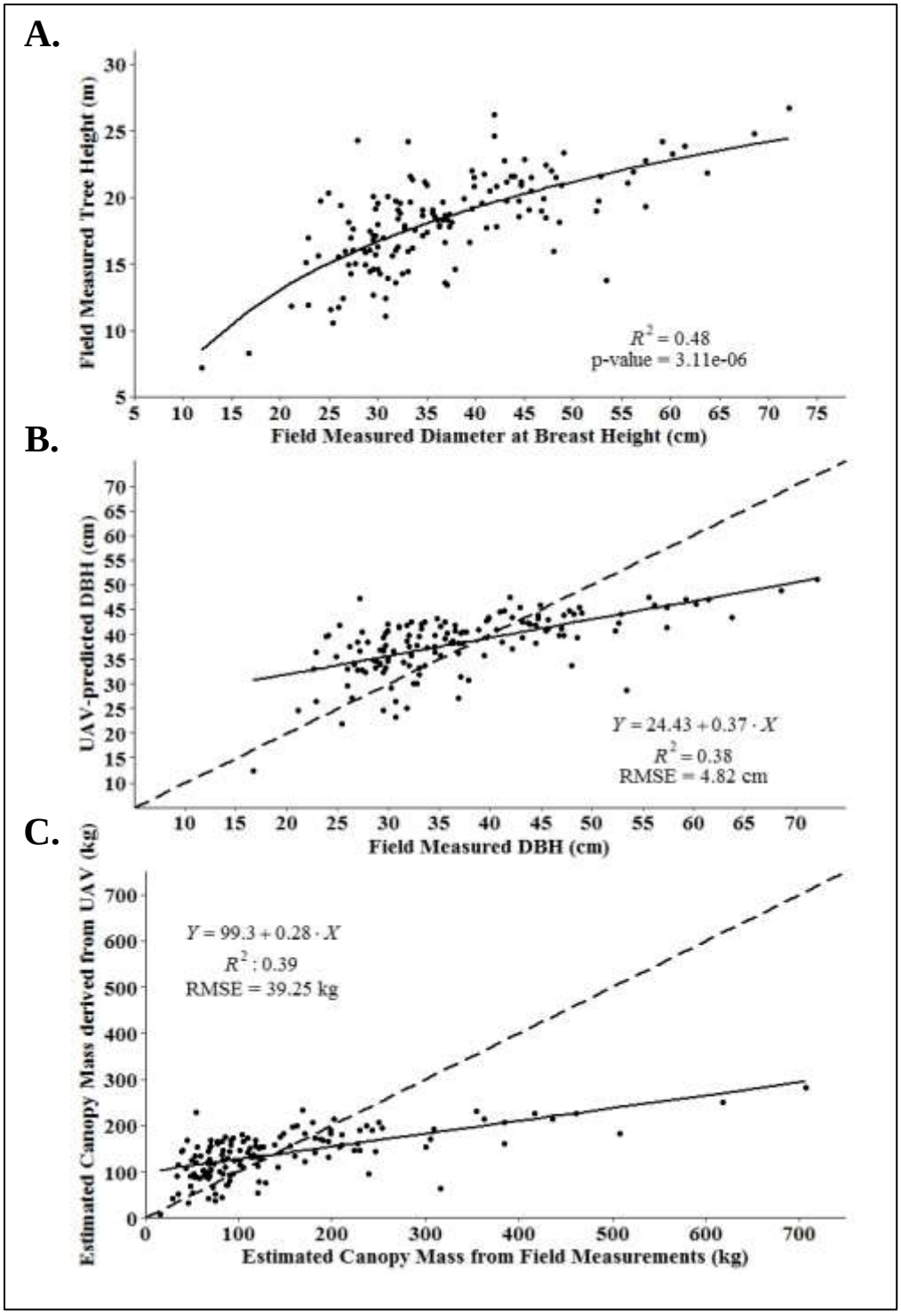

Figure 20: Regression relationships of data used to predict canopy mass. Logarithmic relationship between tree height and DBH that was used to predict DBH from UAV data (Panel A). The relationship of the UAV predicted DBH and field measured DBH (Panel B). Final canopy mass derived from UAV estimates and field measurements (Panel C). Solid lines

represent fitted regression lines for all graphs. Dashed line represents the 1:1 fitted line for linear regressions.

Additional error in canopy bulk density estimates also came from UAV-derived volume estimates. In order to estimate volume, three UAV-derived metrics were used: tree height, base height, and average canopy radius. Overall, UAV-derived tree heights were found to be reasonably accurate (R^2= 0.71, RMSE= 1.83 m). UAV-derived canopy base height was positively correlated to field measurements, but the relationship was relatively weak (R^2= 0.34, p-value = 2.63e-14, RMSE= 2.52 m). When UAV-derived canopy radius was compared to field measurements, the relationship was fairly poor (R^2= 0.26, RMSE= 0.88 m). A comparison of the UAV-derived canopy volume to the canopy volume estimated from field measurements showed that the overall volume estimated using each method was highly variable and contained a poor relationship (R^2= 0.33, p-value= 3.46e-14, RMSE= 246.13 m^3) (Figure 21).

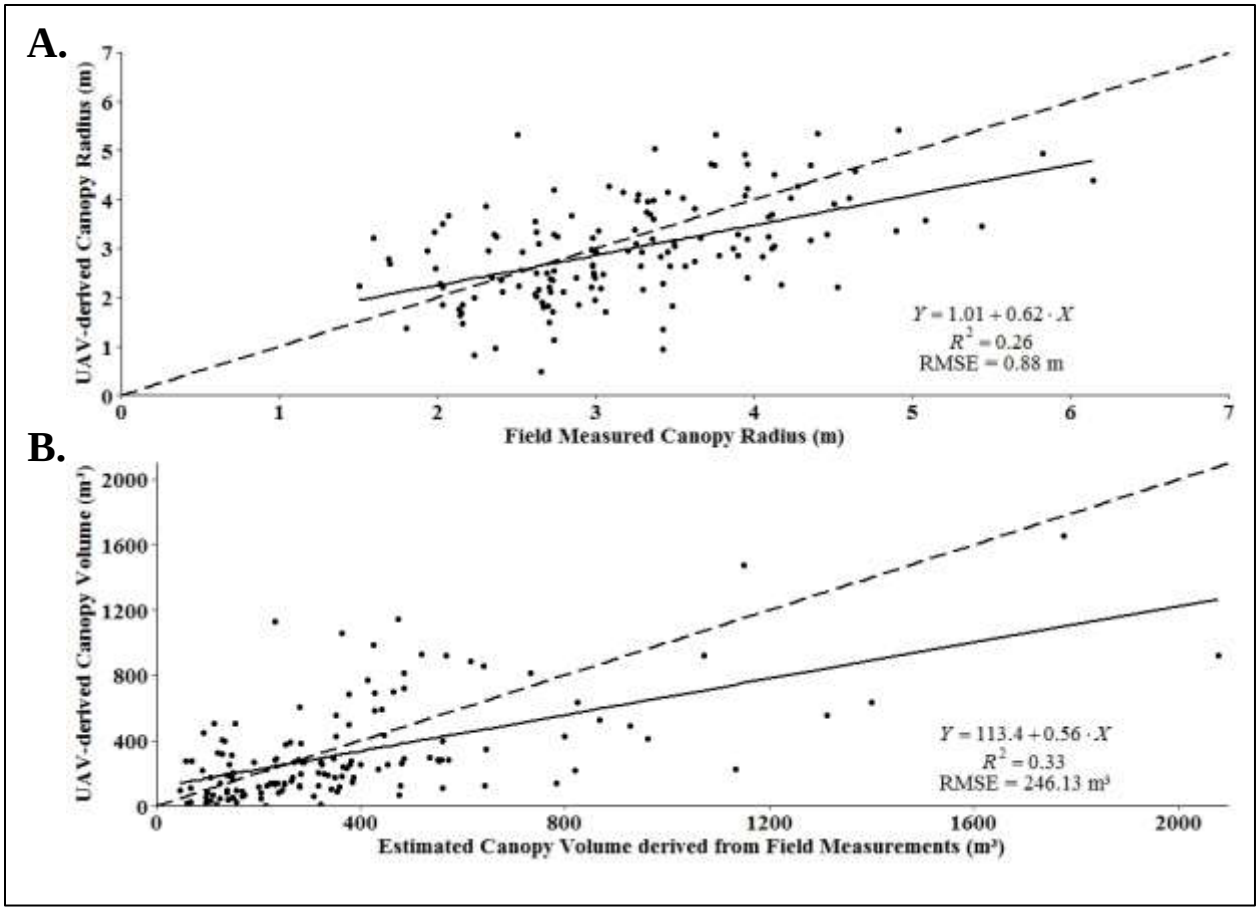

Figure 21: Regression relationships of data used to predict canopy volume. Comparison between UAV-derived and field-measured canopy radii (Panel A). Relationship of final canopy volume estimated from the UAV data and field measurements (Panel B). Solid lines represent fitted regression lines on both graphs. Dashed lines represent 1:1 lines for reference.

The compounding error in both the mass and volume estimates can explain the poor relationship found when comparing canopy bulk density estimates from UAV-derived and field-based measurements. The UAV-derived canopy bulk density and the canopy bulk density estimated from field measurements were not statistically correlated (R^2= 0.00, p-value= 0.34, RMSE= 0.3 kg/m^3).

When attempting to derive canopy bulk density estimates from UAV data, some limitations in the data were highlighted. Due to the fact that slight changes in volume and/or

mass could lead to large changes in canopy bulk density, the method used to estimate canopy bulk density from UAV data was unsuccessful at producing meaningful results. This could be attributed to the nature of UAV data and the impact of visual occlusion on measurements that may be below the canopy. For example, it proved to be difficult to measure both canopy base height, canopy diameter, and canopy bulk density possibly due to the UAV imagery not having a visual line-of-sight of the bottoms and edges of tree canopies- which may oftentimes be overlapping. In general, this is a potential limitation for UAV imagery being used in areas of high canopy cover and attempting to make measurements of objects that may be obstructed by tree canopy (Dandois & Ellis, 2013; Wallace et al., 2016; Goldbergs et al., 2018).

Although, difficult to do with the UAV image-based methods used our study, canopy bulk density has been accurately estimated using aerial lidar. Both Andersen et al (2005) and Erdody and Moskal (2010) estimated canopy bulk density specifically as a canopy fuel metric. Both of these studies were conducted in Washington State, however Andersen et al (2005) estimated canopy fuels in a Douglas-fir dominated forest, and the study by Erdody and Moskal (2010) was conducted in ponderosa pine forest. High correlations between lidar-derived canopy bulk density estimates to those based on field measurements were found by both Anderson et al (2005) and Erdody and Moskal (2010) (R^2 = 0.86, R^2 = 0.83 respectively).

Future Considerations for Tree Segmentation

Due to the stratified sampling design that was specifically aimed at collecting data from areas of varying density, plot data could not be used to interpret overall tree density across the area. In future studies, tree density information could help target the segmentation algorithm to have the best detection rates in areas that are most representative of the survey location as a whole. For

example, if 70% of the study area has density class 2, the segmentation model could compensate accordingly.

In this study, individual tree segmentation algorithms performed differently in areas of low or high tree density. This characteristic of segmenting individual trees from point cloud data makes it difficult to balance under- and over-segmentation in areas of variable tree density. To help overcome this, assuming that canopy cover informs tree density estimates, this study utilized an optimized tree segmentation that adapted the segmentation according to areas of different canopy cover. Two classes, high (> 50%) and low (≤ 50%), of canopy cover were used to select either of two different tree segmentation parameters. It is important to note that both tree segmentation algorithms were used across the entire study area, and the canopy cover classes were only used to select the segmentation outputs accordingly. This study only utilized two canopy cover classes, but more classes could have been used. Overall, the ability to adapt the parameters being used in a tree segmentation algorithm based on other available information (canopy cover, spectral data, etc) could help address the issue of over- and under-segmentation of trees in areas of variable tree density. This concept should be explored more to produce accurate tree segmentations.

Prior to the implementation of the tree segmentation algorithms on the UAV point cloud data, a NDVI raster created from the orthomosaic was used to "colorize" the point cloud points which added a NDVI value to each point. An NDVI threshold was then used to remove all points that did not resemble vegetation. This process was effective at creating a subset point cloud that represented only tree points which was then used in the tree segmentation algorithm. The Li (2012) algorithm used in this study then analyzes each point of the point cloud to aggregate and identify individual trees. However, this process was strictly based on the coordinate location (X,

Y, Z) of each point. Future research may consider incorporating spectral data, such as NDVI, RGB, or others, within the actual decision-making process of the tree segmentation algorithm. Although preliminary analysis of three different tree segmentation algorithms (W. Li et al., 2012; Dalponte et al., 2016; Oles et al., 2018) was conducted as part of this study, other tree segmentation algorithms (Silva et al., 2016; Ayrey et al., 2017) may yield different results and should be tested.

This study performed individual tree segmentation and subsequent measurement of tree attributes using SfM-derived point cloud data and multispectral imagery. This method offers a lower-cost alternative to aerial lidar surveys, but also has associated tradeoffs. Although UAV imagery can be less expensive to acquire than aerial lidar surveys, aerial lidar can cover a considerably larger area than a single, or even several, UAV surveys. Since lidar is an active remote sensing method, lighting conditions and shadows are less of a concern. Additionally, options such as multiple return and full waveform lidar can penetrate tree canopies and perhaps be less affected by visual occlusion and provide better measurements of canopy base height than UAV imagery. There are also some operational restrictions such as takeoff/landing areas that, depending on the area, may be less of a concern with aerial lidar. On the other hand, the lower cost of UAV imaging equipment compared to aerial lidar makes it easier for landowners, or agencies, to purchase equipment and conduct surveys in-house. This option allows a much more flexible temporal frequency of UAV image acquisitions to be defined by the user. Depending on the user's need and objectives, both aerial lidar and UAV imagery may be viable options.

Fire Behavior Modeling

Using UAV data for Modeling Fire Behavior

The LANDFIRE database has traditionally been the major source of data used to model potential crown fire behavior. In this study, UAV data were used as inputs to FlamMap for modeling potential crown fire behavior. The overall effects of using UAV data from the study area was a drastic reduction in the amount of area that was modeled as active and passive crown fire. In the sensitivity analysis conducted in this study, the UAV-derived canopy base height was the single largest influence of this reduction in crown fire area. Canopy base height is the primary factor that determines the transition from surface fire to crown fire. A low canopy base height makes this transition more likely to occur, whereas a high canopy base height reduces the likelihood of crown fire initiation (Cruz et al., 2002; Scott, 2006). When comparing the canopy base height estimates, the UAV estimate showed an average canopy base height between 4-5 m, whereas LANDFIRE data had a mean canopy base height of less than 1 m. Field data were distributed by stratified random sampling, thus not entirely representative of the study area. However, the mean canopy base height from field data was 7.7 m, which may potentially indicate a substantial underestimation from the LANDFIRE data. This difference could explain the discrepancy in the amount of crown fire modeled using each data source. The primary hypothesis regarding UAV-derived crown fire behavior models was that these models would show more variation than LANDFIRE-derived models. The hypothesis was supported by an increased variation in the UAV-derived models, however the dramatic decrease of potential crown fire activity in general was unexpected.

LANDFIRE data used to model crown fire behavior is only available in 30 m resolution, whereas UAV-derived data were estimated from sub-meter data and resampled to 10 m

resolution. This difference in spatial resolution may also be responsible for the differences in data values and the subsequent crown fire models. In general, the UAV data accurately depicted areas of less canopy cover and decreased canopy height. The fine resolution of UAV data relative to LANDFIRE data may be more effective at detecting these areas that were often less than the size of a single LANDFIRE data pixel (30 m). The effects of data resolution may have also lead to the differences in crown fire models from UAV and LANDFIRE data. For example, there were areas where minimal tree cover was present due to small roads, trails, and gaps between trees. Within the UAV imagery, these areas caused decreased estimates for canopy cover and canopy height due to the absence of trees. However, these gaps were often not represented in the LANDFIRE data due to the coarse spatial resolution (Figure 22).

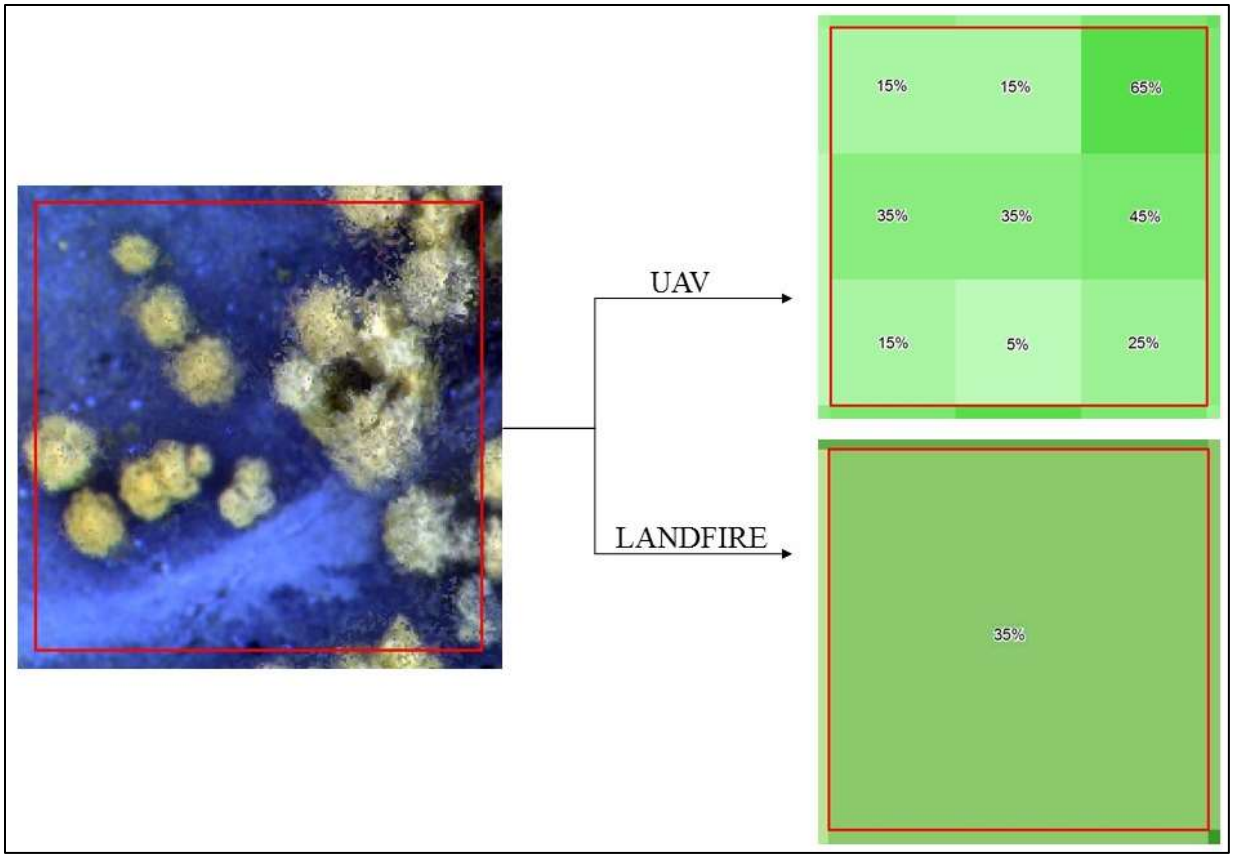

Figure 22: Canopy cover estimates of the same 30 x 30 m area from UAV-derived and LANDFIRE data. Due to the high resolution of UAV data, the UAV canopy cover estimates are able to represent variability from roads and gaps that are not shown in the LANDFIRE data. When modeling crown fire potential with UAV data, these areas tended to model less crown fire causing less crown fire potential across the entire study area in general relative to LANDFIRE-based models.

A limitation of this study was the coarse estimation of base height, and the inability to estimate canopy bulk density. Both of these measurements rely on accurate depictions of canopy edges and bottoms, both of which were difficult to estimate with the UAV data used in this study. However, in future studies, the integration of lidar data may produce better estimates of both of these variables. Additionally, the fire behavior fuel models used by FlamMap to model fire behavior were not estimated in this study. Future advances in remote sensing capabilities and

modeling may provide a means to estimate fire behavior fuel models with reliable accuracy, thus leading to more effective modeling of potential wildfire behavior.

Future Consideration for Modeling Fire Behavior with UAV data

LANDFIRE fuels data is known to have spatially variables accuracies, in which some are very low (Reeves et al., 2009). An analysis of the LANDFIRE spatial fuels variables was conducted by Reeves et al. (2009) by performing an accuracy assessment of the LANDFIRE fuels products by comparing them to Forest Inventory and Analysis (FIA) plot level data. Overall, canopy cover was found to be overestimated. In their study area, the LANDFIRE canopy cover ranged up to 85%, whereas most field-observed stands in the area showed canopy cover ranging from 25 to 55%. Estimates of canopy base height in LANDFIRE were shown to have relatively poor relationships with field-measured base heights with an average R^2 value of 0.09 that was highly variable with ranges between 0 and 0.93 across 12 sites. Canopy bulk density had a better relationship to field estimates with an average R^2 value of 0.58 which ranged from 0.45 to 0.85 across 12 sites.

An accuracy assessment of fuel models was not conducted due to no existing independent data source. Reeves et al. (2009) additionally state that fuel models are difficult to assess due to the lack of instruments and inventory techniques for measuring fuel model, which makes this measurement highly subjective. Additionally, when comparing predicted fire behavior models to those observed after an actual wildfire event, the addition of local data adjustments has shown to more accurately simulate model outcomes (Krasnow et al., 2009). Other studies have shown that LANDFIRE data accuracies should be verified and data adjusted accordingly by the user (Reeves et al., 2006; Rollins, 2009) before attempting to use for making management decisions. The sensitivity analysis conducted in this study showed that the input layers in FlamMap had a

great impact on the potential crown fire modeled across the study area. UAV surveys offer a potential method of providing correction and/or replacing portions of LANDFIRE fuels data with information that can be more representative of local conditions.

The ability for land managers to use UAV data to supplement LANDFIRE data for modeling potential crown fire behavior has applications for both planning and monitoring of forest fuels reduction treatments. For planning purposes, UAV data may provide managers with a tool for treatment prioritization, which may be particularly useful in situations of limited resource availability for fuels reduction treatments. Additionally, the high spatial and temporal resolutions of UAV data could potentially be very useful for monitoring fuels reduction treatments. Rapid feedback from UAV surveys could allow opportunities for adaptive management and treatment calibration that may otherwise be difficult. The precise planning and monitoring made possible with UAV data may be especially beneficial in sensitive management areas such as the wildland urban interface and wildlife habitat.

Chapter 5 Conclusion

This study tested the feasibility of using a fixed-wing UAV with multispectral sensor for estimating forest canopy fuels and structure in a southwestern ponderosa pine forest. The results indicate that UAV surveys can be used to produce accurate estimates for forest characteristics that can be visualized from above the canopy such as: canopy cover, canopy height, and tree density. Canopy cover and canopy height proved to be the most reliable estimates. Tree density estimates are directly related to the accuracy of individual tree segmentation, which tends to underperform in areas of increased tree density. However, tree segmentation can be improved by utilizing adaptive algorithm parameters that adjust according to canopy cover. Accuracy of canopy base height estimates was low, however reasonably comparable to LANDFIRE estimates. Canopy bulk density proved to be the most difficult metric to estimate using the UAV methods in our study, and showed no correlation to estimates using field measurements. As part of this study, forest canopy fuels estimates from UAV data were used to supplement LANDFIRE data and model crown fire behavior across the study area. Crown fire behavior outputs using UAV data yielded a drastic reduction in the total amount of potential crown fire. It is important to note that although the crown fire behavior outputs were very different between LANDFIRE and UAV data, this study did not seek to estimate which models were most accurate to real-life crown fire behavior. However, the sensitivity analysis showed that the input data in FlamMap can have a drastic effect on the crown fire potential modeled in an area. Managers should consider the source and accuracies of the input data when modeling fire behavior and making management decisions. Overall, results from this study show that UAV surveys could be used to estimate forest canopy fuels and structure with reasonable accuracy. These estimates could then be used to adjust, or used in conjunction with, other data such as LANDFIRE making it a

potentially useful tool for forest managers. In general, UAV surveys offer more control of temporal resolution in data collection making it a useful tool for rapid assessments and adaptive management. Although typically more costly and less flexible than UAV surveys, aerial lidar surveys may provide better estimates for the metrics that were difficult to measure using UAV imagery. Future studies should explore the use of both technologies in combination to measure forest canopy fuels and structure. Aerial lidar surveys may be used to develop baseline data for planning, and UAV surveys could be used as a cost-effective intermittent data collection for monitoring purposes. With the increasing need for the management of forest fuels, the combination of these technologies may provide land managers with an effective way of planning and monitoring fuels treatments.

References

Agee, J.K., & Skinner, C.N. (2005). Basic principles of forest fuel reduction treatments. *Forest Ecology and Management, 211*, 83-96

Allen, C.D., Savage, M., Falk, D.A., Suckling, K.F., Swetnam, T.W., Schulke, T., et al. (2002). Ecological restoration of southwestern ponderosa pine ecosystems: a broad perspective. *Ecological Applications, 12*, 1418-1433

Allred, S. (2015). *Ponderosa; Big Pine of the Southwest.* : University of Arizona Press

Andersen, H.E., McGaughey, R.J., & Reutebuch, S.E. (2005). Estimating forest canopy fuel parameters using LIDAR data. *Remote Sensing of Environment, 94*, 441-449

Anderson, H.E. (1982). Aids to determining fuel models for estimating fire behavior. *The Bark Beetles, Fuels, and Fire Bibliography*, 143

Ayrey, E., Fraver, S., Kershaw, J.A., Kenefic, L.S., Hayes, D., Weiskittel, A.R., et al. (2017). Layer Stacking: A Novel Algorithm for Individual Forest Tree Segmentation from LiDAR Point Clouds. *Canadian Journal of Remote Sensing, 43*, 16-27

Baker, M.B. (1986). Effects of ponderosa pine treatments on water yield in Arizona. *Water Resources Research, 22*, 67-73

Coconino National Forest. (2015). Final Environmental Impact Statement for the Flagstaff Watershed Protection Project. *USDA Forest Service Southwest Region, MB-R3-04-27*

Coconino National Forest. (n.d.a). Pipeline Trail No. 42. https://www.fs.usda.gov/recarea/coconino/recarea/?recid=55152 Date Accessed: 11/21/2017.

Coconino National Forest. (n.d.b). Coconino National Forest GIS Data. https://www.fs.usda.gov/detail/r3/landmanagement/gis/?cid=stelprdb5209303 Date Accessed: 02/01/2017.

Combrink, T., Cothran, C., Fox, W., Peterson, J., & Snider, G.B. (2013). Issues in Forest Restoration: Full Cost Accounting of the 2010 Schultz Fire. *ERI White Paper–Issues in Forest Restoration*

Cooper, C.F. (1960). Changes in vegetation, structure, and growth of southwestern pine forests since white settlement. *Ecological Monographs, 30*, 129-164

Covington, W.W., & Moore, M.M. (1994a). Postsettlement changes in natural fire regimes and forest structure: ecological restoration of old-growth ponderosa pine forests. *Journal of Sustainable Forestry, 2*, 153-181

Covington, W.W., & Moore, M.M. (1994b). Southwestern Ponderosa Forest Structure - Changes since Euro-American Settlement. *Journal of Forestry, 92*, 39-47

Covington, W.W., Fule, P.Z., Moore, M.M., Hart, S.C., Kolb, T.E., Mast, J.N., et al. (1997). Restoring ecosystem health in ponderosa pine forests of the Southwest. *Journal of Forestry, 95*, 23-29

Covington, W.W., Fule, P.Z., Hart, S.C., & Weaver, R.P. (2001). Modeling ecological restoration effects on ponderosa pine forest structure. *Restoration Ecology, 9*, 421-431

Cruz, M.G., Alexander, M.E., & Wakimoto, R.H. (2002). Predicting crown fire behavior to support forest fire management decision-making.

Dalponte, M., Coomes, D.A., & Murrell, D. (2016). Tree- centric mapping of forest carbon density from airborne laser scanning and hyperspectral data. *Methods in Ecology and Evolution, 7*, 1236-1245

Dandois, J.P., & Ellis, E.C. (2013). High spatial resolution three-dimensional mapping of vegetation spectral dynamics using computer vision. *Remote Sensing of Environment, 136*, 259-276

Dandois, J.P., Olano, M., & Ellis, E.C. (2015). Optimal altitude, overlap, and weather conditions for computer vision UAV estimates of forest structure. *Remote Sensing, 7*, 13895-13920

Dunford, R., Michel, K., Gagnage, M., Piegay, H., & Tremelo, M. (2009). Potential and constraints of Unmanned Aerial Vehicle technology for the characterization of Mediterranean riparian forest. *International Journal of Remote Sensing, 30*, 4915-4935

Edson, C., & Wing, M.G. (2011). Airborne Light Detection and Ranging (LiDAR) for Individual Tree Stem Location, Height, and Biomass Measurements. *Remote Sensing, 3*, 2494-2528

Erdody, T.L., & Moskal, L.M. (2010). Fusion of LiDAR and imagery for estimating forest canopy fuels. *Remote Sensing of Environment, 114*, 725-737

ESRI. (2015). ArcGIS for Desktop. , *10.4.1.5686*

Feeney, S.R., Kolb, T.E., Covington, W.W., & Wagner, M.R. (1998). Influence of thinning and burning restoration treatments on presettlement ponderosa pines at the Gus Pearson Natural Area. *Canadian Journal of Forest Research, 28*, 1295-1306

Finney, M.A. (2006). An Overview of FlamMap Fire Modeling Capabilities. *USDA Forest Service Proceedings, RMRS-P-41*

Fitzgerald, S.A. (2005). Fire ecology of ponderosa pine and the rebuilding of fire-resilient ponderosa pine ecoystems. *USDA Forest Service, Pacific Southwest Research Station, General Technical Report PSW-GTR-198*

Franklin, S.E., Hall, R.J., Moskal, L.M., Maudie, A.J., & Lavigne, M.B. (2000). Incorporating texture into classification of forest species composition from airborne multispectral images. *International Journal of Remote Sensing, 21,* 61-79

Fule, P.Z., Crouse, J.E., Cocke, A.E., Moore, M.M., & Covington, W.W. (2004). Changes in canopy fuels and potential fire behavior 1880–2040: Grand Canyon, Arizona. *Ecological Modelling, 175,* 231-248

Ganey, J.L., Block, W.M., Jenness, J.S., & Wilson, R.A. (1999). Mexican Spotted Owl Home Range and Habitat Use in Pine-Oak Forest: Implications for Forest Management. *Forest Science, 45,* 127-135

Getzin, S., Wiegand, K., & Schöning, I. (2012). Assessing biodiversity in forests using very high- resolution images and unmanned aerial vehicles. *Methods in Ecology and Evolution, 3,* 397-404

Goldbergs, G., Maier, S.W., Levick, S.R., & Edwards, A. (2018). Efficiency of Individual Tree Detection Approaches Based on Light-Weight and Low-Cost UAS Imagery in Australian Savannas. *Remote Sensing, 10,* 161

Graham, R.T., McCaffrey, S., & Jain, T.B. (2004). Science basis for changing forest structure to modify wildfire behavior and severity. *USDA Forest Service Rocky Mountain Research Station, General Technical Report RMRS-GTR-120*

Homer, C., Huang, C.Q., Yang, L.M., Wylie, B., & Coan, M. (2004). Development of a 2001 National Land-Cover Database for the United States. *Photogrammetric Engineering and Remote Sensing, 70,* 829-840

Hummel, S., Hudak, A.T., Uebler, E.H., Falkowski, M.J., & Megown, K.A. (2011). A comparison of accuracy and cost of LiDAR versus stand exam data for landscape management on the Malheur National Forest. *Journal of Forestry, 109,* 267-273

Hyde, P., Dubayah, R., Walker, W., Blair, J.B., Hofton, M., & Hunsaker, C. (2006). Mapping forest structure for wildlife habitat analysis using multi-sensor (LiDAR, SAR/InSAR, ETM , Quickbird) synergy. *Remote Sensing of Environment, 102,* 63-73

Iizuka, K., Yonehara, T., Itoh, M., & Kosugi, Y. (2018). Estimating tree height and diameter at breast height (DBH) from digital surface models and orthophotos obtained with an unmanned aerial system for a Japanese cypress (Chamaecyparis obtusa) forest. *Remote Sensing, 10,* 13

Jameson, D.A. (1967). The relationship of tree overstory and herbaceous understory vegetation. *Journal of Range Management, 20,* 247-249

Jensen, J.L.R., & Mathews, A.J. (2016). Assessment of image-based point cloud products to generate a bare earth surface and estimate canopy heights in a woodland ecosystem. *Remote Sensing, 8,* 50

Kaye, J.P., Hart, S.C., Fule, F.Z., Covington, W.W., Moore, M.W., & Kaye, M.W. (2005). Initial carbon, nitrogen, and phosphorous fluxes following ponderosa pine restoration treatments. *Ecological Applications, 15*, 1581-1593

Kaye, J.P., Hart, S.C., Cobb, R.C., & Stone, J.E. (2002). Water and nutrient outflow following the ecological restoration of a ponderosa pine- bunchgrass ecosystem. *Restoration Ecology, 7*, 252-261

Keane, R.E., Holsinger, L.M., & Pratt, S.D. (2006). *Simulating historical landscape dynamics using the landscape fire succession model LANDSUM version 4.0.* : US Department of Agriculture, Forest Service, Rocky Mountain Research Station

Keane, R.E., Reinhardt, E.D., Scott, J., Gray, K., & Reardon, J. (2005). Estimating forest canopy bulk density using six indirect methods. *Canadian Journal of forest research, 35*, 724-739

Key, T., Warner, T.A., McGraw, J.B., & Fajvan, M.A. (2001). A comparison of multispectral and multitemporal information in high spatial resolution imagery for classification of individual tree species in a temperate hardwood forest. *Remote Sensing of Environment, 75*, 100-112

Kolb, T.E., Holmberg, K.M., Wagner, M.R., & Stone, J.E. (1998). Regulation of ponderosa pine foliar physiology and insect resistance mechanisms by basal area treatments. *Tree physiology, 18*, 375-381

Krasnow, K., Schoennagel, T., & Veblen, T.T. (2009). Forest fuel mapping and evaluation of LANDFIRE fuel maps in Boulder County, Colorado, USA. *Forest Ecology and Management, 257*, 1603-1612

Lackey, R.T. (1998). Seven pillars of ecosystem management. *Landscape and Urban Planning, 40*, 21-30

Landres, P.B., Morgan, P., & Swanson, F.J. (1999). Overview of the use of natural variability concepts in managing ecological systems. *Ecological Applications, 9*, 1179-1188

Larson, A.J., & Churchill, D. (2012). Tree spatial patterns in fire-frequent forests of western North America, including mechanisms of pattern formation and implications for designing fuel reduction and restoration treatments. *Forest Ecology and Management, 267*, 74-92

Laughlin, D.C., Moore, M.M., Bakker, J.D., Casey, C.A., Springer, J.D., Fulé, P.Z., et al. (2006). Assessing targets for the restoration of herbaceous vegetation in ponderosa pine forests. *Restoration Ecology, 14*, 548-560

Li, W., Guo, Q., Jakubowski, M.K., & Kelly, M. (2012). A New Method for Segmenting Individual Trees from the Lidar Point Cloud. *Photogrammetric Engineering and Remote Sensing, 78*, 75-84

Li, X., & Strahler, A.H. (1985). Geometric-optical modeling of a conifer forest canopy. *IEEE Transactions on Geoscience and Remote Sensing*, 705-721

Lydersen, J.M., North, M.P., Knapp, E.E., & Collins, B.M. (2013). Quantifying spatial patterns of tree groups and gaps in mixed-conifer forests: Reference conditions and long-term changes following fire suppression and logging. *Forest Ecology and Management, 304*, 370-382

Makynen, J., Holmlund, C., Saari, H., Ojala, K., & Antila, T. (2011). Unmanned aerial vehicle (UAV) operated megapixel spectral camera. *, 8186*, 81860Y

Mast, J.N., Fule, P.Z., Moore, M.M., Covington, W.W., & Waltz, A.E. (1999). Restoration of presettlement age structure of an Arizona ponderosa pine forest. *Ecological Applications, 9*, 228-239

Miller, J.D., Safford, H.D., Crimmins, M., & Thode, A.E. (2009). Quantitative evidence for increasing forest fire severity in the Sierra Nevada and southern Cascade Mountains, California and Nevada, USA. *Ecosystems, 12*, 16-32

Mohan, M., Silva, C.A., Klauberg, C., Jat, P., Catts, G., Cardil, A., et al. (2017). Individual Tree Detection from Unmanned Aerial Vehicle (UAV) Derived Canopy Height Model in an Open Canopy Mixed Conifer Forest. *Forests, 8*, 340

Moore, M.M., Huffman, D.W., Fule, P.Z., Covington, W.W., & Crouse, J.E. (2004). Comparison of historical and contemporary forest structure and composition on permanent plots in southwestern ponderosa pine forests. *Forest Science, 50*, 162-176

Moore, M.M., Casey, C.A., Bakker, J.D., Springer, J.D., Fule, P.Z., Covington, W.W., et al. (2006). Herbaceous vegetation responses (1992–2004) to restoration treatments in a ponderosa pine forest. *Rangeland Ecology & Management, 59*, 135-144

Morgenroth, J., & Gomez, C. (2014). Assessment of tree structure using a 3D image analysis technique—A proof of concept. *Urban Forestry & Urban Greening, 13*, 198-203

Mottek Lucas, A. (2015). Flagstaff watershed protection project: creating solutions through community partnerships. *Flagstaff, AZ: Ecological Restoration Institute, Northern Arizona University, ERI White Paper- Issues in Forest Restoration*

Mueller, J.M., Swaffar, W., Nielsen, E.A., Springer, A.E., & Lopez, S.M. (2013). Estimating the value of watershed services following forest restoration. *Water Resources Research, 49*, 1773-1781

Naesset, E., & Bjerknes, K.O. (2001). Estimating tree heights and number of stems in young forest stands using airborne laser scanner data. *Remote Sensing of Environment, 78*, 328-340

National Oceanic and Atmospheric Administration. (n.d.). Data Tools: 1981-2010 Normals. https://www.ncdc.noaa.gov/cdo-web/datatools/normals Date Accessed: 11/21/2017.

Natural Resources Conservation Service. (2017). Web Soil Survey. https://websoilsurvey.nrcs.usda.gov/app/ Date Accessed: 11/24/2017.

Noss, R.F., Beier, P., Wallace Covington, W., Edward Grumbine, R., Lindenmayer, D.B., Prather, J.W., et al. (2006). Recommendations for integrating restoration ecology and conservation biology in ponderosa pine forests of the southwestern United States. *Restoration Ecology, 14*, 4-10

Oles, A., Pau, G., Skylar, O., & Huber, W. (2018). Introduction to EBImage: Image processing and analysis.

Ozdemir, I., & Karnieli, A. (2011). Predicting forest structural parameters using the image texture derived from WorldView-2 multispectral imagery in a dryland forest, Israel. *International Journal of Applied Earth Observation and Geoinformation, 13*, 701-710

Patton, D.R., & Severson, K.E. (1989). WILDHARE: a wildlife habitat relationships data model for southwestern ponderosa pine. *General technical report RM-Rocky Mountain Forest and Range Experiment Station, US Department of Agriculture, Forest Service (USA)*

Popescu, S.C., & Zhao, K. (2008). A voxel-based lidar method for estimating crown base height for deciduous and pine trees. *Remote Sensing of Environment, 112*, 767-781

Prather, J.W., Noss, R.F., & Sisk, T.D. (2008). Real versus perceived conflicts between restoration of ponderosa pine forests and conservation of the Mexican spotted owl. *Forest Policy and Economics, 10*, 140-150

Puliti, S., Orka, H.O., Gobakken, T., & Nasset, E. (2015). Inventory of small forest areas using an unmanned aerial system. *Remote Sensing, 7*, 9632-9654

Reeves, M.C., Ryan, K.C., Rollins, M.G., & Thompson, T.G. (2009). Spatial fuel data products of the LANDFIRE Project. *International Journal of Wildland Fire, 18*, 250-267

Reeves, M.C., Kost, J.R., & Ryan, K.C. (2006). Fuel Products of the LANDFIRE Project. *USDA Forest Service Proceedings, RMRS-P-41*

Reynolds, R.T., Meador, A.J.S., Youtz, J.A., Nicolet, T., Matonis, M.S., Jackson, P.L., et al. (2013). Restoring composition and structure in Southwestern frequent-fire forests: A science-based framework for improving ecosystem resiliency. *USDA Forest Service Rocky Mountain Research Station, General Technical Report RMRS-GTR-310*

Roberts, D.A., Ustin, S.L., Ogunjemiyo, S., Greenberg, J., Dobrowski, S.Z., Chen, J., et al. (2004). Spectral and structural measures of northwest forest vegetation at leaf to landscape scales. *Ecosystems, 7*, 545-562

Rollins, M.G. (2009). LANDFIRE: a nationally consistent vegetation, wildland fire, and fuel assessment. *International Journal of Wildland Fire, 18*, 235-249

Rothermel, R.C. (1972). A mathematical model for predicting fire spread in wildland fuels. *USDA Forest Service Intermountain Forest and Range Experiment Station, Research Paper INT-115*

Saari, H., Pellikka, I., Pesonen, L., Tuominen, S., Heikkila, J., Holmlund, C., et al. (2011). Unmanned Aerial Vehicle (UAV) operated spectral camera system for forest and agriculture applications. , *8174*, 81740H

Sankey, T., Donald, J., McVay, J., & Sankey, J. (2017). UAV lidar and hyperspectral fusion for forest monitoring in the southwestern USA. *Remote Sensing of Environment, 195*, 30-43

Savage, M., Brown, P.M., & Feddema, J. (1996). The role of climate in a pine forest regeneration pulse in the southwestern United States. *Ecoscience, 3*, 310-318

Scott, J.H. (2006). Comparison of Crown Fire Modeling Systems Used in Three Fire Management Applications. *USDA Forest Service Research Paper, RMRS-RP-58*

Scott, J.H., & Burgan, R.E. (2005). Standard Fire Behavior Fuel Models: A Comprehensive Set for Use with Rothermel's Surface Fire Spread Model. *USDA Forest Service Rocky Mountain Research Station, General Technical Report RMRS-GTR-153*

Scott, J.H., & Reinhardt, E.D. (2001). Assessing crown fire potential by linking models of surface and crown fire behavior. *USDA Forest Service Research Paper*, 1

SenseFly. (n.d.a). eBee SenseFly. https://www.sensefly.com/fileadmin/user_upload/sensefly/documents/brochures/eBee_en.pdf Date Accessed: 02/01/2017.

SenseFly. (n.d.b). eMotion 2. https://www.sensefly.com/software/emotion-2/

Silva, C.A., Hudak, A.T., Vierling, L.A., Loudermilk, E.L., O'Brien, J.J., Hiers, J.K., et al. (2016). Imputation of Individual Longleaf Pine (Pinus palustris Mill.) Tree Attributes from Field and LiDAR Data. *Canadian Journal of Remote Sensing, 42*, 554-573

Simonin, K., Kolb, T.E., Montes-Helu, M., & Koch, G.W. (2007). The influence of thinning on components of stand water balance in a ponderosa pine forest stand during and after extreme drought. *Agricultural and Forest Meteorology, 143*, 266-276

Stephens, S.L., Agee, J.K., Fule, P.Z., North, M.P., Romme, W.H., Swetnam, T.W., et al. (2013). Managing forests and fire in changing climates. *Science, 342*, 41-42

Stoddard, M.T., Meador, A.S., Fule, P.Z., & Korb, J.E. (2015). Five-year post-restoration conditions and simulated climate-change trajectories in a warm/dry mixed-conifer forest, southwestern Colorado, USA. *Forest Ecology and Management, 356*, 253-261

Stratton, R.D. (2004). Assessing the effectiveness of landscape fuel treatments on fire growth and behavior. *Journal of Forestry, 102*, 32-40

Stratton, R.D. (2009). Guidebook on LANDFIRE Fuels Data Acquisition, Critique, Modification, Maintenance, and Model Calibration. *USDA Forest Service Rocky Mountain Research Station, General Technical Report RMRS-GTR-220*

Stratton, R.D. (2006). Guidance on Spatial Wildland Fire Analysis: Models, Tools, and Techniques. *USDA Forest Service Rocky Mountain Research Station, General Technical Report RMRS-GTR-183*

Thornton, P.E., Running, S.W., & White, M.A. (1997). Generating surfaces of daily meteorological variables over large regions of complex terrain. *Journal of Hydrology, 190*, 214-251

Tucker, C.J. (1979). Red and Photographic Infrared Linear Combinations for Monitoring Vegetation. *Remote Sensing of Environment, 8*, 127-150

USGS. (2008). Elevation derivatives for national applications. US Geological Survey online database. http://edna.usgs.gov/

Van Mantgem, P.J., Stephenson, N.L., Byrne, J.C., Daniels, L.D., Franklin, J.F., Fule, P.Z., et al. (2009). Widespread increase of tree mortality rates in the western United States. *Science, 323*, 521-524

Wagner, C.V. (1977). Conditions for the start and spread of crown fire. *Canadian Journal of Forest Research, 7*, 23-34

Wallace, L., Musk, R., & Lucieer, A. (2014). An assessment of the repeatability of automatic forest inventory metrics derived from UAV-borne laser scanning data. *IEEE Transactions on Geoscience and Remote Sensing, 52*, 7160-7169

Wallace, L., Lucieer, A., & Watson, C.S. (2014). Evaluating tree detection and segmentation routines on very high resolution UAV LiDAR data. *IEEE Transactions on Geoscience and Remote Sensing, 52*, 7619-7628

Wallace, L., Lucieer, A., Malenovsky, Z., Turner, D., & Vopenka, P. (2016). Assessment of Forest Structure Using Two UAV Techniques: A Comparison of Airborne Laser Scanning and Structure from Motion (SfM) Point Clouds. *Forests, 7*

Westerling, A.L., Hidalgo, H.G., Cayan, D.R., & Swetnam, T.W. (2006). Warming and earlier spring increase western US forest wildfire activity. *Science, 313*, 940-943

Westoby, M.J., Brasington, J., Glasser, N.F., Hambrey, M.J., & Reynolds, J.M. (2012). 'Structure-from-Motion' photogrammetry: A low-cost, effective tool for geoscience applications. *Geomorphology, 179*, 300-314

Woodcock, C.E., & Strahler, A.H. (1987). The factor of scale in remote sensing. *Remote Sensing of Environment, 21*, 311-332

Wulder, M.A., White, J.C., Alvarez, F., Han, T., Rogan, J., & Hawkes, B. (2009). Characterizing boreal forest wildfire with multi-temporal Landsat and LIDAR data. *Remote Sensing of Environment, 113*, 1540-1555

Zachmann, L.J., & Dickson, B.G. (2017). Four Forest Restoration Initiative- Landscape Pattern Analysis.

Zhu, Z., Vogelmann, J., Ohlen, D., Kost, J., Chen, X., & Tolk, B. (2006). Mapping existing vegetation composition and structure for the LANDFIRE prototype project.

Appendix A.

Table of predictor variables used to derive canopy fuels data for LANDFIRE (Reeves et al., 2009). MRLC is the Multi-Resolution Land Characteristic Consortium. DAYMET is a meteorological database. Wx Fire is a fire weather simulation model (Homer et al., 2004; Keane et al., 2006; Rollins, 2009; Thornton et al., 1997; Tucker, 1979; USGS, 2008; Zhu et al., 2006).

Variable	Source; Citation	Units
Satellite Imagery		
Landsat ETM band 1	MRLC; Homer et al (2004)	0.45-0.52 µm
Landsat ETM band 2	MRLC; Homer et al (2004)	0.52-0.60 µm
Landsat ETM band 3	MRLC; Homer et al (2004)	0.63-0.69 µm
Landsat ETM band 4	MRLC; Homer et al (2004)	0.76-0.90 µm
Landsat ETM band 5	MRLC; Homer et al (2004)	1.55-1.75 µm
Landsat ETM band 7	MRLC; Homer et al (2004)	2.08-2.35 µm
Landsat ETM tasseled-cap transformation	MRLC; Homer et al (2004)	unitless
Landsat ETM NDVI	MRLC; Tucker (1979)	unitless
Biophysical Gradients		
Average annual shortwave radiation	DAYMET; Thornton et al (1997)	W m^2
Average annual minimum daily temperature	DAYMET; Thornton et al (1997)	◦C
Average annual maximum daily temperature	DAYMET; Thornton et al (1997)	◦C
Average annual precipitation	DAYMET; Thornton et al (1997)	mm
Average annual vapor pressure deficit	DAYMET; Thornton et al (1997)	mbar
Average annual day length	DAYMET; Thornton et al (1997)	minutes
Average annual relative humidity	DAYMET; Thornton et al (1997)	%
Average annual snowfall	Wx Fire; Keane et al (2006)	cm
Average annual dewpoint temperature	Wx Fire; Keane et al (2006)	◦C
Average annual soil temperature	Wx Fire; Keane et al (2006)	◦C
Soil water transpired by canopy	Wx Fire; Keane et al (2006)	kg m^-2 day^-1
Volumetric water content	Wx Fire; Keane et al (2006)	unitless
Actual evapotranspiration	Wx Fire; Keane et al (2006)	kg h2o year^-1
Degree-days	Wx Fire; Keane et al (2006)	◦C
Days since last rain	Wx Fire; Keane et al (2006)	days
Evaporation	Wx Fire; Keane et al (2006)	kg h2o m^-2 day^-1
Canopy conductance to sensible heat	Wx Fire; Keane et al (2006)	s m^-1
Soil water lost to runoff and ground	Wx Fire; Keane et al (2006)	kg m^-2 day^-1
Potential evapotranspiration	Wx Fire; Keane et al (2006)	kg m^-2 year^-1
Photon flux density	Wx Fire; Keane et al (2006)	µmol m−2
Precipitation	Wx Fire; Keane et al (2006)	cm
Water potential of soil and leaves	Wx Fire; Keane et al (2006)	Mpa
Amount of snowfall	Wx Fire; Keane et al (2006)	cm
Soil water fraction	Wx Fire; Keane et al (2006)	%
Elevation	USGS (2008)	m
Aspect	USGS (2008)	azimuth
Slope	USGS (2008)	%
Vegetation attributes from LANDFIRE		
Existing vegetation type	Zhu et al (2006)	map class
Existing vegetation height	Zhu et al (2006)	map class
Existing vegetation cover	Zhu et al (2006)	map class
Environmental site potential	Rollins (2009)	map class